PNNL-25835

Pacific Northwest
NATIONAL LABORATORY
Proudly Operated by Battelle Since 1965

2016 Update of Hanford Glass Property Models and Constraints for Use in Estimating the Glass Mass to be Produced at Hanford by Implementing Current Enhanced Glass Formulation Efforts

September 2016

JD Vienna
GF Piepel
DS Kim
JV Crum
CE Lonergan
BA Stanfill
BJ Riley
SK Cooley
T Jin

U.S. DEPARTMENT OF ENERGY

Prepared for the U.S. Department of Energy
under Contract DE-AC05-76RL01830

DISCLAIMER

PACIFIC NORTHWEST NATIONAL LABORATORY
operated by
BATTELLE
for the
UNITED STATES DEPARTMENT OF ENERGY
under Contract DE-AC05-76RL01830

Printed in the United States of America

Available to DOE and DOE contractors from the
Office of Scientific and Technical Information,
P.O. Box 62, Oak Ridge, TN 37831-0062;
ph: (865) 576-8401
fax: (865) 576-5728
email: reports@adonis.osti.gov

Available to the public from the National Technical Information Service
5301 Shawnee Rd., Alexandria, VA 22312
ph: (800) 553-NTIS (6847)
email: orders@ntis.gov <http://www.ntis.gov/about/form.aspx>
Online ordering: http://www.ntis.gov

This document was printed on recycled paper.
(8/2010)

PNNL-25835

2016 Update of Hanford Glass Property Models and Constraints for Use in Estimating the Glass Mass to be Produced at Hanford by Implementing Current Enhanced Glass Formulation Efforts

JD Vienna
GF Piepel
DS Kim
JV Crum
CE Lonergan
BA Stanfill
BJ Riley
SK Cooley
T Jin

September 2016

Prepared for
the U.S. Department of Energy
under Contract DE-AC05-76RL01830

Pacific Northwest National Laboratory
Richland, Washington 99352

Executive Summary

Recent glass formulation and melter testing data have suggested that significant increases in waste loading in high-level waste (HLW) and low-activity waste (LAW) glasses are possible over current system planning estimates. In 2013, a set of models and constraints based on these data were developed and published (Vienna et al. 2013). Since that report, roughly 200 additional glasses have been tested and lessons were learned in applying the preliminary set of models and constraints. This report summarizes the advancements in glass formulation and glass property estimation since the publication of Vienna et al. (2013) using the additional data and lessons learned. The report also updates the recommended set of enhanced glass property-composition models and constraints for use in River Protection Project (RPP) planning.

The combined data (although limited in some cases[1]) were evaluated to determine a set of constraints and models that could be used to estimate the maximum loading of specific waste compositions in glass. It is recommended that these models and constraints be used to estimate the likely HLW and LAW glass masses that would result if the current glass formulation studies are successfully completed. It is recognized that some of the models are preliminary in nature and will change in the coming years. In addition, the models do not currently address the prediction uncertainties that would be required before they could be used in plant operations. The models and constraints are only meant to give an indication of rough glass masses and are not intended to be used in quality-affecting activities or decisions. A current program is in place to develop the data, models, and uncertainty descriptions for that purpose.

A fundamental tenet underlying the research reported in this document and in Vienna et al. (2013) was to be less conservative, but still realistic, compared to previous studies. This tenet was followed by implementing current enhanced glass formulation efforts to develop the constraints for estimating the masses of HLW and LAW glasses to be produced. The less conservative approach documented herein should allow for estimating glass masses that may be realized if the current efforts in enhanced glass formulations are completed over the coming years, and are as successful as results from the previous approximately four years of effort indicate they will be. However, at this stage of the work, there is an unquantifiable uncertainty in the ultimate glass mass projections due to model prediction uncertainties that must be considered, along with other system uncertainties, such as waste compositions and amounts to be immobilized, split factors between LAW and HLW, etc. A plan to estimate the impact of those uncertainties has been developed and a future update will document the results.

[1] Data limitations primarily exist for (i) HLW sulfate solubility across the entire composition region, (ii) HLW Product Consistency Test (PCT) response for high alumina glasses, (iii) HLW glass nepheline formation and mass fraction for Hanford glasses with prototypic cooling curves, (iv) LAW melt refractory corrosion, (v) HLW melt spinel settling and equilibrium crystal fraction, (vi) HLW chromium solubility, and (vii) LAW glass PCT and Vapor Hydration Test responses for high alkali glasses.

Recommended Models and Constraints

High-Level Waste Glass Models and Constraints

Models that constrain the composition and loading of high-level waste (HLW) glasses include models to control the nepheline formation in canister-cooled glass, amount of spinel in the melter (c_{Sp}), sulfur tolerance of the melter feed, viscosity of the melt at 1150ºC (η_{1150}), product consistency test (PCT) response, and liquidus temperature (T_L) of zirconia-containing phases. Also reported are component concentration limits for model validity, chromium tolerance, and phosphate tolerance. The recommended models are given below, along with property and component concentration constraints.[1]

The model form for predicting the probability of nepheline formation in HLW glass after canister centerline cooling is given by

$$p = \frac{\exp[\beta_0 + \beta_1 X + \beta_2 Y + \beta_3 X^2]}{1 + \exp[\beta_0 + \beta_1 X + \beta_2 Y + \beta_3 X^2]}\ , \qquad \text{(S.1)}$$

where

p = probability of nepheline formation for the HLW glass

β_i = polynomial model coefficients for the submixture model

X = location of the glass along the horizontal direction in the submixture ternary diagram $X = g^*_{AlFe} + \frac{1}{2} g^*_{SiB}$

Y = location in the vertical direction in the submixture ternary diagram $Y = \frac{\sqrt{3}}{2} g^*_{SiB}$

g^*_{SiB} = normalized concentration of the ternary submixture component involving SiO_2 and B_2O_3, where $g^*_{SiB} = \frac{g_{SiB}}{g_{Alk} + g_{AlFe} + g_{SiB}}$ and $g_{SiB} = g_{SiO_2} + \alpha_6 g_{B_2O_3} + \alpha_7 g_{P_2O_5}$

g^*_{AlFe} = normalized concentration of the ternary submixture component involving Al_2O_3 and Fe_2O_3, where $g^*_{AlFe} = \frac{g_{AlFe}}{g_{Alk} + g_{AlFe} + g_{SiB}}$ and $g_{AlFe} = g_{Al_2O_3} + \alpha_5 g_{Fe_2O_3}$

g^*_{Alk} = normalized concentration of the ternary submixture component involving the alkalis, where $g^*_{Alk} = \frac{g_{Alk}}{g_{Alk} + g_{AlFe} + g_{SiB}}$ and $g_{Alk} = g_{Na_2O} + \alpha_1 g_{Li_2O} + \alpha_2 g_{K_2O} + \alpha_3 g_{CaO} + \alpha_4 g_{MgO}$

[1] See Section 1.3 for discussion of significant figures.

The model coefficients are listed in Table S.1.

Table S.1. Coefficients of the Recommended Model for Nepheline Formation in HLW Glass

Coefficient[(a)]	LR-SM Conservative
α_1 (Li_2O)	0.804
α_3 (CaO)[(b)]	0.294
α_6 (B_2O_3)	1.732
β_0	-64.085
β_1	498.338
β_2	-102.179
β_3	-522.382
Threshold	0.30

(a) In addition to the components listed in this column, Al_2O_3, Na_2O, and SiO_2 also appear in the logistic regression-submixture model (LR-SM) with coefficients of one.

(b) Note that other terms with coefficients α_2, α_4, α_5, and α_7 were found to be insignificant.

The recommended $T_{2\%}$ model for HLW glass is given by

$$T_{2\%} = \sum_{i=1}^{q} a_i g_i + \text{ Selected}\left\{ \sum_{i=1}^{q} a_{ii} g_i^2 + \sum_{i=1}^{q-1} \sum_{j=i+1}^{q} a_{ij} g_i g_j \right\}, \qquad \text{(S.2)}$$

where q is number of HLW glass components in the model, a_i is model coefficient for the i^{th} HLW glass component, g_i mass fraction of the i^{th} HLW glass component (so that $g_1 + \ldots + g_{q=\text{Others}} = 1.0$), a_{ii} is the coefficient for the squared term of the i^{th} component, and a_{ij} is the coefficient of the crossproduct term involving the i^{th} and j^{th} components. The model coefficients are given in Table S.2.

Table S.2. Coefficients of the Recommended $T_{2\%}$ Model for HLW Glasses, in °C

Model Term	Coefficient
Al_2O_3	2058.4195
B_2O_3	-281.516
Bi_2O_3	1543.2359
Cr_2O_3	11944.224
Fe_2O_3	3673.0656
Li_2O	-753.6015
MgO	3553.9322
MnO	3485.9411
Na_2O	-1940.195
NiO	11231.615
RuO_2	84418.014
TiO_2	2574.6514
ZnO	4011.0211
ZrO_2	-987.8832
Others	391.75396
$Al_2O_3 \times Na_2O$	9345.1684
$ZrO_2 \times ZrO_2$	42569.129

The model for the allowable weight percent SO_3 concentration in the HLW melter feed ($w_{SO_3}^{Limit}$) has the form

$$w_{SO_3}^{Limit} = \sum_{i=1}^{q} s_i n_i \tag{S.3}$$

where q is the number of HLW glass components in the model, s_i is the coefficient of the i^{th} component in HLW glass and n_i is the concentration of the i^{th} component in HLW glass normalized to a total mass fraction of 1.0 after removing SO_3. Hence, $n_i = g_i / (1 - g_{SO_3})$, where g_i is the mass fraction of the i^{th} component in HLW glass. The model coefficients are given in Table S.3.

Table S.3. Coefficients for the Recommended w_{SO_3} (in wt%) Model for HLW Glasses

Model Term	Coefficient
Al_2O_3	-3.112
B_2O_3	5.253
CaO	10.679
Cl	-92.942
Li_2O	17.635
Na_2O	2.571
SiO_2	-2.438
V_2O_5	8.638
ZrO_2	-2.696
P_2O_5	4.737
Fe_2O_3	2.375
Others	4.165

Note: The model is based on mass fractions of HLW glass compositions, but predicts w_{SO_3} in wt%.

A model for HLW glass viscosity at 1150°C (η_{1150}) was developed with the form

$$\ln(\eta_{1150}, \text{Pa} \cdot \text{s}) = \sum_{i=1}^{q} b_i g_i \quad \text{(S.4)}$$

where b_i is the coefficient of the i^{th} HLW glass component, g_i is the mass fraction of the i^{th} HLW glass component, and q is the number of HLW glass components in the model. The model coefficients are given in Table S.4.

Table S.4. Coefficients of the Recommended η_{1150} Model for HLW Glass Melts, in ln(Pa·s)

Model Term	Coefficient
Al_2O_3	12.093093
B_2O_3	-6.968649
CaO	-7.867327
Cr_2O_3	10.263034
F	-18.405435
LN_2O_3[(a)]	3.5927373
Li_2O	-34.656075
MnO	-6.137735
Na_2O	-9.383399
NiO	4.1828203
P_2O_5	2.8993337
SiO_2	8.7348186
SrO	-5.661461
TiO_2	-9.632734
UO_3	2.4199882
ZrO_2	6.1936719
Others	-0.982565

(a) LN_2O_3 is the combination of Y_2O_3 and all the rare-earth oxides (which are all assumed to be in the trivalent state).

Models for the natural logarithm of normalized PCT-boron, -lithium, and -sodium responses for HLW glass were developed with the form

$$\ln[\mathrm{PCT}] = \sum_{i=1}^{q} b_i g_i + b2_{Al_2O_3} g_{Al_2O_3}^2 + b3_{Al_2O_3} g_{Al_2O_3}^3 + b4_{Al_2O_3} g_{Al_2O_3}^4 \ , \qquad \text{(S.5)}$$

where ln[PCT] is the response (ln[PCT-B, g/m^2], ln[PCT-Na, g/m^2], or ln[PCT-Li, g/m^2]), q is number of HLW glass components in the model, b_i is the coefficient of the i^{th} component in HLW glass, g_i is the mass fraction of the i^{th} component in HLW glass (so that $g_1 + \ldots + g_{q=\text{Others}} = 1.0$), and $b2_{Al_2O_3}$, $b3_{Al_2O_3}$, $b4_{Al_2O_3}$ are the coefficients for higher-order terms involving the mass fraction of Al_2O_3. The model coefficients are listed in Table S.5.

Table S.5. Coefficients of the Recommended ln[PCT] Models for HLW Glasses, in ln[g/m^2]

Model Term	PCT-B	PCT-Na	PCT-Li
Al_2O_3	-78.7836	-71.6595	-63.9519
B_2O_3	11.8314	7.5035	9.7161
CaO	-4.2608	0.1647	-1.5756
Fe_2O_3	-0.1367	-1.2469	-1.5209
Li_2O	26.6872	23.9739	21.5220
MgO	22.2708	19.8924	16.0853
Na_2O	18.0511	20.0074	13.5925
P_2O_5	-10.1336	-10.0559	-6.3595
SiO_2	-4.5104	-4.5442	-3.3104
SO_3	18.6514	17.5527	16.7191
TiO_2	-7.3229	-7.9836	-4.6582
UO_3	-8.6123	-7.9687	-6.6933
ZnO	-7.3998	-12.3124	-9.9948
ZrO_2	-8.8810	-9.7138	-8.0739
Other	2.9184	3.9227	1.9047
$(Al_2O_3)^2$	638.3727	594.5920	523.1351
$(Al_2O_3)^3$	-2360.5420	-2330.9850	-1983.3580
$(Al_2O_3)^4$	3174.4550	3321.4927	2738.6894

A model for the liquidus temperature (T_L) of zirconium-containing phases in HLW glasses was developed and published previously and is recommended for use here. This model has the form

$$T_L = \sum_{i=1}^{q} t_i g_i \ , \tag{S.6}$$

where q is the number of HLW glass components in the model, while t_i and g_i are the coefficient and mass fraction of the i^{th} component in HLW glass, respectively. The model coefficients are listed in Table S.6.

Table S.6. Coefficients of the Recommended T_L-Zs Model for HLW Glasses, in °C

Model Term	Coefficient
Al_2O_3	3193.3628
B_2O_3	651.39721
LN_2O_3[(a)]	2156.4074
Li_2O	-1904.417
Na_2O	-1947.711
SrO	13011.909
ZrO_2	3747.4241
Others	1259.2233

(a) LN_2O_3 is the combination of Y_2O_3 and all the rare-earth oxides (which are all assumed to be in the trivalent state).

The recommended property constraints are listed in Table S.7 and the recommended component concentration constraints are listed in Table S.8.

Table S.7. HLW Glass Property Constraints

Constraint	Limit
PCT Responses	ln[PCT-B, Na, Li, g/m^2] ≤ 1.386[(a)]
Nepheline	$p \leq 0.3$ (probability)
Spinel	$T_{2\%} \leq 950$°C
Zirconium-containing phases	T_L-Zs ≤ 1050°C if $g_{ZrO_2} > 0.04$ (mass fraction)
Viscosity at 1150°C	$1.386 \leq \ln(\eta_{1150}, \text{Pa·s}) \leq 1.792$[(b)]
P_2O_5 and CaO concentrations	$w_{P_2O_5} \times w_{CaO} \leq 6.5$ (wt%)^2
Salt, SO_3 concentration	$w_{SO_3} \leq w_{SO_3}^{Limit}$ (wt%)
Eskolaite formation	$g_{Cr_2O_3} \leq 0.03$ (mass fraction)
B_2O_3 and SiO_2 concentrations	$g_{SiO_2} + g_{B_2O_3} \geq 0.32$ (mass fraction)

(a) This corresponds to PCT-B, -Na, -Li ≤ 4 g/m^2.
(b) This corresponds to $4 \leq \eta_{1150} \leq 6$ Pa·s.

Table S.8. HLW Glass Component Concentration Constraints, in Mass Fractions

Component	Min	Max
Al_2O_3	0.1900	0.3000
B_2O_3	0.0400	0.2200
Bi_2O_3	0	0.0700
CaO	0	0.1000
CdO	0	0.0150
Cr_2O_3	0	0.0300
F	0	0.0250
Fe_2O_3	0	0.2000
K_2O	0	0.0600
Li_2O	0	0.0600
MgO	0	0.0600
MnO	0	0.0800
Na_2O	0.0410	0.2400
NiO	0	0.0300
P_2O_5	0	0.0450
SiO_2	0.2200	0.5300
SrO	0	0.1010
ThO_2	0	0.0600
TiO_2	0	0.0500
UO_3	0	0.0630
ZnO	0	0.0400
ZrO_2	0	0.1350

The additives recommended for calculation purposes are Al_2O_3, B_2O_3, CaO, Li_2O, MgO, Na_2O, SiO_2, V_2O_5, ZnO, and ZrO_2.

Low-Activity Waste Glass Models and Constraints

Models to constrain the composition and loading of low-activity waste (LAW) glasses include models to control the sulfur tolerance of the melter feed PCT response, Vapor Hydration Test (VHT) response, η_{1150}, and refractory corrosion. Also reported are component concentration limits for model validity, as well as the chromium, halide, phosphate, and alkali tolerance. The recommended models are given below along with property and component concentration constraints.

The model for the allowable weight percent SO_3 concentration in the LAW melter feed ($w_{SO_3}^{Limit}$) is given by

$$w_{SO_3}^{Limit} = \sum_{i=1}^{q} s_i n_i + \text{Selected}\left\{ \sum_{i=1}^{q} s_{ii} n_i^2 + \sum_{i=1}^{q-1} \sum_{j=i+1}^{q} s_{ij} n_i n_j \right\} \quad \text{(S.7)}$$

where s_i is the coefficient of the i^{th} component in LAW glass, n_i is the mass fraction of the i^{th} component in LAW glass normalized after removing SO_3 [$n_i = g_i / (1 - g_{SO_3})$, where g_i is the mass fraction of the i^{th} component in LAW glass], s_{ii} is the coefficient for the squared term of the i^{th} component in LAW glass, s_{ij} is the coefficient of the crossproduct term involving the i^{th} and j^{th} components in LAW glass, and q is the number of normalized LAW glass components in the model. Note that that $n_1 + \ldots + n_{q=\text{Others}} = 1.0$. The model coefficients are listed in Table S.9.

Table S.9. Coefficients of the Recommended w_{SO_3} Model for LAW Glasses, in wt%

Model Term	Coefficient
Al_2O_3	-2.0919
B_2O_3	3.044075
CaO	4.442289
Cl	-22.6535
Cr_2O_3	-13.1414
K_2O	0.615785
Li_2O	2.473926
Na_2O	2.897209
P_2O_5	4.606083
SiO_2	0.240729
SnO_2	-1.77533
V_2O_5	7.534548
ZrO_2	-1.87192
Others	-0.28027
$(Li_2O)^2$	260.203

A model for the average natural logarithm of normalized PCT-boron and -sodium response [ln(*NL*, g/L)] for LAW glasses was developed with the form

$$\ln\left(NL,\ \text{g/L}\right) = \sum_{i=1}^{q} b_i g_i + \text{Selected}\left\{ \sum_{i=1}^{q} b_{ii} g_i^2 + \sum_{i=1}^{q-1} \sum_{j=i+1}^{q} b_{ij} g_i g_j \right\}, \quad \text{(S.8)}$$

where q is number of LAW glass components in the model, b_i is the coefficient of the i^{th} component in LAW glass, g_i is the mass fraction of the i^{th} component in LAW glass (so that $g_1 + \ldots + g_{q=\text{Others}} = 1.0$), b_{ii} is the coefficient for the squared term of the i^{th} component in LAW glass, and b_{ij} is the coefficient of the

crossproduct term involving the i^{th} and j^{th} components in LAW glass. The model coefficients are given in Table S.10.

Table S.10. Coefficients of the Recommended ln(PCT *NL*) Model for LAW Glasses, in ln(g/L)

Model Term	Coefficient
Al_2O_3	-4.7932
B_2O_3	-31.2612
CaO	3.8636
K_2O	-13.5298
Li_2O	-16.6826
MgO	21.4263
Na_2O	-25.2993
P_2O_5	-5.1242
SiO_2	0.3093
SnO_2	-4.4031
TiO_2	-1.7604
ZrO_2	3.8966
Others	6.2375
$B_2O_3 \times B_2O_3$	157.3873
$K_2O \times K_2O$	201.4790
$Al_2O_3 \times Li_2O$	-255.4098
$CaO \times Li_2O$	-128.0130
$Li_2O \times Li_2O$	474.3082
$B_2O_3 \times Na_2O$	81.1682
$K_2O \times Na_2O$	120.3814
$Li_2O \times Na_2O$	391.5456
$Na_2O \times Na_2O$	97.6643

A model for the VHT alteration thickness in ln(*D*, μm) of LAW glasses was developed with the form

$$\ln\left(D,\ \mu\text{m}\right) = \sum_{i=1}^{q} b_i g_i + \text{Selected}\left\{ \sum_{i=1}^{q} b_{ii} g_i^2 + \sum_{i=1}^{q-1} \sum_{j=i+1}^{q} b_{ij} g_i g_j \right\}, \tag{S.9}$$

where q is number of LAW glass components in the model, b_i is the coefficient of the i^{th} component in LAW glass, g_i is the mass fraction of the i^{th} component in LAW glass (so that $g_1 + \ldots + g_{q=\text{Others}} = 1.0$), b_{ii} is the coefficient for the squared term of the i^{th} component in LAW glass, and b_{ij} is the coefficient of the crossproduct term involving the i^{th} and j^{th} components in LAW glass. The model coefficients are given in Table S.11.

Table S.11. Coefficients of the Recommended ln(VHT *D*) Model for LAW Glasses, in ln(μm)

Model Term	Coefficient
Al_2O_3	-3.1247
B_2O_3	9.0537
CaO	-165.0264
Fe_2O_3	-9.3359
K_2O	-68.6719
Li_2O	308.9919
Na_2O	75.8436
SiO_2	-22.5420
SnO_2	-28.5312
TiO_2	-27.0704
ZrO_2	-48.6944
Others	2.5197
CaO×CaO	452.8308
$Li_2O \times Li_2O$	-3040.2579
$K_2O \times Na_2O$	433.9384
$Li_2O \times Na_2O$	-1273.4629
$CaO \times SiO_2$	267.5427
$K_2O \times K_2O$	724.3290
$Li_2O \times SiO_2$	361.8056

A model for LAW melt viscosity at 1150°C (η_{1150}) was developed with the form

$$\ln(\eta_{1150}, \text{Pa} \cdot \text{s}) = \sum_{i=1}^{q} b_i g_i \qquad \text{(S.10)}$$

where q is number of LAW glass components in the model, b_i is the coefficient of the i^{th} component in LAW glass, and g_i is the mass fraction of the i^{th} component in LAW glass. The model coefficients are given in Table S.12.

Table S.12. Coefficients of the Recommended ln(η_{1150}) Model for LAW Glasses, in ln(Pa·s)

Model Term	Coefficient
Al_2O_3	11.67007
B_2O_3	-7.44665
CaO	-7.60545
Fe_2O_3	-0.11082
K_2O	-4.65558
Li_2O	-32.67344
MgO	-4.26291
Na_2O	-9.30809
P_2O_5	7.94147
SiO_2	8.88092
SnO_2	4.73082
TiO_2	-4.93294
V_2O_5	-2.64858
ZnO	-4.51330
ZrO_2	6.91854
Others	2.74032

A model for K3 corrosion at 1208°C is given by the form

$$\ln(k_{1208}) = \sum_{i=1}^{q} k_i g_i + \text{Selected}\left\{ \sum_{i=1}^{q} k_{ii} g_i^2 + \sum_{i=1}^{q-1} \sum_{j=i+1}^{q} k_{ij} g_i g_j \right\} \quad \text{(S.11)}$$

where k_{1208} is neck corrosion distance in the 6-day test at 1208°C (in inches), q is number of LAW glass components in the model, k_i is the coefficient of the i^{th} component in LAW glass, g_i is the mass fraction of the i^{th} component in LAW glass (so that $g_1 + \ldots + g_{q=\text{Others}} = 1.0$), k_{ii} is the coefficient for the squared term of the i^{th} component in LAW glass, and k_{ij} is the coefficient of the crossproduct term involving the i^{th} and j^{th} components in LAW glass. The model coefficients are given in Table S.13.

Table S.13. Coefficients of the Recommended ln(k_{1208}) Model for LAW Glasses, in ln(inch)

Model Term	Coefficient
Al_2O_3	-23.696
B_2O_3	-0.965
CaO	6.590
Cr_2O_3	-85.437
Fe_2O_3	-4.315
K_2O	7.997
Li_2O	44.748
MgO	-37.185
Na_2O	20.337
P_2O_5	117.297
SiO_2	-10.103
SnO_2	-38.779
TiO_2	90.238
V_2O_5	-114.733
ZnO	-12.560
ZrO_2	-11.150
Others	-20.952
$Li_2O \times P_2O_5$	-3092.687
$(MgO)^2$	716.072
$Na_2O \times P_2O_5$	-579.772
$Na_2O \times V_2O_5$	335.374
$SiO_2 \times TiO_2$	-241.722
$SnO_2 \times$Others	2880.688
$V_2O_5 \times$ZnO	1028.765

The recommended property and multicomponent constraints are listed in Table S.14. The waste loading rules give an estimate of the loading of waste in glass, while the property limits, combined with property models described above, allow for optimization of the glass composition along with the recommended component concentration constraints that are listed in Table S.15.

The additives recommended for glass optimization approach calculation purposes are Al_2O_3, B_2O_3, CaO, Li_2O, MgO, SiO_2, SnO_2, V_2O_5, ZnO, and ZrO_2.

Table S.14. LAW Glass Property and Multicomponent Concentration Constraints

Waste Loading Rules	Limit
Alkali content	$w_{Na_2O} + 0.66 w_{K_2O} \le 24\,\text{wt\%}$
Alkali and sulfur content	$w_{Na_2O} + 0.66 w_{K_2O} \le 33.94 - 11.69 w_{SO_3}$, wt%
Sulfur content	$w_{SO_3} \le 1.5\,\text{wt\%}$
Halide content	$g_{SO_3} \le 0.01825 - 0.4936 \times \left(1.761 g_{Cl} + 2.971 g_{Cr_2O_3} - 0.1608 g_{P_2O_5}\right)$
Property	**Limit**
Salt, SO_3 concentration	$w_{SO_3} \le w_{SO_3}^{Limit}$
Combined zirconia, tin, and alumina constraint	$g_{ZrO_2} + g_{SnO_2} + g_{Al_2O_3} \le 0.17$
Alkali minus sum of zirconia, tin, and lime constraint	$g_{Na_2O} + 0.66 g_{K_2O} + 2.07 g_{Li_2O} - g_{ZrO_2} - g_{SnO_2} - g_{CaO} \le 0.15$
PCT response	ln[PCT *NL*, g/L] ≤ 1.386
VHT response	ln[VHT *D*, µm] ≤ 6.116
Viscosity at 1150°C	1.386 ≤ ln[η_{1150}, Pa·s] ≤ 1.792
K-3 neck corrosion at 1208°C	ln[k_{1208}, in] ≤ -3.2189

Table S.15. LAW Glass Single Component Concentration Constraints, in Mass Fractions

Component	Min	Max
Al_2O_3	0.0553	0.1370
B_2O_3	0.0600	0.1370
CaO	0	0.1060
Cl	0	0.0117
Cr_2O_3	0	0.0100
Fe_2O_3	0	0.0997
K_2O	0	0.0589
Li_2O	0	0.0503
MgO	0	0.0350
Na_2O	0.0248	0.2600
P_2O_5	0	0.0340
SiO_2	0.2983	0.5020
SnO_2	0	0.0501
TiO_2	0	0.0341
V_2O_5	0	0.0401
ZnO	0	0.0540
ZrO_2	0	0.0675

Quality Assurance

This task was performed under the U.S. Department of Energy Office of River Protection Inter-Entity Work Order # M0ORV00020 and under Pacific Northwest National Laboratory's (PNNL's) Nuclear Quality Assurance Program (NQAP), which implements the requirements of ASME NQA-1-2012, with mapping to NQA-1-2008 with 2009 addendum and is graded in accordance with NQA-1-2012, Subpart 4.2, "Guidance on Graded Application of Quality Assurance for Nuclear-Related Research and Development." The work reported here has been graded as "Basic Research." No experimentation was conducted as part of the study reported here. The work reported included gathering data from the literature, screening and evaluating the data, fitting glass property models, and recommending constraints for glass formulation based on the literature data and glass formulation experiences. The data used in the evaluations and the models were taken from literature and were not formally evaluated or qualified for acceptability prior to reporting. Calculations and models were not verified and validated. The work has been peer reviewed at PNNL. Therefore, the models reported in this document cannot be used for quality impacting work or decisions as defined in NQA-1 (ASME 2012) or RW-0333P (DOE 2008) (e.g., design basis input, plant operations, waste form compliance). Instead the models and constraints are intended for use in mission planning activities.

Acknowledgments

We gratefully acknowledge the financial support of Mr. William F. Hamel, Jr – Federal Project Director of the U.S. Department of Energy's Waste Treatment and Immobilization Plant (WTP) under the direction of Dr. Albert A. Kruger.

The authors also thank the following people for their technical review and consultations on the work leading to this report:

- David Peeler (PNNL) for peer review of the document
- Kirsten Meier (PNNL) for quality assurance review of the document
- Derek Dixon (PNNL) for his careful technical review of the LAW viscosity dataset
- Rod Gimpel (WTP), Bennett Rieck (WTP), Natalie Kirch (WRPS), and Jeremy Belsher (WRPS) for external technical review of the document
- Albert Kruger (DOE-ORP) for management review

This manuscript was masterfully formatted and edited, respectively, by Susan Tackett and Cary Counts. We thank Mike Schweiger for programmatic support during the conduct of this work.

A large fraction of the data described in this report was generated by the Vitreous State Laboratory at The Catholic University of America (VSL). We are thankful to VSL (in particular Professor Ian Pegg) for sharing VSL data and providing assistance in data evaluation and interpretation.

Acronyms and Abbreviations

ASTM	American Society for Testing and Materials
c_{950}	equilibrium concentration of spinel in the melt at 950°C
CCC	canister centerline cooled
CFR	Code of Federal Regulations
c_{Sp}	equilibrium concentration of spinel in the melt
CVS	Composition Variation Study
D	Vapor Hydration Test response alteration depth after 24-day test
DOE	U.S. Department of Energy
DWPF	Defense Waste Processing Facility
EA	environmental assessment
G2	WTP dynamic flowsheet model
g_i	mass fraction of i^{th} component in glass
HASQARD	Hanford Analytical Services Quality Requirements Document
HDI	How Do I?
HLP	Hanford LAW product acceptance
HLW	high-level waste
HTM	high temperature melter
HTWOS	Hanford Tank Waste Operations Simulator
HWVP	Hanford Waste Vitrification Plant
IDF	Integrated Disposal Facility
ILAW	immobilized low-activity waste
INEEL	Idaho National Engineering and Environmental Laboratory
LAW	low-activity waste
L-BFGS	limited memory-Broyden-Fletcher-Goldfarb-Shanno (algorithm)
LMM	linear mixture model
ln(*NL*)	normalized average loss of ln(*NL* B) and ln(*NL* Na) from an LAW glass after a 7-day PCT
LR	logistic regression
MT	metric ton
NAlk	normalized alkali oxide concentration
ND	nepheline discriminator
NH	normalized halogen concentration
n_i	normalized mass fraction of i^{th} component in glass
NN	neural network
NQA	nuclear quality assurance
NSi	normalized SiO_2 concentration

OB	optical basicity
ORP	Office of River Protection
PCT	Product Consistency Test
PDC	polynomial discriminating curve
PI	prediction interval
PNNL	Pacific Northwest National Laboratory
PQMM	partial quadratic mixture model
QA	quality assurance
QAP	Quality Assurance Plan
R^2	R-squared (coefficient of determination)
RMSE	root mean squared error
RPP	River Protection Project
RSD	relative standard deviation
SM	submixture
SRNL	Savannah River National Laboratory
SwRI	Southwest Research Institute
$T_{1\%}$	temperature at one volume percent crystals in equilibrium with the melt
$T_{2\%}$	temperature at two volume percent crystals in equilibrium with the melt
TCLP	Toxicity Characteristic Leaching Procedure
T_L	liquidus temperature
TWRS	Tank Waste Remediation System
UTL	upper tolerance limit
VFT	Vogel-Fulcher-Tammann
VHT	Vapor Hydration Test
VSL	the Vitreous State Laboratory at the Catholic University of America
w_i	weight percent of the i^{th} component in glass or melter feed
WTP	Hanford Tank Waste Treatment and Immobilization Plant
WVDP	West Valley Demonstration Project
ε	melt electrical conductivity
η	melt viscosity

Contents

Figures

Tables

1.0 Introduction

The Hanford Tank Waste Operations Simulator (HTWOS) and the Hanford Tank Waste Treatment and Immobilization Plant (WTP) dynamic flowsheet model (G2) are software tools used to evaluate the impacts of process assumptions on the Hanford tank waste cleanup mission (Allen et al. 2014, Deng 2014). Both contain modules that calculate the high-level waste (HLW) and low-activity waste (LAW) glass mass to be produced from each batch of tank waste transferred to the WTP. The sum of the glass masses over the life of the Hanford tank waste cleanup mission is a key output of the models. That output may significantly influence cleanup costs and schedules, which form part of the basis for the project baseline (e.g., the River Protection Project [RPP] system plan) (Certa 2011). It is important, therefore, to incorporate the most up-to-date information that dictate waste loading in glasses into these models.

A multi-year program initiated and led by the U.S. Department of Energy (DOE) Office of River Protection (ORP) is being conducted by researchers from Pacific Northwest National Laboratory (PNNL), The Vitreous State Laboratory at the Catholic University of America (VSL), Savannah River National Laboratory (SRNL), and ORP to develop the data and models needed to process the full range of HLW and LAW compositions at high waste loadings in glass (see for examples: Peeler et al. 2015a and 2015b). Vienna et al. (2013) summarized the state-of-the-art in Hanford waste loading estimates in glass and recommend a set of glass property-composition models and constraints that can be used in HTWOS and G2 to estimate the range of likely HLW and LAW glass masses that would result if the current glass formulation studies are continued and the models ultimately implemented. Those models were incorporated into both HTWOS and G2 as options for estimating glass masses and used in various planning cases (see for example: Jenkins et al. 2013 and DOE 2014). Since 2013 significant additional data have been developed along with progress in glass property models and glass formulations. The purpose of this report is to summarize the advancements in glass formulation and glass property estimation since publication of Vienna et al. (2013) and update the recommended set of glass property-composition models and constraints for use in RPP planning.

It is recognized that some of the models are preliminary in nature and will change in the coming years. In addition, the models do not currently address the prediction uncertainties that would be needed before they could be used in plant operations. The models and constraints are only meant to give an indication of rough glass masses and are not intended to be used in quality-affecting activities or decisions. A current research program is in place to develop the data, models, and uncertainty descriptions for those purposes.

A fundamental tenet underlying the research reported in the Vienna et al. (2013) and this document is to be less conservative, yet still realistic, than previous studies when developing constraints for estimating glass masses to be produced by implementing current enhanced glass formulation efforts. The less conservative approach documented herein should allow the estimating glass masses that may be realized if the current efforts in enhanced glass formulations are completed over the coming years and are as successful as early indications suggest they may be. Because of this approach, there is an unquantified uncertainty in the ultimate glass mass projections due to model prediction uncertainties that must be considered, along with other system uncertainties, such as waste compositions and amounts to be immobilized, split factors between LAW and HLW, etc. A plan has been developed to obtain a reasonable estimate of the prediction and vitrification plant operation uncertainties which will be documented in a future study.

1.1 HLW Property Constraints and Loading Limitations

Estimates of HLW glass masses are based on optimizing the loading of the waste batch in a borosilicate glass, while simultaneously meeting a full range of predicted property and composition limits or constraints. The constraints typically considered for HLW glasses are:

- Constraints to avoid the accumulation of crystals in the melter during normal operating conditions and extended periods of melter idling. These constraints generally are of the form of limits on the concentration of spinel and other phases in equilibrium at a specific temperature.
- Constraints on viscosity (η) at the processing temperature to ensure sufficient processing rate and flow of glass while minimizing corrosion of melter construction materials.
- Constraints on electrical conductivity (ε) at the processing temperature to ensure sufficient energy can be supplied by the power source without exceeding current density limits of the power system. Note that electrical conductivity rarely influences the loading of HLW in glass, so it was not modeled or recommended as a constraint for the purposes of this work.
- Product Consistency Test (PCT) response limits for waste form acceptance dictated by the WTP contract and the *Waste Acceptance Product Specification* (WAPS, DOE 1996).
- Waste form phase stability constraints to avoid the risk of forming nepheline and other phases that may dramatically change the PCT responses of glass in an unpredictable way.
- Salt accumulation constraints to avoid excessive corrosion of melter construction materials and increase radionuclide volatility.

Model validity or data availability constraints to maintain glass compositions within the ranges over which the predictive models and formulation approaches are valid. Three sets of models and constraints have been used for HLW glass mass estimates at Hanford (with slight variations). These include:

1. The WTP Algorithm (also referred to as: WTP Baseline, WTP Commissioning, and 2008) models and constraints. These models (Piepel et al. 2008) were developed under the WTP project and QA program appropriate for plant operation, have been reviewed and approved by DOE-ORP and a preliminary Technical Review Group for application in waste form compliance, and are incorporated in the *Preliminary Immobilized High-Level Waste Formulation Algorithm* (Vienna and Kim 2014) for use in plant commissioning. They were developed based on a limited set of tank waste feed (AY-102/C-106, AZ-101, AZ-102, and AY-101/C-104) and used modest waste loadings, slightly above the contract minimum waste loading limits (TS-1.1 in DOE 2000). Because three of the four waste compositions had high iron content (primarily PUREX waste), the WTP algorithm does not cover the breadth of expected waste compositions. Since the objective of the development work that generated these models was to successfully commission the new HLW vitrification plant, they do not challenge the possible range of waste loadings. All tank wastes could likely be processed using these models but would result in double or more the necessary amount of HLW glass.
2. The 2009 (also referred to as: HTWOS, Glass Shell Version 2, System Plan) models and constraints. These models were originally documented in Vienna et al. (2009) then were updated in McCloy and Vienna (2010). They were developed to estimate more realistic, yet still conservative, HLW glass masses based on the wealth of glass property data developed by PNNL,

VSL, SRNL, and others but not all used in the WTP Algorithm models. These models were implemented in HTWOS (Bergmann 2010) and G2 (Gimpel 2009) codes and were applied in the *RPP System Plan*, Revisions 5 (Certa et al. 2010), 6 (Certa et al. 2011), and 7 (DOE 2014) and virtually all WTP dynamic flowsheet models since 2009 (e.g., Jenkins et al. 2010). These models, and the data used to produce them, are not fully QA compliant for plant operation and so should be used only as an estimation tool.

3. The Enhanced (also referred to as: 2013, Kruger) models and constraints documented by Vienna et al. (2013). These models were developed to allow for a systematic estimate of the potential impacts of the ongoing enhanced glass formulation program on RPP mission assumptions. The available data from enhanced glass formulations generated from roughly 2006 through 2012 were incorporated in these models and constraints. They were the first set of models and constraints aimed at non-conservative, yet still realistic, glass mass estimates. They were implemented in both HTWOS and WTP G2 models to estimate glass masses in sensitivity cases of the life-cycle mission glass mass estimates (Jenkins et al. 2013, DOE 2014). These models, and the data used to produce them, are not fully QA compliant for plant operation and so should be used only as an estimation tool.

These three sets of models and constraints are contrasted in Table 1.1 and Figure 1.1 below. The objective of this report is to update the third set of models and constraints (i.e., enhanced) by incorporating (i) data collected between 2012 and 2016 and (ii) lessons learned from the implementation and validation of those models and constraint sets.

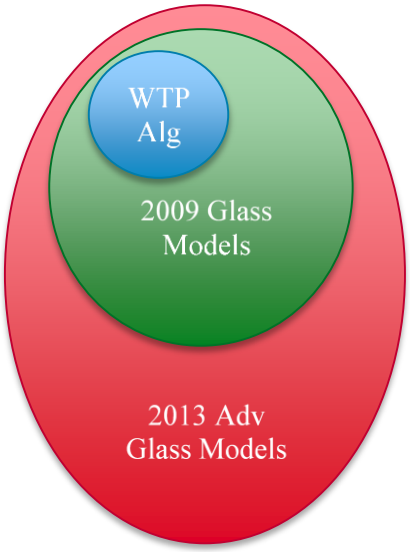

Figure 1.1. Graphical Representation of HLW Models and Constraints

Table 1.1. Attributes of HLW Models and Constraints Sets

Model/Constraint	WTP Baseline	HTWOS 2009	Enhanced 2013
Full QA for plant operation	Yes	No	No
Waste loading	Conservative	Modest, yet still conservative	Highest practical based on current data
Tanks considered	AY-101/C-104, AZ-101, AZ-102, AY-102/C-106	All	All
Intended Purpose	WTP Commissioning	Mission Planning	Mission Planning
Spinel limit	1 vol%, 950°C	1 vol%, 950°C	2 vol%, 950°C
Al_2O_3 concentration limit in glass	13 wt%	20 wt%	28 wt%
Cr_2O_3 concentration limit in glass	0.6 wt%	1.2 wt%	3 wt%
Estimated full mission glass cans*	18,400 (Leach) 31,600 (No Leach)	10,800 (Leach) 19,500(no Leach)	8,000 (Leach) 13,500 (no Leach)

* Glass mass estimates described in Appendix A of Vienna et al. (2013) for "Leach" waste feeds and Jenkins et al. 2013 for "no Leach" waste feeds.

The loading of Hanford HLW in glass has repeatedly been found (Vienna et al. 2013) to be most strongly influenced by:

- Model-validity constraints (particularly Al_2O_3, Cr_2O_3, F and CaO in the case of WTP Baseline; SiO_2 and B_2O_3 in the case of 2013 Enhanced).
- Combined nepheline, spinel, viscosity, and PCT constraints. As multicomponent constraints, the optimization process would simultaneously meet as many constraints as degrees of freedom available (e.g., number of glass-forming additives).
- Sulfur or salt accumulation constraints
- Phosphate and phosphate-calcium constraints.

Additional effort for the results in this report focused on evaluating and updating the most influential constraints and property models. In addition, several lessons were learned by the implementation and informal validation of the 2013 Enhanced models and constraints. For example:

- The previous approach of using a neural network model top predict nepheline formation was both impractical and not as predictive as previously applied model approaches (e.g., see Vienna et al. 2016).
- Dividing composition space into local (or sub) regions can significantly reduce prediction uncertainties. For example PCT response models for low-, intermediate-, and high-Al_2O_3 concentration regions were more precise than global models covering the entire composition region. Unfortunately, these sub-region models resulted in step-function changes in predicted responses at the boundaries causing problems in formulation optimization routines.
- Modeling spinel crystal fraction as functions of both temperature and composition results in significantly less precise (and potentially less accurate) models than predicting composition effects

on either temperature of a fixed crystal fraction (e.g., 2 vol%) or crystal fraction at a fixed temperature (e.g., 950°C).

Modeling approaches were changed in the current study to address these lessons learned.

1.2 LAW Property Constraints and Loading Limitations

The loading of LAW in glass has been found to be limited by two factors (Kim et al. 2011; Kim and Vienna 2012; Matlack et al. 2007b; Muller et al. 2010; Vienna t al. 2013):

- Alkali content of the glass (primarily Na_2O, but also K_2O in some wastes), which causes poor chemical durability in general and more specifically fails the current WTP contract constraints for PCT and Vapor Hydration Test (VHT) responses (DOE 2000).
- Salt formation in the melter that is promoted by SO_3 concentration and to lesser extents Cr_2O_3, Cl, and F.

The fraction of waste limited by each of these two factors depends on the constraint sets and waste composition estimates used. Three methods of estimating the loading of LAW glass have been used to estimates masses of LAW glass:

1. The DOE-2004 (also referred to as HTWOS, Vienna 2004) model determines loading of LAW by the lesser of 20 wt% Na_2O or 0.8 wt% SO_3 in glass. Note that other models are based on melter feed while this model is based on glass after volatile loss). This model (Hamel et al. 2003, Vienna et al. 2004) was an attempt in 2003-2004 to estimate the waste loading that would result from higher waste loading glass development, testing, and demonstration that was likely to occur shortly after WTP commissioning. Hence, this model was expected to result in more accurate estimates of waste loading in glass for the Hanford mission. This model was not developed under a QA program based on NQA-1 nor has it been demonstrated at greater than crucible scale. This model was applied in HTWOS in 2004 and used in the *RPP System Plan* (revisions 3 [Certa et al. 2008], 3A [Certa et al. 2008], 4 [Certa et al. 2009], 5 [Certa et al. 2010], 6 [Certa et al. 2011] and 7 [DOE 2014]), usually as the baseline case.
2. The WTP Baseline (also referred to as Algorithm, 2009, 2007, Isabelle Rule) model determines the target glass composition for production during operation. The model in various forms has been documented in several places (Muller et al. 2004, Vienna 2005, Kim and Vienna 2012, Arakali et al. 2011, Jenkins et al. 2013). This model is based on the interpolation of successfully tested glass compositions (up to pilot scale) with reasonable estimated composition variation (due to uncertainty and process variation). The glass loading is determined by 21.5 wt% Na_2O+0.66 K_2O, 0.7 wt% SO_3, or Na_2O wt% < 35.875 to 42.5 SO_3 wt% in melter feed (Muller et al. 2004) with additional constraints for Cr_2O_3, Cl, F, and P_2O_5 (Vienna and Kim 2007). This model was developed under a full QA program and thus could be applied to plant operation and is the basis of the WTP design. However, this model is significantly more conservative in waste loading than is necessary or appropriate for application across the full mission. Application in the WTP glass formulation algorithm includes uncertainty quantification; although applications in WTP G2 and HTWOS do not.
3. The Enhanced 2013 (also referred to as Kruger) model determines the waste loading of LAW by the lesser of 24 wt% Na_2O or 1.5 wt% SO_3 with additional constraints for halides. This model

(Vienna et al. 2013) was an attempt in 2013 to estimate the waste loading that would result from higher waste loading glass development, testing, and demonstration that was likely to occur shortly after WTP commissioning. Hence, this model was expected to result in more accurate estimates of loading in glass for the Hanford mission (e.g., an updated model to meet the objectives of the DOE-2004 model). This model was not developed under a QA program. However, it is based on significant melter and crucible testing. This model was applied in sensitivity cases in the *RPP System Plan* revision 7 (DOE-2014), the *Tank Utilization Assessment* (Jenkins et al. 2013), and estimates for the Secretary of Energy (Kim 2013).

These three sets of models and constraints are contrasted in Figure 1.2 and Table 1.2 below. The objective of this report is to update the third set of constraints and limits (i.e., Enhanced) by incorporating data collected between 2012 and 2016 and lessons learned from the implementation and validation of those models and constraint sets.

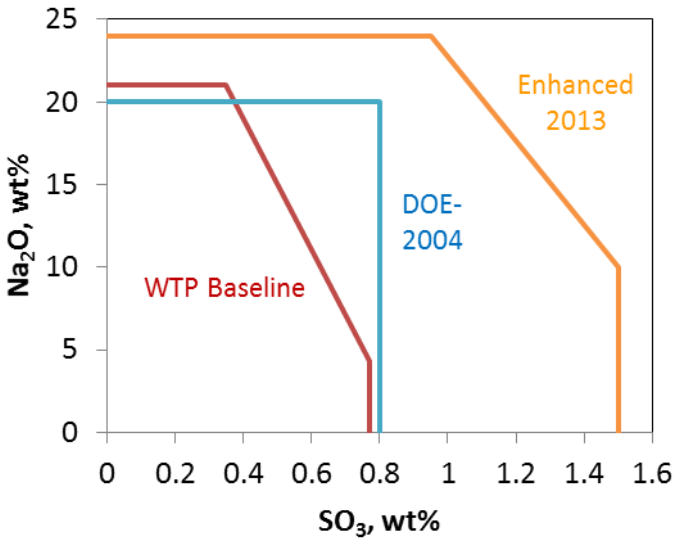

Figure 1.2. Comparison of Na_2O and SO_3 Concentrations in LAW Waste Loading Rules

Table 1.2. Attributes of LAW Models and Constraints Sets

Model/Constraint	WTP Baseline	DOE-2004	Enhanced 2013
Max Na_2O	21 wt%	20 wt%	--
Max Na_2O+0.66 K_2O	21.5 wt%	--	24 wt%
Max SO_3	0.7 wt%	0.8 wt%	1.5 wt%
Na_2O and SO_3 Line	$Na_2O \leq 35.875\text{-}42.5SO_3$	--	$Na_2O+0.66K_2O \leq 33.94\text{-}11.69SO_3$
Additional constraints	Cl and F vs SO_3, Cr_2O_3 vs P_2O_5 and K_2O	--	Cl and F vs SO_3, Cl, F, and Cr_2O_3 vs SO_3
Life-Cycle Glass*	797,829 MT	647,822 MT	482,723 MT

* Glass mass estimates described in Kim (2013)

In addition to the loading limits for LAW glass, a series of property constraints must be met that determine the overall glass composition and in some cases may reduce the overall waste loading in glass (see Kim and Vienna 2012 for example). These properties include:

- Constraints on viscosity (η) at the processing temperature to ensure sufficient processing rate and flow of glass while minimizing corrosion of melter construction materials.
- Constraints on electrical conductivity (ε) at the processing temperature to ensure sufficient energy can be supplied by the power source without exceeding current density limits of the power system.
- PCT response limits for waste form acceptance dictated by the WTP contract (DOE 2000).
- VHT response limits for waste form acceptance dictated by the WTP contract (DOE 2000).
- Salt accumulation constraints to avoid excessive corrosion of melter construction materials and increase radionuclide volatility.
- Model validity or data availability constraints to maintain glass compositions within the ranges over which the predictive models and formulation approaches are valid.

In the case of the WTP Baseline approach, glasses are formulated by first determining the waste loading based on rules described above (Table 1.2), then the concentrations of glass-forming chemicals are obtained by interpolating between successful glasses that span the range of loadings (Muller et al. 2004). The properties with associated uncertainties are evaluated. If any property exceeds its associated limit, the composition is adjusted until all property constraints are met as described by Kim and Vienna (2012). In the case of the DOE-2004 and Enhanced 2013 models and constraints, the glass composition is determined by optimizing the additive concentrations to simultaneously meet the loading limits and all property constraints. A current effort is in progress to develop a method of interpolating between successful high loading formulations (e.g., Muller et al. 2015a). However, at the time of this report, those methods are not yet ready for use.

Additional effort for the results in this report focused on evaluating and updating the most influential constraints and property models. In addition several lessons were learned by the implementation and informal validation of the 2013 Enhanced models and constraints. The previous approach of using a neural network model for the VHT response was both impractical and not as predictive as previously applied model approaches. Combined LAW and HLW sulfur solubility modeling was found to perform worse than individual LAW and HLW glass sulfur solubility models. Confusion was caused by reporting two different approaches to limiting halides in the Enhanced 2013 model report. Modeling approaches were changed in the current study to address these lessons learned.

1.3 A Note on Significant Figures

Throughout this document, model coefficients and other values are reported with a higher number of figures than may be significant. Also, not all model coefficients were reported to the same number of significant figures in software output. Ideally, the appropriate number of figures to report should be evaluated in detail so that the predicted property values are accurate to the same number of figures to which as the property is typically measured. However, no such evaluations were performed. We therefore suggest using all reported figures in the model coefficients for consistency with example calculations supplied in this report.

1.4 Assessing Model Goodness of Fit

Sections 2.0 and 3.0 present models for various properties of enhanced HLW and LAW glasses, respectively. For each glass property with quantitative values, several numerical statistics and a graphical method are used to assess how well the model performs for (i) the data used to fit the models, and (ii) validation data not used to fit the model.

In some cases there were no separate validation data because all appropriate data within the desired HLW or LAW glass composition region were used in model fitting. In such cases, a data-splitting approach was used. With this approach, the modeling dataset was split into five subsets (referred to as "groups"). The groups were selected by ordering the property values in the modeling dataset from smallest to largest, and numbering them 1, 2, 3, 4, 5, 1, 2, …, etc. Each number represents a representative group of approximately 20% of the data, which roughly span the same range of property values. Then, each group was used as a validation data set, with the model being fit to the remaining four groups of data.

The model goodness of fit was summarized using the coefficient of determination (R^2), which describes the fraction of the variation in the data that is accounted for by the model. Three other variations of the R^2 statistics were also used: (i) R^2 adjusted for the number of coefficients used to fit the model (R^2_{Adj}), (ii) R^2 in which each data point is "left out of the fit" in evaluating how well the model predicts the property for each data point (R^2_{Pred}), and (iii) R^2 calculated from data used to validate the model that was not used in model fitting (R^2_{Val}). The R^2_{Pred} statistic estimates the fraction of variability that would be explained in predicting new observations drawn from the same composition space. Generally $0 < R^2_{Pred} < R^2_{Adj} < R^2 < 1$. However, it is possible for very poor fitting models or models with very influential points that R^2_{Pred} or R^2_{Val} can be negative.

Another statistic used to assess model goodness of fit that is reported in Sections 2.0 and 3.0 is the root mean square error (RMSE). It is the square root of the mean squared difference between predicted and measured response values. The RMSE is an estimate of the experimental plus measurement standard deviation if the model does not have a statistically significant lack-of-fit. The formulas and additional discussion of RMSE and the various R^2 statistics are given in Appendix A.

Finally, *predicted vs. measured plots* were also used to assess model performance. Such a plot has the predicted property values (or their natural logarithm for some models) of the modeling dataset on the y-axis, and the measured property values (or their natural logarithms) on the x-axis. The plot also contains a 45º line corresponding to predicted values equaling measured values. Groups of points that tend to be above (below) the 45º line for certain ranges of measured property values correspond to the model overpredicting (underpredicting) the property in that range of values. The scatter of points around the 45º line roughly indicates the precision of model predictions. Finally, some of the predicted vs. measured plots contain 90% or 95% prediction intervals (PI)[1], which correspond to the uncertainty in model predictions for single new data points. Not all of the predicted vs. measured plots have PIs included

[1] PIs with 90% confidence were used for processing properties, while PIs with 95% confidence were used for properties with repository acceptance constraints.

because different technical staff using different software developed various property models and predicted vs. measured plots.

2.0 HLW Glass Models and Constraints

Section 2.0 describes the models to be used in estimating HLW glass properties including: nepheline limits (Section 2.1), spinel limits (Section 2.2), sulfur tolerance (Section 2.3), eskolaite limits (Section 2.4), viscosity (Section 2.5), PCT response (Section 2.6), zirconium-containing phases (Section 2.7), and phosphate limits (Section 2.8). The proposed HLW glass formulation approach is given in Section 2.9 followed by example calculations in Section 2.10.

2.1 Nepheline Limit

High-alumina waste glasses are prone to nepheline precipitation during canister centerline cooling (CCC). If sufficient nepheline forms, the chemical durability of the glass can be significantly impacted. Overly conservative constraints have been developed and used to avoid the deleterious effects of nepheline formation in the WTP Baseline and HTWOS 2009 constraint sets (Li et al. 1997, Vienna and Kim 2014, Vienna et al. 2009). The constraints used have been shown to significantly limit the loading of waste in glass at Hanford and therefore the cost and schedule of cleanup. The Enhanced 2013 model report recommended the use of a neural network (NN) model to constrain the composition and avoid nepheline formation on CCC. That model was difficult to implement, was extremely challenging to quantify uncertainties and ultimately did not validate well with a new dataset that was not used to develop the model (see Vienna 2016 for further discussion). Since the 2013 models report, a new 90-glass study was performed to develop an improved understanding of the impacts of glass composition on the formation of nepheline during CCC. The CCC crystallinity data from these glasses were combined with 657 glasses found in the literature (Vienna et al. 2013).

Vienna et al. (2016) proposed a ternary submixture (SM) model to identify the glass composition region prone to nepheline precipitation. The details of this model are given in Vienna et al. (2016) but are summarized here for completeness, because a new model described subsequently uses aspects of the Vienna et al. (2016) model.

The ternary submixture model of Li et al. (1997) was extended to include the effects of other component concentrations (B_2O_3, CaO, Fe_2O_3, K_2O, Li_2O, MgO, and P_2O_5) that have either been measured or hypothesized to effect nepheline formation in HLW glasses. Ultimately, a submixture ternary with axes of $SiO_2 + 1.98B_2O_3$, $Na_2O + 0.653Li_2O + 0.158CaO$, and Al_2O_3 was found to divide glasses that precipitate nepheline during CCC from those that do not as shown in Figure 2.1.

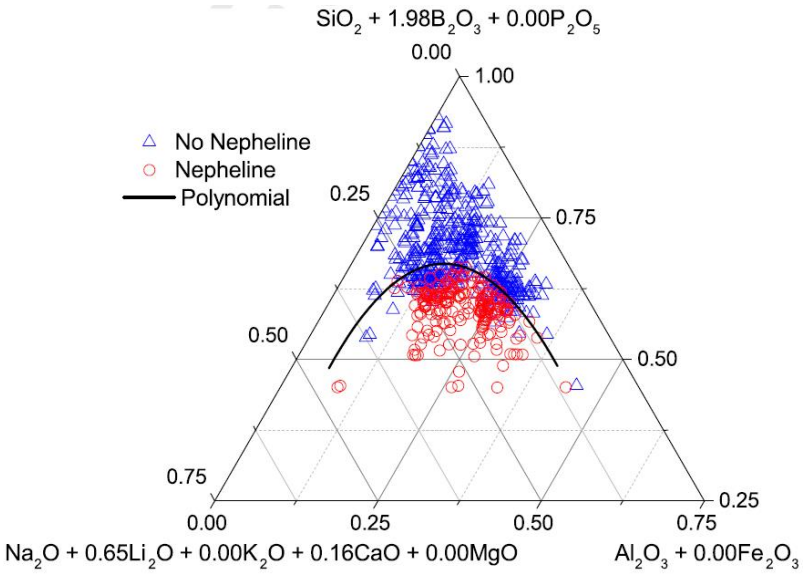

Figure 2.1. Submixture Ternary Diagram with Conservative Polynomial Line Fit to Discriminate HLW Glasses that Form Nepheline after Canister Centerline Cooling (from Vienna et al. 2016)

In this work, the SM model was extended using logistic regression (LR) as described in the following subsections. Section 2.1.1 describes the dataset used to develop the new LR model. Section 2.1.2 presents the structure of the polynomial discriminating curve (PDC) version of the SM discussed by Vienna et al. (2016) using formats that can be extended to statistical analyses and generalized fitting methods. Section 2.1.3 discusses the form of a modified SM developed using LR, referred to as a LR-SM. Section 2.1.4 presents the results from fitting the LR-SM to experimental data. Sections 2.1.5 and 2.1.6 discuss the method and application of bootstrapping to estimate prediction uncertainties of the LR-SM model. Section 2.1.7 compares the LR-SM and PDC-SM methods and Section 2.1.8 recommends the method to be used in formulation efforts.

2.1.1 Description of Data on Nepheline Formation after Canister Centerline Cooling

A large and growing dataset of simulated HLW glasses has been previously reported for the study of crystal formation on CCC (Vienna et al. 2013). Table 2.1 and Table 2.2 summarize 657 existing waste glasses with CCC heat treatment crystallinity data from the literature plus the 90 new compositions (last two rows in Table 2.1). Figure 2.2 shows a pairwise scatterplot matrix of the major component concentrations in these glasses. It is clear from the figure that three glasses significantly extended the range of P_2O_5 (0.036 to 0.09 mass fraction), one glass significantly extended the range of Li_2O (0.081 to 0.126 mass fraction) and one glass significantly increases the range of MgO (0.08 to 0.12 mass fraction). These five glasses were originally excluded from any model fitting, however, their inclusion or exclusion was found not to impact model parameters or goodness of fit and ultimately they were included in the final dataset.

It is worth noting that glasses designed for a number of different waste streams, processing plants, and using different CCC heat treatments were included in this dataset. It is anticipated that using such a diverse dataset in modeling will likely increase the model prediction uncertainty. The data and models are

not fully QA compliant and therefore are not intended to be used in quality-affecting activities or decisions (e.g., design basis input, plant operations, waste form compliance). Instead the models and constraints are intended for use in mission planning activities.

Table 2.1. Summary of Data for HLW Glasses Used in Developing and Evaluating Models for Nepheline Formation after Canister Centerline Cooling[(a)]

Glass Family	#	Lab	Heat Treatment	Citation
IWL	17	PNNL	WTP CCC	Kim et al. 2011
A	6	PNNL	WTP CCC	Hrma et al. 2010, Rodriguez et al. 2011
PNNL-Al-24-X	13	PNNL	WTP CCC	Rodriguez et al. 2011
HLW-E-ANa-X	24	PNNL	WTP CCC	Rodriguez et al. 2011
HAL	19	PNNL/SRNL	WTP CCC	Rodriguez et al. 2011, Kim et al. 2008
EM07/09	47	PNNL	WTP CCC	Schweiger et al. 2011
EM09-Li	10	PNNL	WTP CCC	Rodriguez et al. 2011
HLW-E-Al	14	VSL	WTP CCC	Rodriguez et al. 2011, Matlack et al. 2007
HLW-E-ANa	13	VSL/PNNL	WTP CCC	Rodriguez et al. 2011, Matlack et al. 2007
HWI-Al	23	VSL	WTP CCC	Rodriguez et al. 2011, Matlack et al. 2008 and 2010a
HWI-ALS	13	VSL	DWPF CCC	Matlack et al. 2010b
NP	20	PNNL	WTP CCC	Li et al. 1997
CVS1, CVS2	121	PNNL	HWVP CCC	Hrma et al. 1994
CVS3	39	PNNL	HTM CCC	Vienna et al. 1996
ICCM	15	SRNL	DWPF CCC	Peeler et al. 2002
SB4NEPH	12	SRNL	DWPF CCC	Rodriguez et al. 2011, Peeler et al. 2005
NEPH2	28	SRNL	DWPF CCC	Rodriguez et al. 2011, Peeler et al. 2006
NEPH3	16	SRNL	DWPF CCC	Rodriguez et al. 2011, Fox et al. 2006
NP2	25	SRNL	DWPF CCC	Rodriguez et al. 2011, Fox et al. 2008
NE3	29	SRNL	DWPF CCC	Rodriguez et al. 2011, Fox et al. 2009
EM	30	SRNL	DWPF CCC	Johnson and Edwards 2009
SRNL-JB	18	SRNL	DWPF CCC	Boerstler and Amoroso 2011
SRNL-JB02	20	SRNL	DWPF CCC	Boerstler and Amoroso 2011
SB5NEPH	40	SRNL	DWPF CCC	Fox et al. 2007
US	45	PNNL/SRNL	DWPF CCC	Fox et al. 2008
Ph1-3	45	PNNL	WTP CCC	Kroll et al. 2016
Ph4 (EWG)	45	PNNL	WTP CCC	Chou et al. 2016

(a) PNNL – Pacific Northwest National Laboratory, VSL – The Catholic University of America, SRNL - Savannah River National Laboratory, DWPF - Defense Waste Processing Facility, HWVP - Hanford Waste Vitrification Plant, HTM – High Temperature Melter.

Table 2.2. Component Ranges (mass fractions) of 747 HLW Glasses with Data on Nepheline Formation after Canister Centerline Cooling. These ranges specify the model validity region.

Component	Min	Max
Al_2O_3	0	0.3900
B_2O_3	0	0.2660
Bi_2O_3	0	0.1640
CaO	0	0.1820
CdO	0	0.0134
Cr_2O_3	0	0.0297
F	0	0.0250
Fe_2O_3	0	0.2000
K_2O	0	0.0614
La_2O_3	0	0.0155
Li_2O	0	0.1255[(a)]
MgO	0	0.1201[(a)]
MnO	0	0.0609
Na_2O	0.0200	0.3900
Nd_2O_3	0	0.0855
NiO	0	0.0291
P_2O_5	0	0.0900*
SiO_2	0.1740	0.6000
SrO	0	0.1008
TiO_2	0	0.0212
UO_3	0	0.1568
ZnO	0	0.0200
ZrO_2	0	0.1600

(a) If the five extreme glass compositions were excluded, the resulting maximum concentrations of Li_2O, MgO, and P_2O_5 would be 0.081, 0.08, and 0.036 mass fractions, respectively.

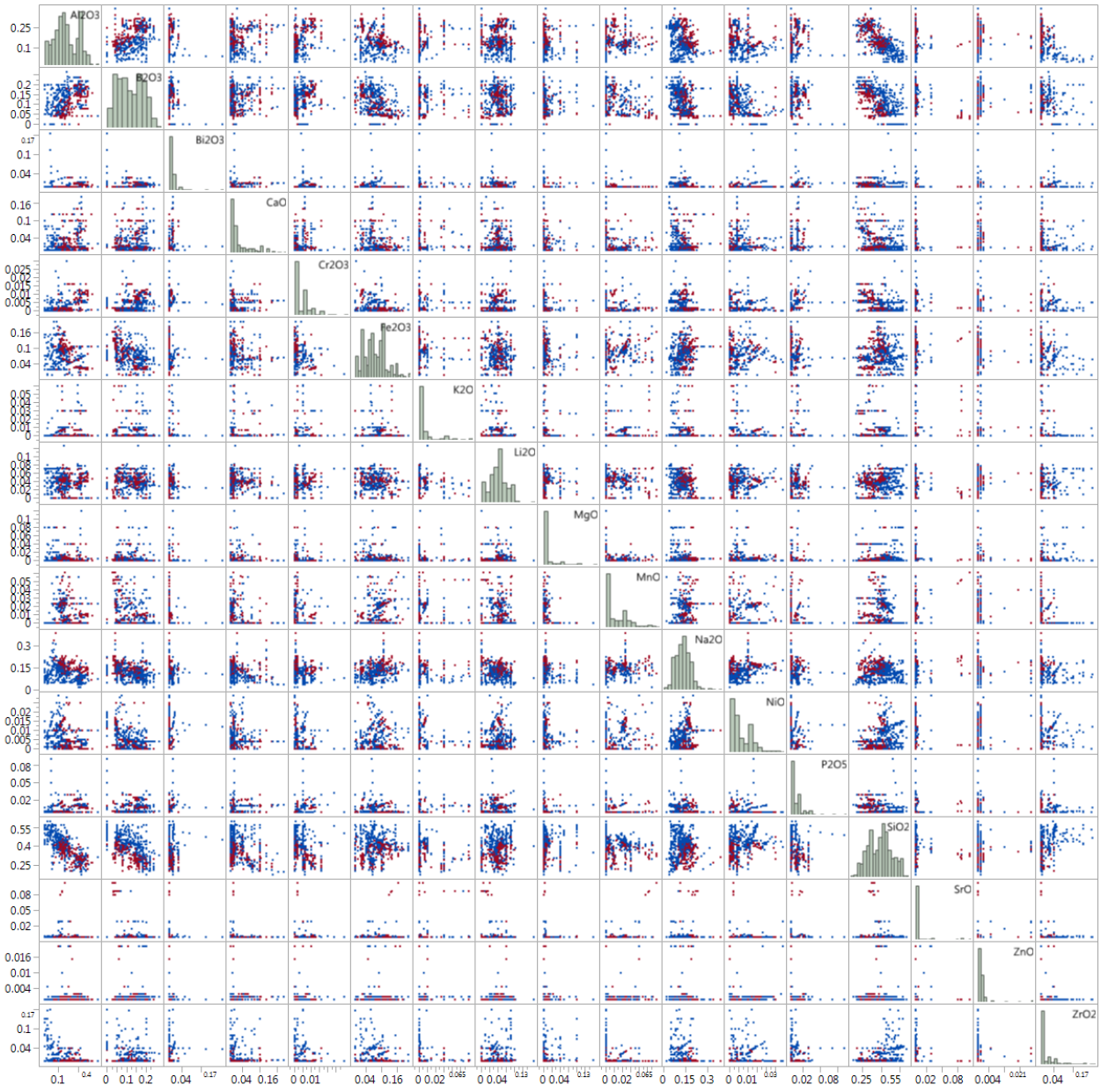

Figure 2.2. Scatterplot Matrix of 747 HLW Glasses Used to Model Nepheline Formation After Canister Centerline Cooling. Component concentrations are shown in mass fractions. Red points precipitated nepheline, while blue points did not.

2.1.2 Structure of the Polynomial Discriminating Curve-Submixture Model

In the PDC-SM approach of Vienna et al. (2016), multicomponent HLW glasses were projected onto a submixture ternary. Then, a polynomial curve was fitted to experimental data to partition the submixture ternary into two regions in which nepheline is predicted to form or not form after CCC. The submixture ternary had three submixture components expressed as linear combinations of glass oxide components. The first submixture component includes alkali and alkaline earth oxides, and is given by

$$g_{Alk} = g_{Na_2O} + \alpha_1 g_{Li_2O} + \alpha_2 g_{K_2O} + \alpha_3 g_{CaO} + \alpha_4 g_{MgO} \quad (2.1)$$

The second submixture component includes Al_2O_3 and Fe_2O_3

$$g_{AlFe} = g_{Al_2O_3} + a_5 g_{Fe_2O_3}, \quad (2.2)$$

while the final submixture component includes SiO_2, B_2O_3, and P_2O_5

$$g_{SiB} = g_{SiO_2} + a_6 g_{B_2O_3} + a_7 g_{P_2O_5}. \quad (2.3)$$

For each submixture component, g_i represents the mass fraction of the i^{th} HLW glass component and $\alpha_1, \ldots, \alpha_7$ are coefficients to be estimated using experimental data. Each of the α_j coefficients is assumed to be non-negative (i.e., $\alpha_j \geq 0$) for $j = 1, \ldots, 7$. In order to form a submixture ternary, the submixture components g_{Alk}, g_{AlFe}, and g_{SiB} must be rescaled to sum to one

$$g_i^* = \frac{g_i}{g_{Alk} + g_{AlFe} + g_{SiB}}, \; i = Alk, AlFe, and SiB \quad (2.4)$$

where g_{Alk}, g_{AlFe}, and g_{SiB} are defined in Equations (2.1), (2.2) and (2.3), respectively. The asterisk on g_i^* g_i^* denotes rescaled mass fractions of the three submixture components. Note that there is no coefficient for the mass fraction of the first oxide in each of the three submixture components (namely Na_2O, Al_2O_3, and SiO_2), because the sum-to-one constraint

$$g_{Alk}^* + g_{AlFe}^* + g_{SiB}^* = 1 \quad (2.5)$$

would otherwise make the coefficients non-identifiable.

Vienna et al. (2016) transformed the three rescaled submixture components (which are mathematically dependent because of Equation (2.5)) to two Cartesian-coordinate variables denoted *X* and *Y* (which are mathematically independent) to enable formation of a ternary plot in Excel. The formulas for *X* and *Y* are

$$X = g_{AlFe}^* + \frac{1}{2} g_{SiB}^* \text{ and } Y = \frac{\sqrt{3}}{2} g_{SiB}^* \; . \quad (2.6)$$

The form of the PDC-SM model developed by Vienna et al. (2016) was a quadratic polynomial model in *X* and a predicted value for *Y*, denoted $\hat{Y}$, given by

$$\hat{Y} = a + bX + cX^2 \quad (2.7)$$

where *a*, *b*, and *c* are coefficients to be estimated by fitting the model to data. This model is the equation of a PDC so that HLW glass compositions with (*X*, *Y*) points on or above the curve in Equation (2.7) are

predicted not to form nepheline after CCC, while HLW glass compositions with (*X*, *Y*) points below the curve are predicted to form nepheline after CCC.

The difference between the observed and predicted values for *Y* is given by

$$Y - \hat{Y} = -\frac{(b-\sqrt{3})g^*_{SiB} + 2b\, g^*_{AlFe}}{2} - \frac{c\,(2g^*_{AlFe} + g^*_{SiB})^2}{4} - a, \tag{2.8}$$

where *a*, *b*, and *c* are the coefficients from Equation (2.7). Vienna et al. (2016) estimated the 10 PDC-SM coefficients ($\alpha_1, \ldots, \alpha_7$, *a*, *b*, *c*) by minimizing the sum of squared $Y - \hat{Y}$ values that correspond only to misclassified data points. Note that the difference defined in Equation (2.8) is equivalent to the distance denoted *P* in Equation (3) of Vienna et al. (2016).

2.1.3 Nepheline Model Form and Fitting Methodology

The LR-SM discussed in this section is based on the same submixture and ternary ideas as the PDC-SM, but there are some key differences. The PDC-SM approach uses a PDC to predict whether or not nepheline will form after CCC. The LR-SM approach uses logistic regression to predict the probability that nepheline will form after CCC. Then, different threshold values for the probability of nepheline formation can then be used to predict whether or not nepheline will form after CCC of a given HLW glass. Another difference between the LR-SM and the PDC-SM is the way in which the model coefficients are estimated. For the LR-SM, the model coefficients are estimated by maximizing the Bernoulli likelihood

$$\prod_{i=1}^{n} p_i^{z_i} (1-p)^{1-z_i}\ , \tag{2.9}$$

where z_i = 1 (0) if nepheline is present (absent) after CCC of the i^{th} HLW glass and p_i is the probability that nepheline forms after CCC of the i^{th} HLW glass composition. The rescaled submixture ternary compositions (g^*_{Alk}, g^*_{AlFe}, g^*_{SiB}) are first mapped onto a two-dimensional coordinate system represented by (*X*, *Y*) pairs. Then the (*X*, *Y*) pairs are connected to the probability of nepheline formation p_i through the logit transformation

$$\ln\left(\frac{p_i}{1-p_i}\right) = \beta_0 + \beta_1 X_i + \beta_2 Y_i + \beta_3 X_i^2\,, \tag{2.10}$$

where X_i and Y_i are defined in Equation (2.6) and "ln" denotes the natural logarithm. In addition to this model, the following model with two additional terms was investigated:

$$\ln\left(\frac{p_i}{1-p_i}\right) = \beta_0 + \beta_1 X_i + \beta_2 Y_i + \beta_3 X_i^2 + \beta_4 Y_i^2 + \beta_5 X_i Y_i\,. \tag{2.11}$$

However, the additional model terms did not improve the predictive accuracy of the LR-SM in Equation (2.10). It is interesting to note that the model in Equation (2.11) is equivalent to the model

$$\ln\left(\frac{p_i}{1-p_i}\right) = \gamma_1 g^*_{Alk} + \gamma_2 g^*_{AlFe} + \gamma_3 g^*_{SiB} + \gamma_{12} g^*_{Alk} g^*_{AlFe} + \gamma_{13} g^*_{Alk} g^*_{SiB} + \gamma_{23} g^*_{AlFe} g^*_{SiB}, \quad (2.12)$$

which for convenience does not include the "*i*" subscripts on the right-hand side. Note Equation (2.12) has a Scheffé full quadratic mixture experiment model (Cornell 2002) on the right-hand side. The LR-SM in Equation (2.10) is equivalent to a specific reduced form of the model in Equation (2.12). However, this topic is not discussed further because the LR-SM model of the form in Equation (2.10) was used.

Finally, note that the form of the model described by Equation (2.10) directly parallels the parabola approach described in Vienna et al. (2016). In particular, Equation (2.10) can be rewritten in a form similar to Equation (2.7) as follows

$$Y = \frac{\ln\left(\frac{p_i}{1-p_i}\right) - \beta_0}{\beta_2} + \frac{-\beta_1}{\beta_2} X + \frac{-\beta_3}{\beta_2} X^2. \quad (2.13)$$

Note that the first term on the right-hand side of Equation (2.13) is not a constant that is the same for all HLW glasses in the dataset as is the coefficient *a* in Equation (2.7). Specifically, the first term in Equation (2.10) depends on the probability of nepheline formation for each HLW glass, which will not be constant across the dataset used to fit the model.

A final key difference is that the LR-SM approach uses all data points to fit the model, whereas the PDC-SM approach uses only the data points that misclassify nepheline formation to fit the model. Hence, the PDC-SM approach gives weights of zero to glasses for which nepheline formation is correctly classified. On the other hand, the LR-SM approach uses all data points (with equal weights) and is then able to predict the probability of nepheline formation for any HLW glass composition (whether used to fit the model or not).

The seven coefficients $(\alpha_1, \ldots, \alpha_7)$ of the scaled submixture components and the four regression coefficients (b_0, b_1, b_2, b_3) in the LR-SM were estimated using the limited memory-Broyden-Fletcher-Goldfarb-Shanno (L-BFGS) algorithm implemented in the "stan" software (Stan Development Team 2015, Chapter 7.2 of Nocedal and Wright 2006). The coefficients $a_1, \ldots, a_7$ were restricted to be non-negative, as described in Section 2.1.1. A dataset of 747 HLW glass compositions and results on whether or not nepheline formed after CCC (see Vienna et al. 2016) were used to estimate the model coefficients.

The LR-SM in Equation (2.10) predicts the natural logarithm of the odds ratio (the probability that nepheline forms divided by the probability that nepheline does not form) for a given (i.e., i^{th}) HLW glass. The probability of nepheline forming after CCC of a given HLW glass can be calculated for that glass using

$$p = \frac{\exp[\beta_0 + \beta_1 X + \beta_2 Y + \beta_3 X^2]}{1 + \exp[\beta_0 + \beta_1 X + \beta_2 Y + \beta_3 X^2]}, \quad (2.14)$$

where "exp" is the exponential function, X and Y are defined in Equation (2.6), and the g_i^* in the equations for X and Y are defined in Equation (2.4). To use the LR-SM to predict whether or not nepheline will form after CCC, a threshold value of p_i must be chosen. Typically a threshold value of p_i = 0.5 is used, but another value can be specified to strike a desirable balance between two types of misclassifications: false positive (FP) and false negative (FN). In this context, a FN (predicting nepheline will not form when in reality it does) is considered worse than a FP. Therefore, the threshold value for p_i was chosen by a post-hoc analysis to achieve a desirable balance between the two misclassification types achieved with different threshold values.

The L-BFGS optimization method produces maximum likelihood estimates for the 11 coefficients as well as estimates of the coefficient uncertainties, but the non-negativity constraints placed on the a_j coefficients violate the assumptions necessary for such estimates of uncertainty to be reliable. We therefore used a standard nonparametric bootstrap (Chapter 6 of Efron and Tibshirani 1994) to estimate uncertainties in the 11 coefficient estimates. In short, the entire dataset was sampled with replacement to generate a bootstrap sample that was the same size as the original dataset (747 data points). The 11 coefficients were re-estimated using the resampled data exactly as was done for the original data. Note that this process results in different estimates of the a_j coefficients, and hence a different rescaling, for each bootstrap sample of 747 data points. This bootstrap sampling and model fitting process was repeated 2000 times to produce a distribution of possible estimates for each of the 11 coefficients. The resulting standard deviation of each coefficient's distribution is an estimate of the uncertainty in the estimate of each coefficient.

2.1.4 Results of Fitting the Logistic Regression-Submixture Model to Nepheline Formation Data

Coefficient estimates with bootstrap standard deviations for different variations of the LR-SM approach are reported in Table 2.3 along with the number of FN and FP misclassifications in the full dataset as well as in the subset of glasses from nepheline study Phases 1-4 (P1-4) when the threshold for p_i in Equation (2.10) is set to 0.47. The threshold value 0.47 was chosen after computing the FN and FP misclassification rates for various thresholds and selecting the threshold that resulted in the lowest possible FN rate while maintaining a moderate FP rate (Figure 2.3). The four different variations of the LR-SM approach are differentiated by the inclusion or exclusion of P_2O_5 and/or K_2O. In addition to Al_2O_3, Na_2O_3, and SiO_2 (which did not have coefficients to estimate, as discussed in Section 2.1.2), only the components included in Table 2.3 were found to be important in predicting nepheline formation of HLW glasses after CCC. Specifically, Fe_2O_3 and MgO were removed from all variations of the model because their estimated coefficients were statistically indistinguishable from zero. The same two components were found to be insignificant in the PDC-SM approach of Vienna et al. (2016).

The four model variations shown in Table 2.3 result in similar misclassification (FN and FP) rates for the full dataset. This can be visualized by the nearly indistinguishable lines in Figure 2.3, which plots FN versus FP rates for different threshold values of p_i. For the Phases 1 through 4 set of glasses, the FN and FP misclassification percentages in Table 2.3 are also similar for the four model variations. Comparing the misclassification percentages for the full and P1-4 dataset, the percentages of FNs are similar, but the percentages of FPs are higher for the P1-4 dataset than for the full dataset. A likely explanation for this observation is because the P1-4 dataset covered a smaller composition region than the full dataset, which would increase the chances of FPs in the P1-4 dataset.

Table 2.3. Estimated Coefficients and Standard Deviations for Nepheline Formation in HLW Glasses Along with Misclassification Counts for the Logistic Regression-Submixture Models with and without P_2O_5 and/or K_2O in the Submixtures Using a p_i = 0.47 Threshold

P_2O_5 and K_2O Status		P_2O_5, K_2O		No P_2O_5		No K_2O		No P_2O_5, K_2O	
Estimated Coefficients and Standard Deviations									
Coeff.	Comp.[a]	Estimate	SD[b]	Estimate	SD[b]	Estimate	SD[b]	Estimate	SD[b]
α_1	Li_2O	0.7808	0.1524	0.8012	0.1560	0.7870	0.1544	0.8040	0.1556
α_2	K_2O	0.2045	0.1423	0.1827	0.1415	–	–	–	–
α_3	CaO	0.2835	0.0549	0.2896	0.0592	0.2889	0.0538	0.2940	0.0547
α_6	B_2O_3	1.6782	0.1106	1.7307	0.1136	1.6863	0.1111	1.7317	0.1151
α_7	P_2O_5	0.8333	0.5975	–	–	0.7414	0.5623	–	–
β_0	–	-66.414	15.159	-65.527	15.089	-64.684	14.487	-64.085	14.430
β_1	–	516.178	77.780	508.658	76.481	503.731	73.141	498.338	72.013
β_2	–	-106.016	11.347	-103.900	10.937	-103.860	10.958	-102.179	10.497
β_3	–	-540.637	79.825	-533.755	78.626	-527.064	74.830	-522.382	73.812
Misclassification Counts (Percentages) with p_i = 0.47 Threshold									
FN[c]		29/212 (13.7%)		28/212 (13.2%)		31/212 (14.6%)		30/212 (14.2%)	
FP[d]		29/535 (5.4%)		31/535 (5.8%)		28/535 (5.2%)		29/535 (5.4%)	
FN P1-4[e]		4/38 (10.5%)		4/38 (10.5%)		5/38 (13.2%)		5/38 (13.2%)	
FP P1-4[f]		7/52 (13.5%)		9/52 (17.3%)		6/52 (11.5%)		7/52 (13.5%)	

(a) In addition to the components listed in this column, Al_2O_3, Na_2O, and SiO_2 also appear in the LR-SMs with coefficients of one.

(b) Standard deviation estimates are based on a bootstrap sample size of 2000.

(c) FN = false negative, where xx/yyy means there were yyy positives in the full dataset with xx of them being falsely predicted by a model as negatives.

(d) FP = false positive, where xx/yyy means there were yyy negatives in the full dataset with xx of them being falsely predicted by a model as positives.

(e) FN P1-4 = false negative, where xx/yy means there were yy positives in the P1-4 dataset with xx of them being falsely predicted by a model as negatives.

(f) FP P1-4 = false positive, where xx/yy means there were yy negatives in the P1-4 dataset with xx of them being falsely predicted by a model as positives.

Because the coefficients of P_2O_5 and K_2O did not appear to be significantly different from zero and the predictive accuracy of the four models did not differ significantly, the LR-SM model with P_2O_5 and K_2O removed (last column of Table 2.3) was chosen. The classification results using this LR-SM with three different threshold values for p_i (0.10, 0.47, and 0.90) are illustrated in Figure 2.4.

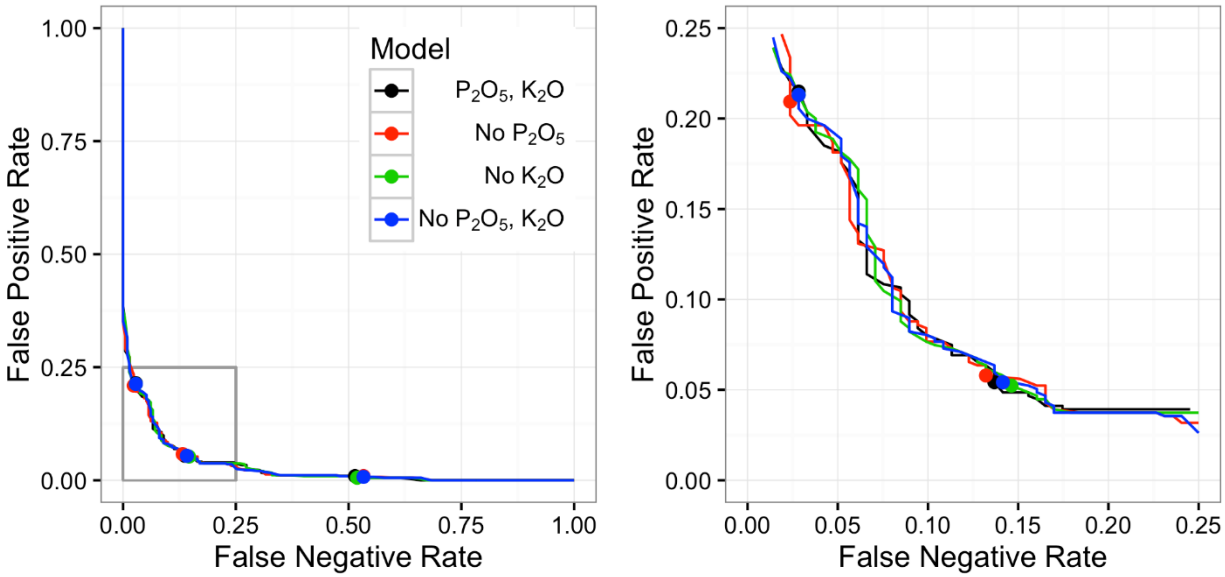

Figure 2.3. Plot of the False Negative and False Positive Misclassification Rates for the Full Dataset Using the Four Logistic Regression-Submixture Models (Table 2.3) for Nepheline Formation After Canister Centerline Cooling of HLW Glasses. The plotted points depict the FN and FP misclassification rates for threshold values of 0.1, 0.47 and 0.9 (from left to right). The figure on the right is a detailed view of the area outlined in gray in the figure on the left.

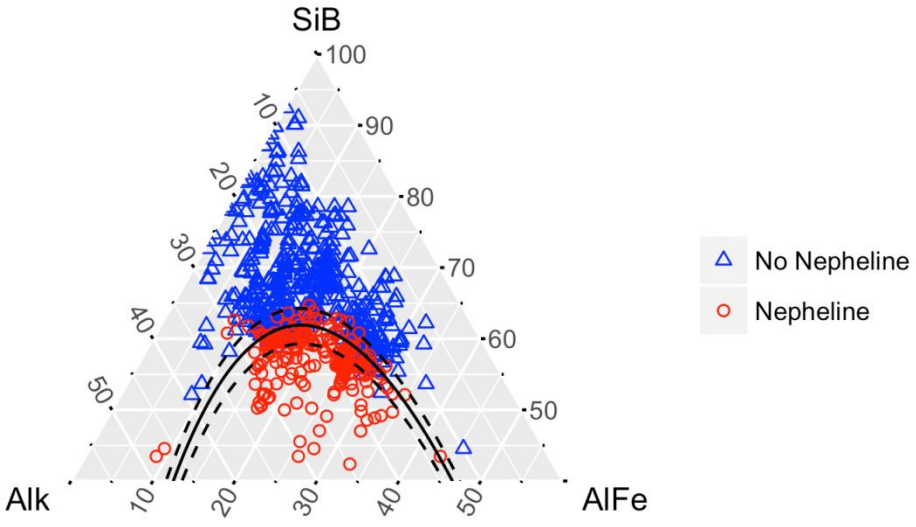

Figure 2.4. Plot of the Submixture Ternary and Discriminating Curves Corresponding to Predicted Probabilities of Nepheline Formation Equal to 0.10, 0.47, and 0.90 (from top to bottom) Using the Logistic Regression-Submixture Model in the Last Column of Table 2.3

The plotting symbols in Figure 2.4 are red circles for HLW glass compositions that formed nepheline after CCC, and blue triangles for glass compositions that did not form nepheline after CCC. The solid black line represents the discriminating curve obtained using the p_i = 0.47 threshold, which produces the misclassification rates reported in the last column of Table 2.3. Glass compositions below the solid black line have predicted probabilities of nepheline formation greater than 0.47, while glass formulations above the solid line have predicted probabilities of nepheline formation less than 0.47. Similarly, the top and bottom dashed black lines correspond to predicted 0.10 and 0.90 probabilities of nepheline formation, respectively. For example, points below the lower dashed black line have predicted probabilities of nepheline formation greater than 0.90. As a final example, points above the upper dashed black line have probabilities of nepheline formation less than 0.10. Hence, using p_i = 0.10 as a threshold would reduce the number of FNs (red circles above the top, dashed black line) compared to the number of FNs (red circles above the solid black line) when using p_i = 0.47 as a threshold. However, using p_i = 0.10 instead of p_i = 0.47 as the threshold would also increase the number of FPs (blue triangles below the top, dashed black line and the solid black line, respectively).

2.1.5 A Nonparametric Tolerance Limit Approach that Accounts for the Uncertainties in the LR-SM Model in Classifying Whether an HLW Glass Composition Forms Nepheline after Canister Centerline Cooling

Figure 2.4 does not take into account the uncertainties associated with the LR-SM in the last column of Table 2.3. Specifically, Figure 2.4 does not take into account the uncertainties of the submixture ternary coefficient (i.e., $\alpha_1, \ldots, \alpha_7$) estimates nor the uncertainties of the LR coefficient (i.e., $\beta_0, \ldots, \beta_3$) estimates. Hence, the uncertainties in the coefficients estimated using the nonparametric bootstrap are not reflected in Figure 2.4. The bootstrap procedure used to quantify coefficient uncertainty produced n = 2000 distinct scaled submixture ternaries and discriminating curves, which results in n = 2000 figures similar to Figure 2.4. The method chosen to account for these uncertainties in the LR-SM and classify whether a given HLW glass is predicted to form nepheline is described next. In what follows, a generic n is used to provide the flexibility for choosing the value chosen in implementing the approach.

To develop a nepheline classification method based on the LR-SM that accounts for the uncertainty in the predicted probability of nepheline formation for each glass, a nonparametric upper tolerance limit (UTL) approach (Beal 2012) was applied together with the bootstrap approach for quantifying uncertainties. In particular, the n vectors of model coefficient estimates from n nonparametric bootstrap samples can be used to produce n predicted probabilities of nepheline formation for each glass in the full dataset. Figure 2.5 illustrates the distribution of n = 2000 predicted probabilities of nepheline formation for three example glasses (Neph-NN-1-2, IWL-SLC20-1, and EWG-OL-03208) from the full dataset. Note that the n = 2000 vectors of model coefficient estimates can be applied to any arbitrary HLW glass composition within the composition validity region of the model to produce n = 2000 predicted probabilities of nepheline formation. Hence, a HLW glass need not be one of the ones in the model-development dataset.

A nonparametric U%/V% upper tolerance limit (U%/V% UTL) provides at least U% confidence that at least V% of the population of possible probabilities of nepheline formation for a given HLW glass are less than the UTL. Here "possible probabilities" refers to the probabilities of nepheline formation for a

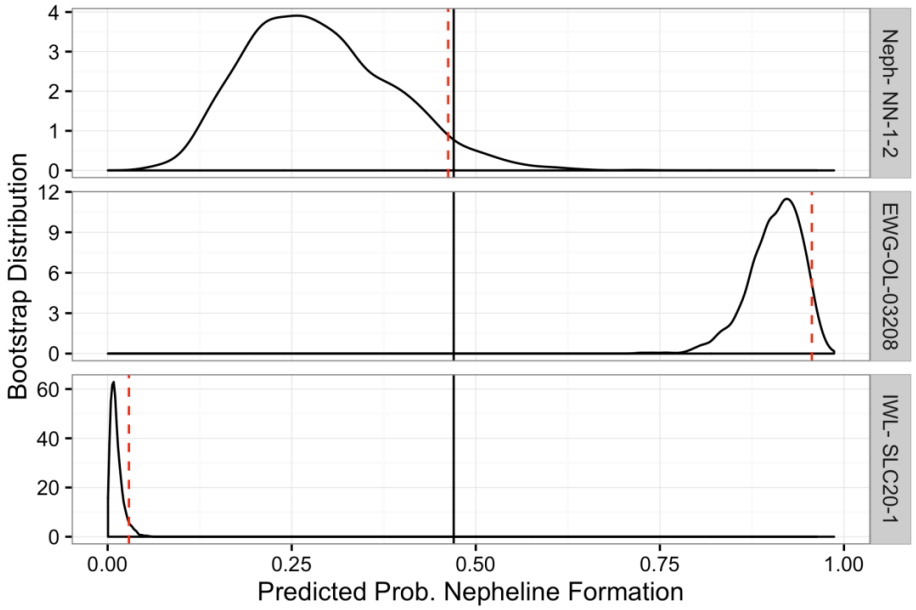

Figure 2.5. Illustration for Three Example Glasses of the Bootstrap Distribution of n = 2000 Predicted Probabilities of Nepheline Formation Using a Logistic Regression-Submixture Model of the Form Given in the Last Column of Table 2.3. For each glass, (i) the solid black vertical line represents a threshold of 0.47 for the predicted probability of nepheline formation, and (ii) the dashed red vertical line depicts the nonparametric 95%/95% UTL for the distribution of predicted probabilities of nepheline formation.

given HLW glass that could conceptually be obtained if the same size dataset on the same glasses were collected a large number of times and each time a LR-SM model was fitted to the resulting data. With this U%/V% UTL approach, instead of (i) a single predicted probability of nepheline formation from the fitted LR-SM being compared to the 0.47 threshold value to assess whether a given HLW glass will form nepheline after CCC, (ii) a U%/V% UTL is compared to the 0.47 threshold value. In this way the uncertainties in the estimated coefficients of the LR-SM are accounted for to conservatively assess whether a given HLW glass might form nepheline after CCC.

In this situation, a U%/V% UTL is obtained by first sorting the n predicted probabilities of nepheline formation for a given HLW glass from smallest to largest. Then the m^{th} largest value (referred to as the k^{th} order statistic, where $k = n - m + 1$) is calculated according to the following formula (Beal 2012). The k^{th} order statistic is then the U%/V% UTL. The value of k is the smallest integer value that satisfies

$$1-\frac{U}{100} \le \sum_{i=0}^{k} \left(\frac{n!}{i!\,(n\text{-}i)!}\right)\left(\frac{V}{100}\right)^{i}\left(1-\frac{V}{100}\right)^{n-i} \qquad (2.15)$$

where

k = value corresponding to the k^{th} order statistic of the predicted probabilities of nepheline formation for a given HLW glass

U = confidence in percent (e.g., 90, 95, or 99) desired for use in the U%/V% UTL statement

V = percentage of the population (e.g., 90, 95, or 99) of predicted probabilities of nepheline formation for a given HLW glass after CCC about which it is desired to make a U%/V% UTL statement

n = number of bootstrap samples.

Note that the formula in Equation (2.15) is based on the binomial distribution rather than the usual formula for nonparametric UTLs based on the incomplete beta function. This difference is because the literature notes that the incomplete beta function is overly conservative when $n(1-V/100)>5$. For n = 2000, this quantity takes values of 200 and 100 for V = 90 and 95, respectively. The quantity would be even larger for larger values of n. These values are very much greater than 5, so the use of Equation (2.15) is warranted. Further, Equation (2.15) provides the exact solution to this problem, whereas historical formulas and tables using the incomplete beta function are approximations.

Table 2.4 contains the values of k calculated using Equation (2.15) for common choices of U and V with values of n = 2000, 1000, 500, and 200. Table 2.4 shows that for n = 2000 the k values for the k^{th} order statistic correspond to slightly larger percentiles [i.e., 100(k/2000)] of the distribution than the nominal V values. The values are only slightly larger because of the large number of bootstrap samples (n = 2000) used. The percentiles corresponding to the k^{th} order statistics do not increase much when moving from n = 2000 to n = 1000 and 500. The increase is more noticeable for n = 200, but not substantial. Ultimately it was decided to use n = 2000 for calculating nonparametric U%/V% UTLs in order to reduce the noise inherent in the bootstrap procedure.

Table 2.4. Values of k for the k^{th} Order Statistic Out of n = 2000, 1000, 500, or 200 Bootstrap Samples for Selected Combinations of U and V to Use as the Nonparametric U%/V% Upper Tolerance Limit with the Logistic Regression-Submixture Model for Nepheline Formation in HLW Glasses

n	U[(a)]	V[(a)]	k	100(k/n)
2000	90	90	1817	90.85
	95	95	1916	95.80
	99	99	1990	99.50
1000	90	90	912	91.20
	95	95	961	96.10
	99	99	997	99.70
500	90	90	459	91.80
	95	95	483	96.60
	99	99	499	99.80
200	90	90	185	92.50
	95	95	195	97.50
	99	99	200	100.00

(a) It is not necessary that U = V, but doing so is common. The k values can be calculated for other combinations of U and V if desired.

2.1.6 Steps of the Logistic Regression-Submixture Model and Nonparametric Upper Tolerance Limit Approach for Predicting whether Nepheline May Form in an HLW Glass after Canister Centerline Cooling

This section provides the steps of the process for applying the proposed LR-SM plus nonparametric U%/V% UTL approach for predicting whether a given HLW glass will form nepheline after CCC.

Step 1: Using the glass composition of the given HLW glass in mass fractions, calculate g_{Alk}, g_{AlFe}, and g_{SiB} using Equations (2.1) to (2.3), with the estimated values of a_1, a_3, and a_6 from the last column of Table 2.3

Step 2: Calculate g^*_{Alk}, g^*_{AlFe}, and g^*_{SiB} for the given HLW glass composition according to Equation (2.4), and verify that these three values sum to 1.0 per Equation (2.5).

Step 3: Calculate *X* and *Y* using the formulas in Equation (2.6).

Step 4: Using the estimates of $\beta_0, \beta_1, \beta_2$, and β_3 in the last column of Table 2.3, calculate the predicted probability of nepheline formation in the given HLW glass after CCC (denoted p_i) using Equation (2.14). If $p_i \geq 0.47$ (the threshold value chosen in Section 2.1.4) then the HLW glass is predicted to form nepheline after CCC. However, this prediction does not account for the uncertainties in the coefficient estimates of $a_1, a_3, a_6, b_0, b_1, b_2$, and b_3.

Step 5: To account for the uncertainties in the coefficient estimates, repeat 2000 times the calculations in Steps 1 to 4 using the $n = 2000$ bootstrap sets of coefficient estimates. The result will be 2000 values of p_i for the given HLW glass. Sort these 2000 values of p_i from smallest to largest. Then, the *U*%/*V*% UTL on the probability of nepheline formation for the given HLW glass is given by the k^{th} order statistic of the $n = 2000$ values (denoted $p^{(k)}$), where $k = 1817$, 1916, or 1990 depending on whether *U*%/*V*% = 90/90, 95/95, or 99/99 is chosen.

Step 6: Finally, after accounting for uncertainties in the LR-SM model given in the last column of Table 2.3, the given HLW glass is predicted not to form nepheline with at least *U*% confidence at least *V*% of the time[1] when $p^{(k)} < 0.47$. If $p^{(k)} \geq 0.47$, there is not at least *U*% confidence that at least *V*% of the time the given HLW glass is predicted not to form nepheline. This statement unfortunately is somewhat awkward, involving a double negative, but is the statistically correct way to make the statement. Calculating a U%/V% UTL = $p^{(k)}$ and comparing it to the threshold 0.47 provides for conservatively avoiding glasses that have a high enough probability of forming nepheline after CCC, when accounting for uncertainties in the LR-SM model in the last column of Table 2.3.

The use of the *U*%/*V*% UTL approach is now illustrated for the three example glasses (Neph-NN-1-2, IWL-SLC20-1, and EWG-OL-03208) discussed in Kroll et al. (2016). The 95%/95% UTL value for each of the three glasses is shown as a dashed red line on each distribution in Figure 2.5. If the dashed red line is below the threshold value of 0.47 (represented as a solid black vertical line), there is at least 95% confidence that at least 95% of the time the glass is not predicted to form nepheline. It follows that glasses Neph-NN-1-2 and IWL-SLC20-1 are predicted to not result in nepheline formation because the 95%/95%

[1] Here, "at least *V*% of the time" refers to the data collection and modeling process conceptually being repeated a large number of times, and that at least *V*% of the times the given HLW glass after CCC would not form nepheline.

UTL for each distribution is below 0.47. Conversely, it cannot be stated with 95% confidence that 95% of the time EWG-OL-03208 is not predicted to result in nepheline formation. Hence, the EWG-OL-03208 glass should be classified as if nepheline formation may occur. For these three glasses, comparing the 95%/95% UTLs to the 0.47 threshold yields correct classifications (i.e., nepheline forming or not).

2.1.7 Comparison of Logistic Regression-Submixture and Polynomial Discriminating Curve-Submixture Models

This subsection compares the results from three LR-SMs to the results from the two PDC-SMs reported in Table V of Vienna et al. (2016). The first two LR-SMs utilize $p = 0.47$ and 0.30 as the thresholds for classifying whether a given HLW glass may form nepheline after CCC. Neither of these directly accounts for the uncertainties in the estimated model coefficients. However, the version with the 0.30 threshold was chosen as an indirect way to account for uncertainties. The third version of the LR-SM uses the nonparametric 95%/95% UTL approach applied to results from fitting the LR-SM model form to $n = 2000$ bootstrap samples of the model-development dataset. This third approach compares the 95%/95% UTL to the $p = 0.47$ threshold, and directly accounts for the uncertainties in the estimated coefficients of the LR-SM model.

For each of the three LR-SMs and two PDC-SMs, Table 2.5 includes coefficient estimates, threshold values or data weights as applicable, and misclassification counts for the entire dataset as well as those for the P1-4 subset of data discussed previously. Compared to the "PDC-SM Optimal" model, the LR-SM using a threshold of $p = 0.47$ has slightly different misclassification rates for the full dataset (30/212 vs. 29/212 for FN, and 29/535 vs. 33/535 for FP). Compared to the "PDC-SM Conservative" model, the LR-SM using a threshold of $p = 0.30$ has a better FP misclassification rate for the P1-4 dataset (13/52 vs. 25/52) while only increasing the FN count to one. For the full dataset, the FN rate increases more significantly (0/212 to 17/212) but the FP rate falls dramatically (133/535 to 50/535). Finally, the 95%/95% UTL approach represents a proper composition dependent uncertainty and has roughly the same misclassification rates as the conservative LR-SM (threshold value $p = 0.30$) and returns modest FN and FP rates in both the full dataset (17/212 and 51/535, respectively) and P1-4 subset (1/38 and 14/52, respectively).

2.1.8 Recommended Models for Predicting whether Nepheline May Form in an HLW Glass after Canister Centerline Cooling

The "Conservative LR-SM" with coefficients listed in Table 2.5 with a threshold of 0.30 is recommended. Steps 1 to 4 in Section 2.1.6 give concise instructions for using this model. Using the "Conservative LR-SM" with a conservative threshold of 0.30 is a more practical approach (compared to the 95%/95% UTL approach) for mission planning calculations. Also the misclassification results, at least for the modeling dataset, match closely to the more rigorous approach of a using a 95%/95% UTL to account for modeling uncertainties.

Table 2.5. Comparison of Logistic Regression-Submixture Models (LR-SM) to Polynomial Discriminating Curve-Submixture Models (PDC-SM) (from Vienna et al. 2016) for Nepheline Formation in HLW Glasses

Coefficient[a]	Optimal LR-SM	Conservative LR-SM	95%/95% UTL with LR-SM	Coefficient[a]	Optimal PDC-SM	Conservative PDC-SM
α_1 (Li_2O)	0.804	0.804	N/A[b]	α_1 (Li_2O)	1.031	0.653
α_2 (K_2O)	-	-	N/A	α_2 (K_2O)	0.390	0.000
α_3 (CaO)	0.294	0.294	N/A	α_3 (CaO)	0.307	0.158
α_6 (B_2O_3)	1.732	1.732	N/A	α_6 (B_2O_3)	1.739	1.982
β_0	-64.085	-64.085	N/A	a	-0.559	-0.592
β_1	498.338	498.338	N/A	b	4.671	4.922
β_2	-102.179	-102.179	N/A	c	-4.997	-5.171
β_3	-522.382	-522.382	N/A	–	–	–
Threshold	0.47	0.30	0.47	Weight	1	1E+07
FN[c]	30/212	17/212	17/212	FN[a]	29/212	0/212
FP[d]	29/535	50/535	51/535	FP[b]	33/535	133/535
FN P1-4[e]	5/38	1/38	1/38	FN P1-4	4/38	0/38
FP P1-4[f]	7/52	13/52	14/52	FP P1-4	8/52	25/52

(a) In addition to the components listed in this column, Al_2O_3, Na_2O, and SiO_2 also appear in the LR-SMs and PDC-SMs with coefficients of one.

(b) N/A = not applicable. The U%/V% UTL approach discussed in Section 2.1.5 and summarized in Section 2.1.6 does not provide/use a single set of model coefficients.

(c) FN = false negative, where xx/yyy means there were yyy positives in the full dataset with xx of them being falsely predicted by a model as negatives.

(d) FP = false positive, where xx/yyy means there were yyy negatives in the full dataset with xx of them being falsely predicted by a model as positives.

(e) FN P1-4 = false negative, where xx/yy means there were yy positives in the P1-4 dataset with xx of them being falsely predicted by a model as negatives.

(f) FP P1-4 = false positive, where xx/yy means there were yy negatives in the P1-4 dataset with xx of them being falsely predicted by a model as positives.

2.1.9 Future Plans

The "Conservative LR-SM" is intended to be effective at conservatively separating HLW glass compositions that are likely to form nepheline during one of many CCC schedules. Future testing should focus on glasses representative of Hanford high-alumina waste glasses with the current WTP CCC schedule. This is likely to reduce the prediction uncertainty for compositions and plant operating plans important to Hanford. In addition to generating "pass-fail" data, the concentration of nepheline formed and its impact on PCT response will be measured and modeled. It is clear from many studies that some nepheline can be tolerated while still maintaining adequate PCT responses as shown in Figure 2.6. After the fraction of nepheline and its impact on PCT can be predicted, less conservative approaches can be taken to formulation glass for Hanford high-alumina wastes.

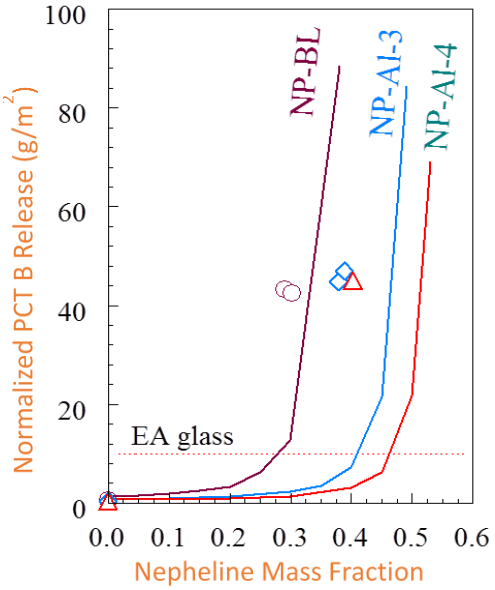

Figure 2.6. Plot Showing the Effect of Nepheline Mass on Normalized PCT-boron Release for Example HLW Glasses (from Riley et al. 2001)

2.2 Spinel Limits

As discussed previously (Vienna et al. 2013), crystal fraction and crystal size in laboratory testing and melter modeling can potentially be useful as predictors of melter failure caused by spinel build-up (Hrma 2002, Hrma et al. 2003, Hrma and Vienna 2003, Hrma 2010). Preceding the establishment of crystal size and fraction restrictions, limits on the spinel formation (in the form of liquidus temperature (T_L) constraints) were used to control glass composition at the Defense Waste Processing Facility (DWPF) and the West Valley Demonstration Project (WVDP) (Jain et al. 1992, Jantzen 1991a, Jantzen and Brown 2007a,b). An arbitrary distinction of a 1 vol% spinel temperature limit ($T_{1\%}$) at 950°C was adopted (Vienna and Kim 2014) as a place holder until a less arbitrary constraint is available. This constraint was viewed as too conservative, which prompted additional work to develop a replacement constraint.

Previous studies utilizing test melters (Jantzen 1986, Rankin et al. 1982) and data from the DWPF melter (Jantzen et al. 2004) have shown that the most likely process to cause failure due to spinel formation is the clogging of the pour-spout riser by crystal accumulation as suggested by Maytas et al. (2010a,b). As discussed in Section 2.1 of Vienna et al. (2013), a limit of 2 vol% at 950°C represents a reasonable compromise between the overly conservative $T_{1\%}$ limit and the incomplete data suggesting concentrations as high as 4.5 vol% could be acceptable (Matyas et al. 2013) and 4.2 vol% demonstrated in short term melter tests (Matlack et al. 2009b). Until sufficient data on spinel accumulation in the melter is obtained, a spinel fraction at 950°C limit of 2 vol% is recommended.

There are three approaches to limit the spinel fraction at 950°C to 2 vol%: (i) model the spinel equilibrium fraction as functions of both temperature and composition, (ii) model the equilibrium fraction of spinel at 950°C, and (iii) model the temperature at an equilibrium spinel fraction of 2 vol%. The first of

these three approaches has been implemented in the past, but the other two approaches have also now been investigated.

The equation generally utilized to model the equilibrium crystal fraction as a function of temperature, based on the freezing point depression equation for an ideal mixture, is

$$c_{Sp} = c_{sp,0}\left\{1-\exp\left[-B_L\left(\frac{1}{T}-\frac{1}{T_L}\right)\right]\right\}, \tag{2.16}$$

where T is the absolute temperature in K, $c_{sp,0}$ is the equilibrium fraction of spinel as T approaches 0K, and B_L is a fit parameter related to the enthalpy of crystallization of the universal gas constant (Hrma and Vienna 2003).

The coefficients $c_{Sp,0}$, T_L, and B_L can be expressed as functions of melt composition (typically as linear mixture models, LMMs). Over a relatively narrow range of low c_{Sp} values, the model in Equation (2.16) can be approximated by

$$c_{Sp} \cong a + bT, \tag{2.17}$$

where a and b are linear fit coefficients. These coefficients can be expressed as LMMs, yielding the equation

$$c_{Sp} \cong \sum_{i=1}^{q}\left(a_i g_i + b_i T g_i\right), \tag{2.18}$$

where

q = number of HLW glass components

a_i = temperature-independent coefficient of the i^{th} component

b_i = temperature-dependent coefficient of the i^{th} component

g_i = mass fraction in the melt of the i^{th} component, such that $g_1 + \ldots g_q = 1$.

T = temperature (not necessarily absolute temp) in ºC (Hrma and Vienna 2003).

A set of c_{Sp}, T, and composition data was compiled and fitted to the simplified model in Equation (2.18) by Vienna et al. (2013). The fit was not precise (with a RMSE of 0.47 vol% spinel). However, at that time the model was thought to be sufficient for estimating the mass of glass to be produced from Hanford HLW (Vienna et al. 2013). This model tended to overpredict small crystal fractions and underpredict high crystal fractions with more realistic predictions focused around 1.5 vol% (see Figure 2.7). Not surprisingly, new glasses formulated with predicted c_{950} concentrations of 2 vol% were underpredicted with high uncertainty (see Chou et al. 2016).

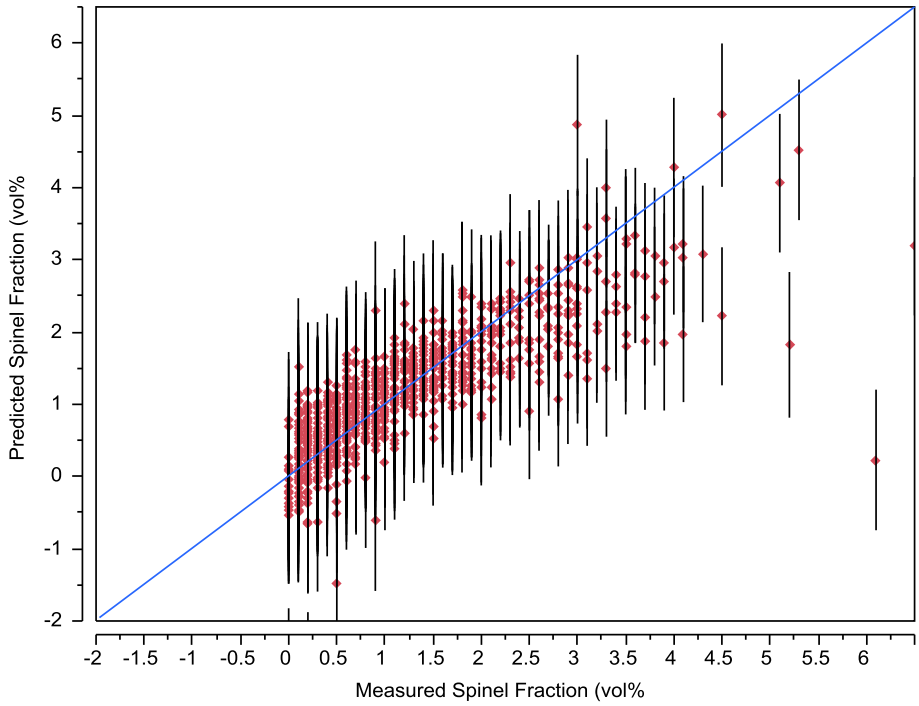

Figure 2.7. Predicted vs. Measured Plot of c_{sp} Values with 95% Prediction Intervals (vol%) Using HLW Glasses (from Vienna et al. 2013)

In a new study, an attempt was made to reduce the uncertainty and improve the accuracy of model prediction by using the other two modeling approaches (i.e., modeling either c_{950} or $T_{2\%}$ as a function of composition). These models were developed using (i) the data of 730 glasses reported in Vienna et al. (2013), (ii) additional data reported in the literature (glass families and references listed in Table 2.6), and (iii) data from a new study with compositions and equilibrium crystal fractions listed in Table 2.7 and Table 2.8, respectively. The composition of Others in this new study (with mass fractions summing to 0.058), includes Ag_2O = 0.0005, Bi_2O_3 = 0.012, CaO = 0.013, F = 0.002, K_2O = 0.0045, La_2O_3 = 0.005, MgO = 0.003, P_2O_5 = 0.013, and PbO = 0.005.

Because the compositions with c_{950} and $T_{2\%}$ data are slightly different, the datasets are described independently in the following Sections 2.1 and 2.2.

Table 2.6. Summary of Existing Data on HLW Glasses used in Evaluating Predictive Models for Limiting Spinel Formation[a]

Glass Family	#	Lab	Citation
IWL	10	PNNL	Kim et al. 2011
SP	20	PNNL	Mika et al. 2007
MS	23	PNNL	Hrma 1999, Wilson et al. 2002
HLW-E	142	VSL	Rodriguez et al. 2011, Matlack et al. 2007
HAL	19	PNNL	Rodriguez et al. 2011, Kim et al. 2008
EM07	38	PNNL	Schweiger et al. 2011
Ni/Fe/Cr/Al/Mn/Ru	11	PNNL	Matyas et al. 2012
HLW-ALG	65	VSL	Kot et al. 2006
HWI-Al	20	VSL	Rodriguez et al. 2011, Matlack et al. 2008/2010a
HWI-ALS	12	VSL	Matlack et al. 2010b
HLW02/03	101	VSL	Piepel et al. 2007, Piepel et al. 2008
HLW05/06	65	VSL	Kot et al. 2005
HLW07	40	VSL	Kruger et al. 2013
HLW-BP-X	10	VSL	Vienna et al. 2013
US	39	PNNL	Riley et al. 2009
LSi	30	PNNL	Vienna et al. 2013
SPA	36	PNNL	Vienna et al. 2013
ICCM	13	PNNL	Vienna et al. 2013
WTP-TI	15	PNNL	Vienna et al. 2013
CCIM	9	PNNL	Vienna et al. 2013
INEL	4	VSL	Vienna et al. 2013
HLW-Bi	4	VSL	Vienna et al. 2013
HLW-N101	12	VSL	Vienna et al. 2013
HLW-NG	20	VSL	Vienna et al. 2013

(a) PNNL – Pacific Northwest National Laboratory, VSL – the Vitreous State Laboratory at the Catholic University of America

Table 2.7. Glass Compositions (in mass fractions) for 11 Varied Components (Al_2O_3 to ZrO_2) and One Fixed Component (Others) Comprising the HLW Spinel Phase 1 Test Matrix

Glass ID	Al_2O_3	B_2O_3	Cr_2O_3	Fe_2O_3	Li_2O	MnO	Na_2O	NiO	RuO_2	SiO_2	ZrO_2	Others
CT16-IL-01	0.10066	0.09500	0.01580	0.15000	0.01979	0.01000	0.17500	0.00550	0.00025	0.36000	0.01000	0.05800
CT16-IL-02	0.13023	0.09500	0.00700	0.07000	0.02865	0.03000	0.17500	0.01631	0.00025	0.36000	0.02956	0.05800
CT16-IL-03	0.13000	0.14000	0.01000	0.10000	0.01650	0.02000	0.15000	0.01100	0.00050	0.34150	0.02250	0.05800
CT16-IL-04	0.18615	0.16050	0.01580	0.07000	0.00830	0.03000	0.17500	0.00550	0.00075	0.28000	0.01000	0.05800
CT16-IL-05	0.19000	0.09500	0.00700	0.07392	0.02900	0.03000	0.15203	0.00550	0.00075	0.34880	0.01000	0.05800
CT16-IL-06	0.13695	0.17000	0.00700	0.07000	0.00830	0.03000	0.12444	0.00550	0.00025	0.36000	0.02956	0.05800
CT16-IL-07	0.19000	0.17000	0.00700	0.10281	0.02900	0.01000	0.12871	0.00550	0.00025	0.28873	0.01000	0.05800
CT16-IL-08	0.18067	0.17000	0.00700	0.07000	0.01402	0.01000	0.17500	0.00550	0.00025	0.28000	0.02956	0.05800
CT16-IL-09	0.12083	0.16558	0.00700	0.07000	0.00830	0.01000	0.17500	0.01750	0.00075	0.35704	0.01000	0.05800
CT16-IL-10	0.13000	0.14000	0.01000	0.10000	0.01650	0.02000	0.15000	0.01100	0.00050	0.34150	0.02250	0.05800
CT16-IL-11	0.13699	0.17000	0.01580	0.07398	0.02900	0.01000	0.12998	0.00550	0.00075	0.36000	0.01000	0.05800
CT16-IL-12	0.18263	0.09500	0.00700	0.07000	0.02662	0.01000	0.17500	0.00550	0.00025	0.36000	0.01000	0.05800
CT16-IL-13	0.09500	0.17000	0.00700	0.15000	0.00966	0.03000	0.11750	0.00594	0.00025	0.34665	0.01000	0.05800
CT16-IL-14	0.15268	0.12394	0.01580	0.07000	0.00830	0.01000	0.17500	0.01603	0.00025	0.36000	0.01000	0.05800
CT16-IL-15	0.12802	0.09500	0.00700	0.15000	0.00830	0.01000	0.16744	0.00550	0.00075	0.34043	0.02956	0.05800
CT16-IL-16	0.14488	0.17000	0.00700	0.07000	0.02900	0.01000	0.11750	0.01750	0.00075	0.34581	0.02956	0.05800

Note: The mass fractions of the 12 components all sum to exactly 1.00000.

Table 2.8. Crystal Fractions, and the Phases Present, Versus Temperature for the HLW Spinel Test Phase 1 Test Matrix Glasses

	Spinel/Crystal Content (wt%) by Temperature (ºC)				
Glass ID	Quench	950	900	850	Phases Present (by XRD)
CT16-IL-1	3.7	4.6	4.9	5.5	Spinel
CT-16-IL-2	2.1	3.6	4.0	5.3	Spinel + $KAlSi_2O_6$
CT-16-IL-3	3.4	4.4	5.1	5.9	Spinel
CT-16-IL-4	4.2	5.2	4.4	8.0	Spinel + Nepheline
CT-16-IL-5	3.0	4.2	18.7	26.5	Spinel + $Na_{6.65}Al_{6.24}Si_{9.76}O_{32}$
CT-16-IL-6	1.9	3.3	4.1	5.0	Spinel + $Na_2Al_2(B_2O_7)$ + $Mn^{2+}Mn^{3+}{}_6SiO_{12}$
CT-16-IL-7	3.4	5.3	5.8	6.8	Spinel
CT-16-IL-8	1.7	2.3	2.7	3.3	Spinel
CT-16-IL-9	1.5	2.3	3.3	3.8	Spinel
CT-16-IL-10	3.2	4.2	4.6	4.6	Spinel
CT-16-IL-11	2.4	2.9	3.3	3.6	Spinel
CT-16-IL-12	1.5	2.3	15.0	2.3	Spinel, $Na_{6.65}Al_{6.24}Si_{9.76}O_{32}$
CT-16-IL-13	3.0	6.2	6.7	8.2	Spinel + Fe_2O_3 (Hematite) (9%) + $Na_2Al_2B_2O_7$ (5%)
CT-16-IL-14	4.3	5.0	5.2	5.6	Spinel
CT-16-IL-15	2.6	4.3	5.1	8.3	Spinel + Fe_2O_3 Hematite + $Na_{6.65}Al_{6.24}Si_{9.76}O_{32}$
CT-16-IL-16	2.8	4.6	5.2	5.6	Spinel

2.2.1 Model for Equilibrium Spinel Fraction at 950°C

The first modeling approach discussed is modeling the equilibrium spinel concentration at 950°C as a function of HLW glass composition. The data used for modeling cover the HLW glass composition region given in Table 2.9 and are shown graphically in a scatterplot matrix in Figure 2.8.

Table 2.9. HLW Glass Component Concentration Ranges (in mass fractions) for Validity of the c_{950} Model

Component	Min	Max
Al_2O_3	0.0180	0.2900
B_2O_3	0.0430	0.2200
CaO	0	0.1420
Cr_2O_3	0	0.0450
Fe_2O_3	0	0.2130
K_2O	0	0.1120
Li_2O	0	0.0601
MnO	0	0.0800
Na_2O	0.0358	0.2500
NiO	0	0.0300
P_2O_5	0	0.0648
SiO_2	0.2140	0.5300
SrO	0	0.1000
TiO_2	0	0.0209
ZnO	0	0.0450
Others	0.0012	0.1990

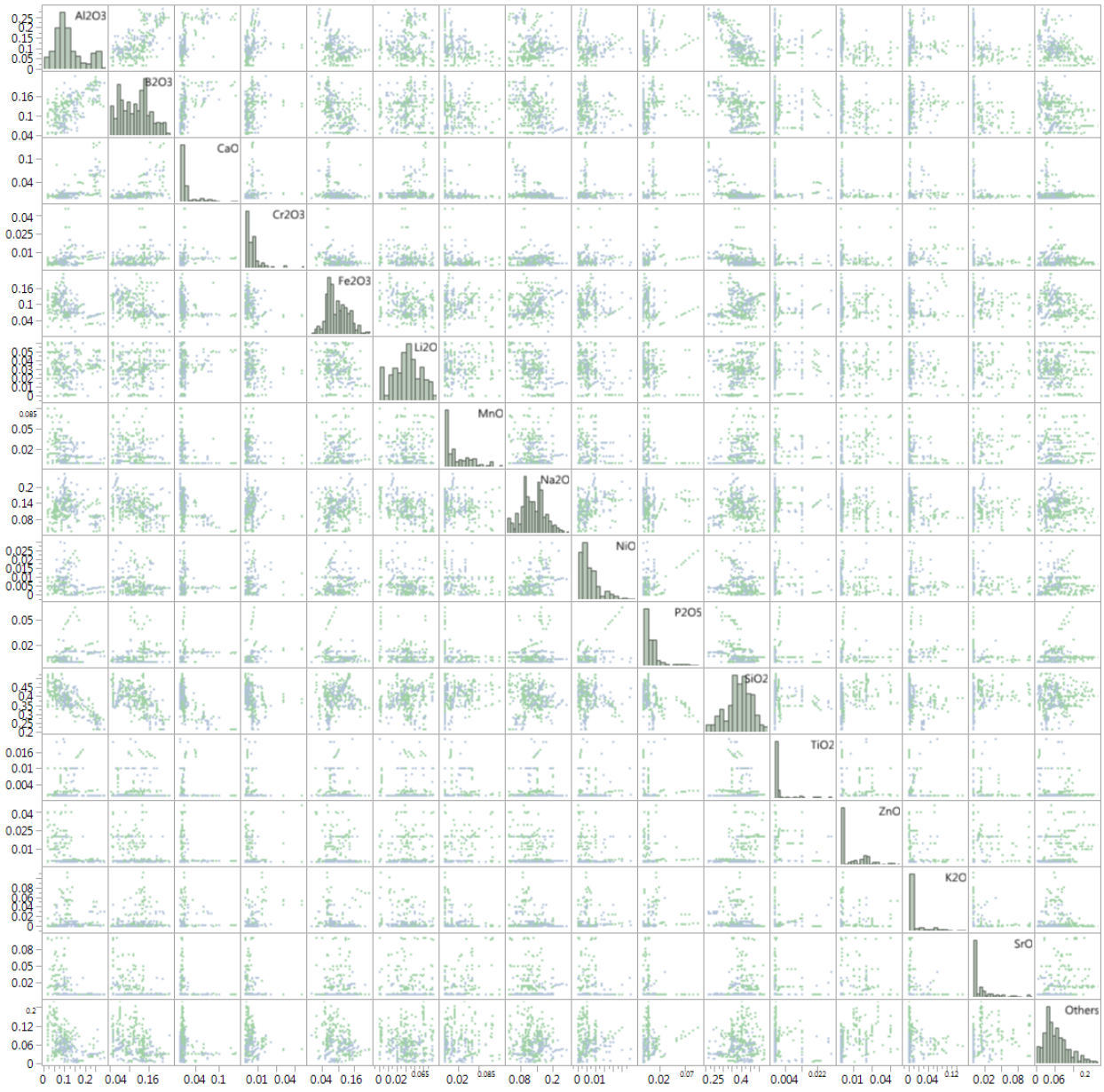

Figure 2.8. Scatterplot Matrix for HLW Glass Compositions (in mass fractions) Used to Model c_{950}

The dataset for modeling c_{950} was generated using a combination of data from PNNL and VSL. The total number of glasses intended for use in the model was 730. However, 87 glasses had no values measured at 950°C and hence were removed from the dataset. Also, to improve the model goodness of fit, glasses with extreme c_{950} data were removed including 158 glasses with $c_{950} = 0$, and 7 glasses with $c_{950} >$ 6 vol% (HLW03-07, HLW03-08, HLW03-10, HLW06-30, HLW06-31, HLW-E-Al-8, and HLW-E-ANa-16). Also, in preliminary fitting, two of the five HLW glasses with SiO_2 concentrations < 0.20 mass fraction were found to be outliers (based on Studentized residuals > 3.5). Therefore, all five glasses with SiO_2 concentrations < 0.20 mass fraction were removed from the dataset. Additionally, HLW-E-ES-09 was found to be a compositional outlier due to high TiO_2 content (> 0.02 mass fraction) and was removed from the dataset as well. During the model fitting, six additional glasses were also identified as model-fit

outliers with Studentized residuals > 3.5 (LSi-Li-05, HLW03-01, HLW03-09, HLW06-07, HLW06-19, HLW-ALG-46, and HLW-E-Al-9). These glasses were removed from the dataset used for the final model fits. The resulting final glass model validity region is summarized in Table 2.9.

The data for the remaining 440 HLW glasses were used to fit a LMM and a partial quadratic mixture model (PQMM). The LMM was of the form

$$c_{950} = \sum_{i=1}^{q} a_i g_i \tag{2.19}$$

where

q = number of HLW glass components in the model

a_i = model coefficient for the i^{th} HLW glass component

g_i = mass fraction of the i^{th} HLW glass component, so that $g_1 + \ldots + g_{q=\text{Others}} = 1.0$.

The PQMM (Piepel et al. 2002) was of the form

$$c_{950} = \sum_{i=1}^{q} a_i g_i + \text{Selected}\left\{ \sum_{i=1}^{q} a_{ii} g_i^2 + \sum_{i=1}^{q-1} \sum_{j=i+1}^{q} a_{ij} g_i g_j \right\} \tag{2.20}$$

where q, a_i, and g_i are as previously defined, a_{ii} is the coefficient for the squared term of the i^{th} component, and a_{ij} is the coefficient of the crossproduct term involving the i^{th} and j^{th} components. Only selected quadratic terms can be chosen because of the constraint $g_1 + \ldots + g_{q=\text{Others}} = 1.0$. See Piepel et al. (2002) for more discussion of PQMMs.

Table 2.10 lists the coefficients and summary statistics for the LMM and PQMM fit to the c_{950} data. The LMM and PQMM, with R^2 values of 0.7034 and 0.7302, account for over 70% and 73% fractions of the variability in the data, respectively, although larger values would be better. Also, RMSE = 0.5825 and 0.5519 for the LMM and PQMM, respectively, are much larger than what the experimental and measurement uncertainty is for c_{950}. This suggests these models have some lack-of-fit (LOF). The average R^2_{Val} value for the PQMM is almost identical to the R^2_{Pred} value of 0.70. Hence, the PQMM should give predictions of unknown data within the model-validity region (Table 2.9) nearly as well as for the model-fit data. However, the model appears to have some LOF.

Figure 2.9 shows the predicted versus measured plot for the PQMM. The figure indicates that the PQMM tends to overpredict smaller values of c_{950} (< 1) and to underpredict larger values of c_{950} (> 3). The scatter of points around the 45º line in Figure 2.9 is fairly large in general, which supports the previous indication of some model LOF. It is believed that the high scatter is due, at least in part, to the combination of data from PNNL and VSL which use different experimental method and have shown differences in results in previous studies.

Table 2.10. Coefficients for the Linear Mixture Model (LMM) and Partial Quadratic Mixture Model (PQMM) for c_{950} (in vol% and mass fractions of oxides) of HLW Glasses

Model Term	LMM Coefficient	PQMM Coefficient
Al_2O_3	15.7907	17.064329
B_2O_3	-5.1773	-6.988394
CaO	-14.7991	-14.25455
Cr_2O_3	83.6096	72.638851
Fe_2O_3	23.0435	20.646002
Li_2O	-15.4088	-16.27009
MnO	16.8047	91.361724
Na_2O	-14.9755	-16.45675
NiO	86.2595	88.862223
P_2O_5	-6.3533	-9.001111
SiO_2	-3.1977	-1.445045
TiO_2	-3.6153	-20.10877
ZnO	17.9636	19.803191
ZrO_2	10.7290	(a)
K_2O	-9.5954	3.8116497
SrO	-6.9026	-7.827833
RuO_2	281.9318	(a)
Others	7.8413	8.3602731
$MnO \times SiO_2$	-	-178.7683
$Al_2O_3 \times K_2O$	-	-116.663
Model Fit Summary		
# data points	440	439
# model terms	17	18
RMSE	0.5825	0.5519
R^2	0.7034	0.7302
R^2_{Adj}	0.6915	0.7193
R^2_{Pred}	0.6728	0.7023
R^2_{Val}	-	0.7000

(a) These components were included in Others for this model.

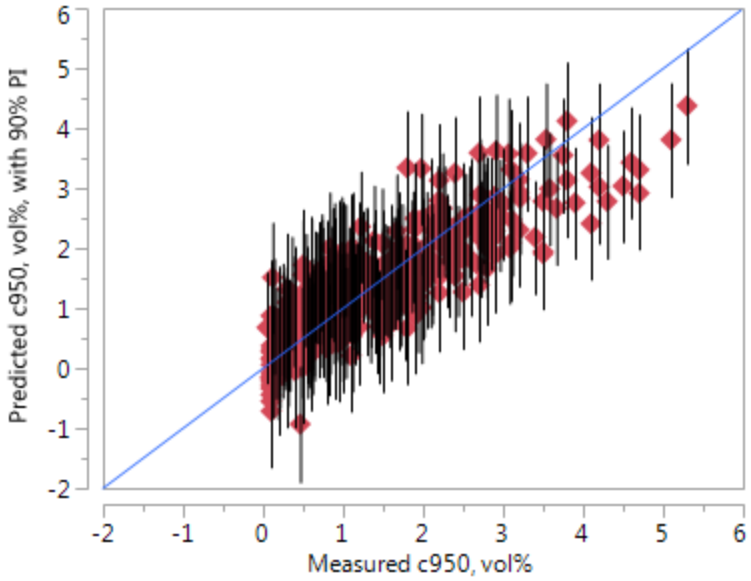

Figure 2.9. Predicted vs. Measured Plot of c_{950} Values with 90% Prediction Intervals (vol%) Using the Partial Quadratic Mixture Model for HLW Glasses

2.2.2 Model for Temperature at 2 vol% Spinel

This subsection discusses modeling the temperature at an equilibrium spinel fraction of 2 vol% ($T_{2\%}$) as a function of HLW glass composition. The data used for modeling $T_{2\%}$ over the composition region given in Table 2.11 are shown graphically in a scatterplot matrix in Figure 2.10. Similar to the c_{950} model, the $T_{2\%}$ model was generated using a combination of data from PNNL and VSL, beginning with the 730 glasses. Many (280) glasses did not have a 2 vol% value measured and/or did not have sufficient data to interpolate a temperature for the 2% value. Additionally, any glasses that did not crystallize spinel as the major phase at or near $T_{2\%}$ were removed (106 glasses). To improve the goodness of fit, a glass with extreme $T_{2\%}$ data (HLW03-12, $T_{2\%} < 500$°C) was removed from the modeling dataset. During the model fitting, three additional glasses were also identified as model-fit outliers with Studentized residuals > 3.0 (LSi-Li-05, HLW03-38, and WTP-TL-03). Two of these three glasses (LSi-Li-05 and WTP-TL-03) were identified as outliers in the original study documents (Jiřička et al. 2003 and Vienna et al. 2003, respectively). All three glasses were removed from the final model fits. Ultimately, 340 data points were used to fit the model. The resulting final model validity region is summarized in Table 2.11.

Table 2.11. HLW Glass Component Concentration Ranges (in mass fractions) for Validity of the $T_{2\%}$ Model

Component	Min	Max
Al_2O_3	0.019	0.30
B_2O_3	0.03	0.22
Bi_2O_3	0	0.0738
CaO	0	0.14
CdO	0	0.02
Cr_2O_3	0	0.045
F	0	0.02
Fe_2O_3	0	0.2128
K_2O	0	0.082
La_2O_3	0	0.012
Li_2O	0	0.0632
MgO	0	0.06
MnO	0	0.08
Na_2O	0.0358	0.25
NiO	0	0.03
P_2O_5	0	0.0548
SiO_2	0.020	0.53
SO_3	0	0.008
SrO	0	0.10
ThO_2	0	0.0597
TiO_2	0	0.0525
UO_3	0	0.065
ZnO	0	0.045
ZrO_2	0	0.096

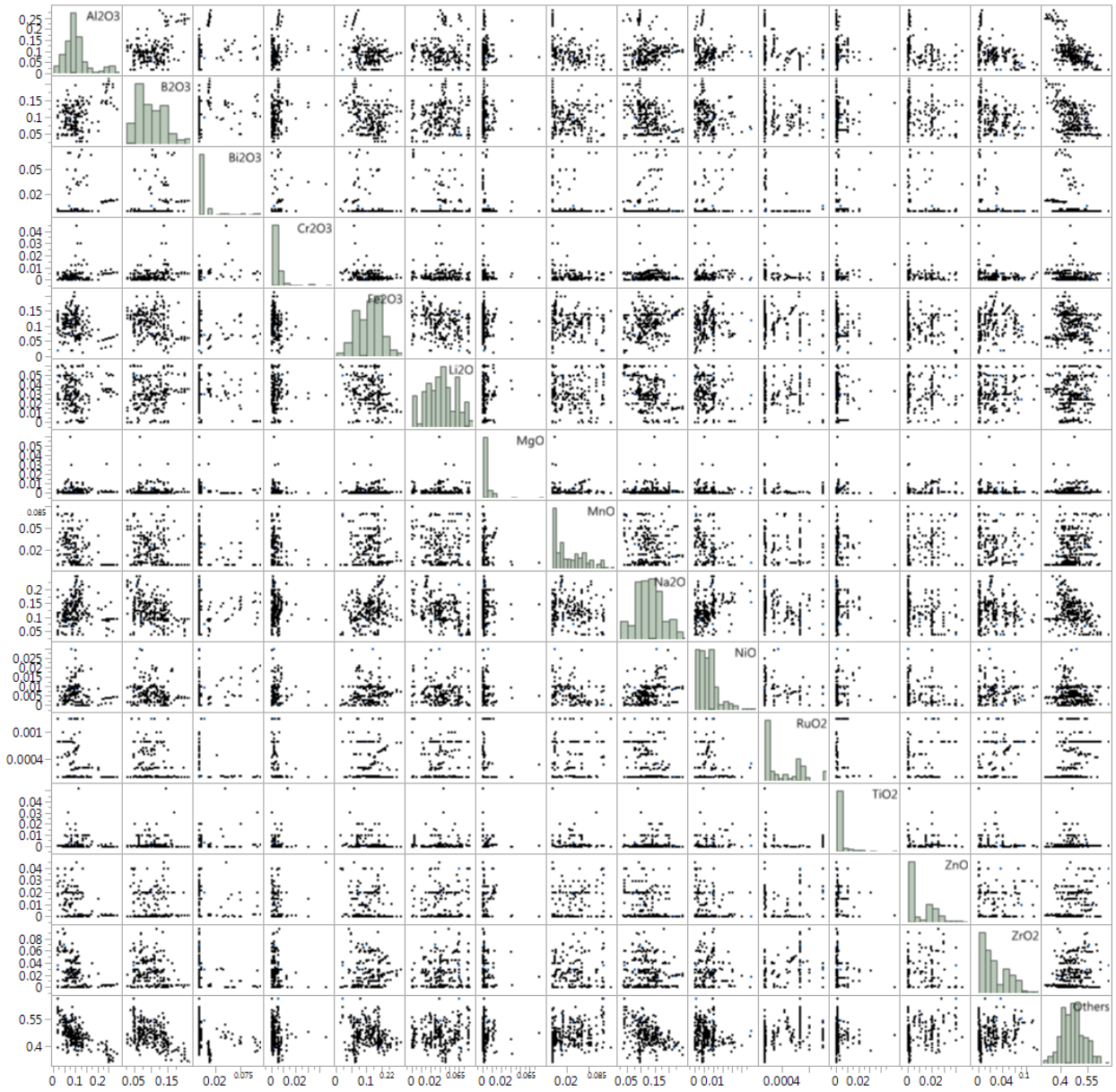

Figure 2.10. Scatterplot Matrix for HLW Glass Compositions (in mass fractions) Used to Model $T_{2\%}$

The data for the remaining 340 glasses were used to fit a LMM and a PQMM, where the model forms are the same as in Equations (2.19) and (2.20), except with $T_{2\%}$ on the left hand sides. The fits of the LMM and PQMM for $T_{2\%}$, as represented by the various R^2 values, were determined similarly as for the c_{950} models, as described in Section 2.2.1. Table 2.12 lists the coefficients and summary statistics for the $T_{2\%}$ LMM and PQMM. The LMM and PQMM, with R^2 values of 0.6945 and 0.7292 respectively, account for over 69% and 72% of the variability in the data, although larger values would be better. Also, RMSE = 77.98 and 73.64 for the LMM and PQMM, respectively, are much larger than what the experimental and measurement uncertainty is for $T_{2\%}$. This suggests these models have some LOFs. The average R^2_{Val} for the PQMM is almost identical to the R^2_{Pred} value of 0.697. Hence, the PQMM should give predictions

of unknown data within the model-validity region (Table 2.11) nearly as well as for the model-fit data. However, the model appears to have some LOF.

Table 2.12. Coefficients for the Linear Mixture Model (LMM) and Partial Quadratic Mixture Model (PQMM) for $T_{2\%}$ (in vol% and mass fractions of oxides)

Model Term	LMM Coefficient	PQMM Coefficient
Al_2O_3	2988.319	2058.4195
B_2O_3	-523.853	-281.516
Bi_2O_3	1778.341	1543.2359
Cr_2O_3	11750.02	11944.224
Fe_2O_3	3440.954	3673.0656
Li_2O	-686.862	-753.6015
MgO	3421.658	3553.9322
MnO	3596.64	3485.9411
Na_2O	-1123.95	-1940.195
NiO	10034.92	11231.615
RuO_2	71492.63	84418.014
TiO_2	1985.837	2574.6514
ZnO	4310.519	4011.0211
ZrO_2	1762.619	-987.8832
Others	294.2597	391.75396
$Al_2O_3 \times Na_2O$	-	9345.1684
$ZrO_2 \times ZrO_2$	-	42569.129
Model Fit Summary		
# data points	340	340
# model terms	14	16
RMSE	77.98	73.64
R^2	0.6945	0.7292
R^2_{Adj}	0.6813	0.7157
R^2_{Pred}	0.6638	0.6970
R^2_{Val}	-	0.6970

Figure 2.11 shows the predicted versus measured plot of $T_{2\%}$ values for the PQMM fit. Predicted values below roughly 800°C tend to be over predicted. This has little practical importance for the proposed application of limiting $T_{2\%}$ to 950°C. There is considerable scatter of the data point around the 45º line, which is the source of the model LOF mentioned previously. This scatter is thought to be caused, at least in part, by combining data from PNNL and VSL which use different methods and have seen some differences in results.

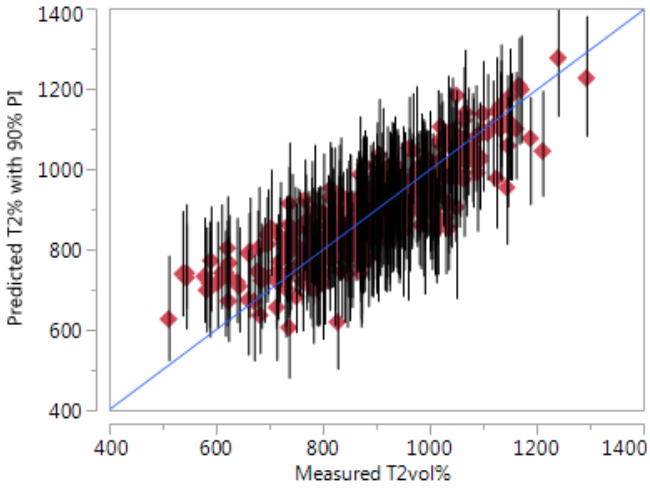

Figure 2.11. Predicted vs. Measured Plot of $T_{2\%}$ Values with 90% Prediction Intervals (vol%) Using the Partial Quadratic Mixture Model for HLW Glasses

2.2.3 Recommended Crystal Constraint

To determine which of the two crystal models and corresponding constraints to use, we consider first the goodness of fit and potential for biased prediction at the desired placeholder constraint of 2 vol% at 950ºC. The c_{950} model data range from 0 (at which it is cutoff) to 5.5 vol% with a median of 1.1 vol% (mean of 1.37 vol%), and are highly skewed toward the low end of range. The $T_{2\%}$ data are symmetrically distributed around roughly 900ºC with a minimum of 511ºC and maximum of 1293ºC. The c_{950} model tends to overpredict smaller values of c_{950} (< 1) and to underpredict larger values of c_{950} (> 3).

The RMSE of the c_{950} and $T_{2\%}$ models are 0.552 vol% and 73.6ºC, respectively. To compare these, we considered typical example spinel forming glasses as shown in Figure 2.12. The slopes dc/dT range from -0.0092 to -0.0041 with an average of -0.0075. Estimating the average vol% impact of change in 73.6ºC is 0.55 vol%. We also considered the number of data points and the distribution of data, which slightly favor the $T_{2\%}$ model. Finally, the validation statistics slightly favor the c_{950} model.

Considering all of the above pros and cons, we recommend using the $T_{2\%}$ model with a 2 vol% limit as the place holder constraint until the crystal settling model becomes available. The data and models are not fully QA compliant and therefore are not intended to be used in quality-affecting activities or decisions (e.g., design basis input, plant operations, waste form compliance). Instead the models and constraints are intended for use in mission planning activities.

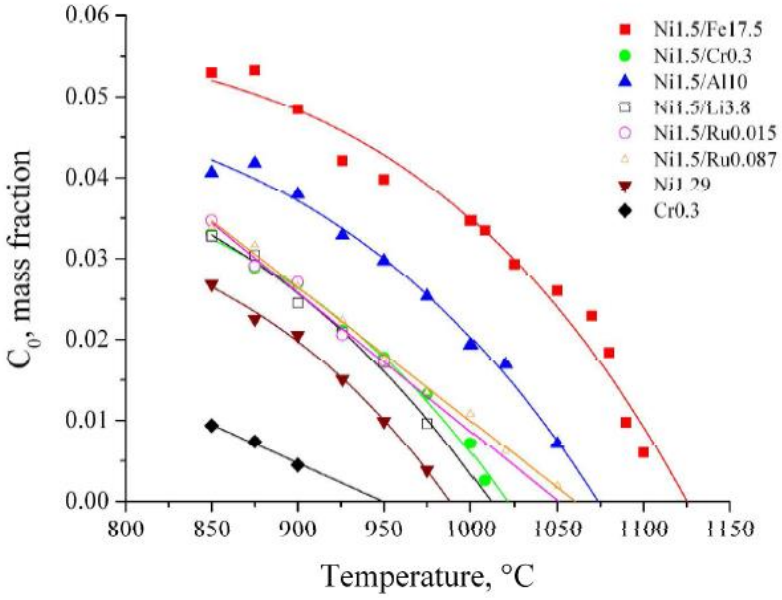

Figure 2.12. Equilibrium Crystal Fraction vs. Temperature for Example Representative HLW Glasses (from Matyas 2013)

2.2.4 Future Plans

Recent results have demonstrated successful melter processing with higher concentrations of spinel in the melt. It was determined by Hrma et al. (2001) that the allowable spinel fraction is likely to be controlled by a combination of crystal size and fraction which are both functions of melt composition. Therefore Matyas et al. (2010, 2012, and 2013) have begun development and validation of spinel crystal accumulation models. These models need to be expanded to a broader composition region of interest for Hanford HLW and be fully validated in scaled melter tests. Efforts will continue to develop data and models to predict crystal accumulation in the melter.

2.3 Sulfur Tolerance

Sulfur is commonly observed as sulfate ion in the glass network, although solubility is limited to between 0.3 and 2.0 wt % depending upon the glass composition. Above the sulfur solubility limit for a glass, it also forms sulfates rich in alkali, alkaline earths, and chromate. Sulfate rich salts can form in the cold cap region during the feed-to-glass melt conversation process leading to a molten salt layer above the glass melt. Understanding sulfur solubility in the HLW glass melts is important to avoid creation of separated molten salts in the melters. To accomplish this, it is important to predict the solubility of SO_3 in glass melts as a function of glass composition.

Empirical mixture models for sulfur solubility were previously examined for the HLW and LAW glasses. Vienna et al. (2013) recommended a combined LAW and HLW sulfate solubility model based on the data available at that time. However, crucible tests performed since that model was generated showed

it significantly underpredicted the measured sulfate solubility for HLW glasses (see Figure 2.13). Although the model was found to be conservative, a more accurate model is desired. There were enough differences between the HLW and LAW melter feed compositions that separate models are now required. This subsection describes the development of a sulfate solubility model for HLW glasses only.

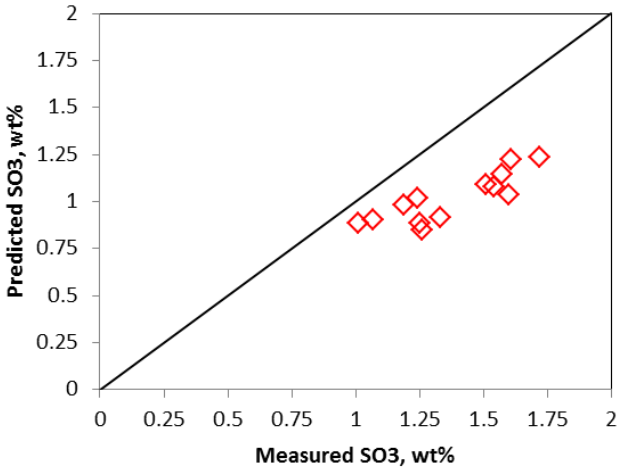

Figure 2.13. Validation Results of Sulfate Solubility Model for Recent HLW Glasses (from Vienna et al. 2013)

2.3.1 Sulfate Solubility Data for HLW Glasses

Measured SO_3 solubility data were available for 61 Hanford HLW glasses collected by two different methods: saturation and bubbling plus seven glasses measured for SO_3 tolerance during melter testing. Only data for the saturation and bubbling methods (61 glasses) were considered for modeling. The following HLW glasses were considered for fitting the SO_3 solubility model:

- HWI-Al-19, HLW-NGFe2, HLW-E-Bi-6, HLW-EANa-22, HLW-E-Al-27, HLW-ALG-03, HLWS-1 to HLWS-20 (Matlack et al. 2012)
- HLW98-77 to -96, HLW02-15 to -50, HLW03-01 and -03, HLW04-07S1 and -09, HLW06-16 to -32 (Kot et al. 2006)
- HLWS-21 to -33 (Matlack et al. 2013).

Two glasses (HLW06-27 and -29) were found to be extreme in ZrO_2 concentration (g_{ZrO_2} = 0.115) and were found to be outliers in initial model fitting. Therefore, the model validity region was reduced to $g_{ZrO_2} \leq 0.0884$ and the two glasses were excluded from the dataset used to fit the final model. Figure 2.14 shows a scatterplot matrix of the compositions for the 59 glasses. The glass compositions with SO_3 normalized out were used for the purpose of modeling SO_3 solubility. Table 2.13 lists the minimum and maximum measured SO_3 solubility and individual component ranges for the data used to develop the HLW SO_3 model. The melter data were not used for modeling because true solubility was not measured

using melters. However, the melter data are shown in figures for comparison purposes as was done for the LAW glass sulfate solubility model (Vienna et al. 2014).

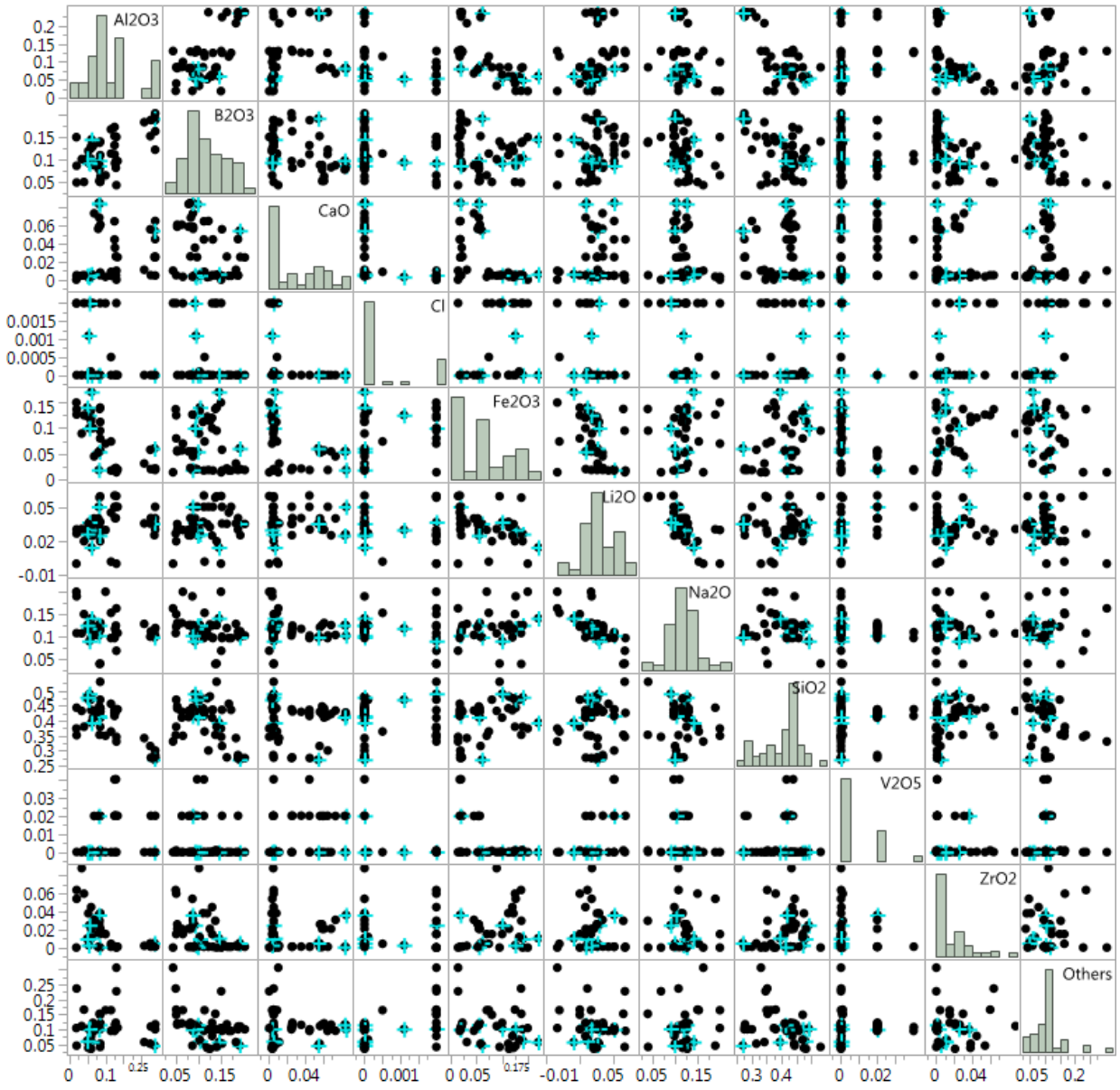

Figure 2.14. Scatterplot Matrix and Histograms of HLW Glass Compositions for Modeling SO_3 Solubility. Blue + symbols are for melter glasses not used in fitting of the model.

Table 2.13. Component Ranges (mass fractions) for Validity of the SO_3 Solubility Model for HLW Glasses

Component	Min	Max
Al_2O_3	0.0188	0.2387
B_2O_3	0.0431	0.2030
Bi_2O_3	0	0.0670
CaO	0	0.0856
CdO	0	0.0165
Cr_2O_3	0	0.0099
F	0	0.0079
Fe_2O_3	0.0140	0.1707
K_2O	0	0.0164
La_2O_3	0	0.0123
Li_2O	0	0.0607
MgO	0	0.0117
MnO	0	0.0800
Na_2O	0.0400	0.2000
Nd_2O_3	0	0.0080
NiO	0	0.0168
P_2O_5	0	0.0508
PbO	0	0.0091
SiO_2	0.02703	0.5305
SO_3	0.0053	0.0178
SrO	0	0.1032
ThO_2	0	0.0596
TiO_2	0	0.0100
UO_3	0	0.0652
ZnO	0	0.0401
ZrO_2	0	0.0884

2.3.2 Model for Sulfate Solubility of HLW Glasses

To model the effect of HLW glass composition on SO_3 solubility (w_{SO_3}), the glass compositions were renormalized with SO_3 removed. The LMM

$$w_{SO_3},\text{wt\%} = \sum_{i=1}^{q} s_i n_i \tag{2.21}$$

was investigated, where

q = number of HLW glass components in the model

s_i = coefficient of the i^{th} component

n_i = mass fraction of the i^{th} component normalized after removing SO_3, so that $n_1 + \ldots + n_{q=\text{Others}} = 1.0$

Components that did not significantly contribute to the model were combined into the Others component based on (i) one of the LMM reduction approaches discussed by Piepel et al. (2009) and (ii) knowledge of component effects on sulfate solubility. Two components (Na_2O and Fe_2O_3) were near the last components considered for combining into Others, but were left in the model because they are major components and would significantly increase the concentration of the Others component in all glasses.

The current dataset is not ideal for several components. Crossproduct and squared terms (for PQMMs) were evaluated, but were not found to significantly improve the model fit for this current dataset of glasses. Hence, a LMM was fit to the modeling dataset of 59 glasses, with the coefficients and the various goodness-of-fit statistics (see Section 1.4) listed in Table 2.14.

The R^2_{Pred} and R^2_{Val} values of 0.821 and 0.827 are significantly lower than the R^2 value of 0.893. This is thought to be due to the relatively small size of the data set and the few data points that appear to be significant outliers (HLWS-19, HLWS-16, and HLW02-24; all with high Studentized residuals). However, no justification could be found for removing these data points from the modeling dataset.

The RMSE should estimate the experimental and measurement uncertainty in determining SO_3 solubility values if the LMM does not have a significant LOF. However, the, RMSE = 0.1344 is larger than what the experimental and measurement uncertainty in SO_3 solubility is typically seen to be. Hence, this indicates the LMM has some LOF.

Table 2.14. SO_3 Solubility Linear Mixture Models for HLW Glasses

Model Term	Coefficient
Al_2O_3	-2.4906
B_2O_3	4.9038
CaO	10.6949
Cl	-34.2573
Fe_2O_3	0.4100
Li_2O	13.1713
Na_2O	3.0563
SiO_2	-1.5986
V_2O_5	6.8123
ZrO_2	-2.7024
Others	2.6712
Model Fit Summary	
# of data points	59
# model terms	11
Mean of SO_3 Solubility Values, wt%	1.0789
RMSE	0.1334
R^2	0.8926
R^2_{Adj}	0.8702
R^2_{Pred}	0.8209
R^2_{Val}	0.8274

Figure 2.15 shows the predicted versus measured plot of w_{SO_3} values for the LMM fit. Measured values above roughly 1.4 wt% tend to be underpredicted. This suggests that the model is somewhat conservative over this subrange and could be improved to improve future estimation of glass mass. There is considerable scatter of the data point around the 45° line, which contributes to the model LOF mentioned previously.

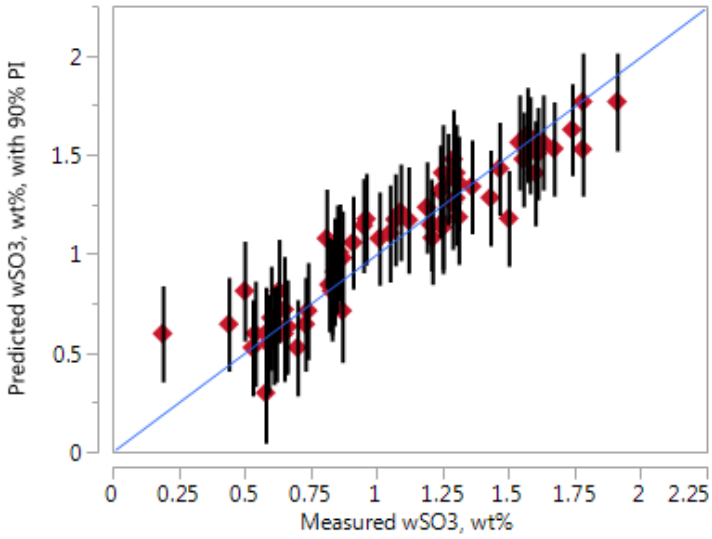

Figure 2.15. Predicted vs. Measured SO_3 Solubility (wt%) for HLW Glasses with 90% Prediction Intervals

The data and models are not fully QA compliant and therefore are not intended to be used in quality-affecting activities or decisions (e.g., design basis input, plant operations, waste form compliance). Instead the models and constraints are intended for use in mission planning activities.

2.3.3 Future Plans

The modeling dataset for SO_3 solubility of HLW glasses used in this report provides incomplete coverage of the current component ranges for the enhanced high-SO_3 HLW glass composition region. Hence, additional SO_3 solubility data are needed to properly cover the composition space of high-SO_3 HLW glasses at Hanford. Many other HLW glasses have been tested (many with lower concentrations of SO_3), but SO_3 solubility was not determined for them. New data points should be statistically designed to provide, at a minimum, good coverage of the extreme vertices. Particular attention will be given to extend the range of Cr_2O_3 in the dataset. Also, if possible, addition of HLW glasses using a space-filling experimental design should be implemented to provide complete coverage of the HLW glass composition space. These data points will provide a more complete dataset to determine the component effects on SO_3 solubility of HLW glasses for Hanford.

2.4 Eskolaite Formation

If the content of chromium in the melter feed is too high, one or a combination of three things will most likely occur (Hrma 2006):

1. A chromate- (and sulfate-) containing salt will accumulate on the melt surface. This typically, but not always, occurs in melts high in sulfate, nitrate, and other salt-forming compounds.
2. Transition metal spinel, $(Fe,Ni,Mn,Zn)(Fe,Cr)_2O_4$, will form. This typically occurs in melts with relatively high concentrations of iron, nickel, manganese, and/or zinc.

3. Eskolaite, Cr_2O_3, will form. This typically occurs only in melts that are relatively low in sulfur, nitrate, iron, nickel, manganese, and/or zinc.

Additionally, chromate species, such as $Na_2Cr_2O_7$, are semi-volatile and partition to some extent to the off-gas system, where they are captured and eventually recycled back to the melter (e.g., Jantzen 1991b). This volatile loss is partially offset by the addition of small amounts of chromium from corrosion/erosion of high-chromium melter materials such as K-3 and Inconel 690.

2.4.1 Investigation of Eskolaite Formation

The formation of salt in waste glasses is clearly influenced by the chromium content of the feed, as seen in the sulfate solubility model for LAW glasses, but less so with HLW glasses (likely because of the higher prevalence of three valent chromium in HLW). The Cr_2O_3 content of the melt also strongly increases the amount of spinel formed at a given temperature as seen in the spinel models described in Section 2.2.

A series of high Cr_2O_3 glasses were formulated and tested in the DM-100 melter (Matlack et al. 2009b). The Cr_2O_3 content of these glasses extended up to 6 wt%. Crucible-scale testing of these glasses showed that for the glasses specifically formulated to have low sulfur and transition metals (e.g., those prone to eskolaite formation), the fraction of eskolaite in the melt after 70-hour heat treatments at 950°C roughly corresponded to the total Cr_2O_3 content of the glass. This is shown in Figure 2.16, where the blue data points ("ES series" glasses) have eskolaite concentrations roughly equal to the maximum amount of all Cr_2O_3 precipitated in the form of eskolaite. There is a slightly higher eskolaite fraction for the glasses with >3 wt% Cr_2O_3, which is likely caused by the inclusion of some Al_2O_3 and/or Fe_2O_3 in the eskolaite, because they are known to form solid solutions (Hrma et al. 2006). Also shown in the plot is a single "M-series" glass that precipitated both spinel and eskolaite and became an outlier to the general trend observed in glasses that precipitated eskolaite only—only the eskolaite fraction is shown on the plot.

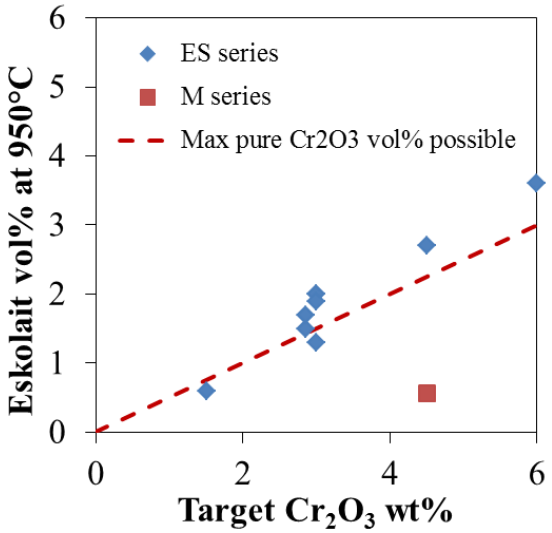

Figure 2.16. Eskolaite vol% in High-Cr_2O_3 Crucible-Scale Glasses Heat Treated at 950°C for 70 Hours (data from Matlack et al. 2009b)

Eskolaite crystals are typically small, plate-like crystals that do not settle readily in glass melts. An example of the morphology is shown in Figure 2.17. It is thus theorized that on an equal volume basis, eskolaite is less likely to cause melter-operation problems than spinel that typically grows to an octahedron or similar.

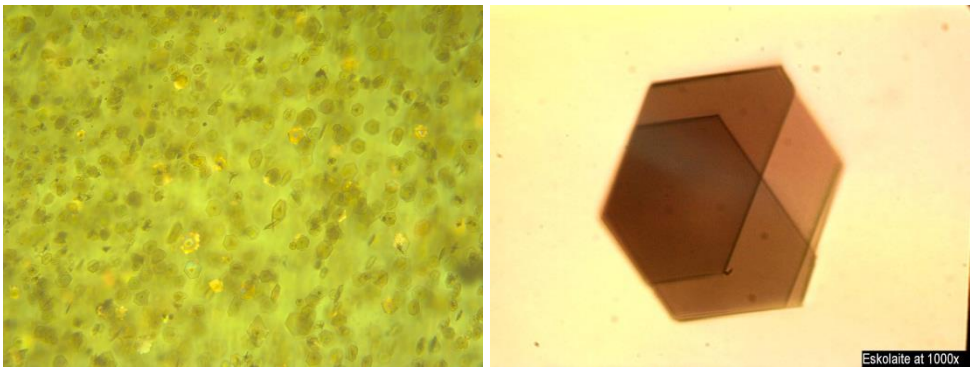

Figure 2.17. Optical Micrographs of Eskolaite in High-Cr_2O_3 HLW Glasses

Two melter tests were performed to develop an initial indication of the eskolaite behavior in the melter (Matlack et al. 2009b). In the first melter test, a glass with 2 vol% eskolaite was fabricated (2 vol% was obtained from crucible-scale glass heat treated at 950°C for 70 hours). In the second melter test a glass with 4.2 vol% combined eskolaite and spinel was fabricated (4.2 vol% was obtained from crucible-scale glass heat treated at 950°C for 70 hours). These melter tests were operated for roughly 50 hours each of continuous feeding in the DM-100 melter. The melter was then idled for 181 to 299 hours. The results did not indicate any potential problems with this amount of crystals. However, the results are too limited (up to only 299 hours) to clearly determine if this amount of crystals could be processed over extended time periods. Additionally, it was shown that during idling, the spinel settled significantly faster than either eskolaite or hematite crystals, which is consistent with the theory based on particle morphology.

By assuming that eskolaite and spinel can be tolerated equally well in the melter, preliminary limits for Cr_2O_3 in glass can be postulated. Taking a conservative assumption that all of the Cr_2O_3 precipitates in the form of either high-chromium spinel ([Fe,Mn,Ni,Zn]Cr_2O_4) or eskolaite (Cr_2O_3), the maximum amount of crystal formed for each mass fraction increase in Cr_2O_3 would range between 0.46 and 0.77 vol% (assuming densities of 2.5, 5.2, and 4.6 for melt, eskolaite, and spinel, respectively). This maximum value represents 72 to 120% of the effect of Cr_2O_3 on c_{950}. This suggests that using the c_{950} model will give a reasonable estimate of the maximum fraction of crystals to form in high Cr_2O_3 glasses. If all Cr_2O_3 crystallized as eskolaite and there was a 2 vol% limit on eskolaite at 950°C, then the maximum $w_{Cr_2O_3}$ would be 4 wt%. This compares well with the spinel limit model validity range of up to 4.5 wt% Cr_2O_3. Recommended Cr_2O_3 concentration limit is given in Section 2.9 where all single component model validity constraints are discussed.

2.4.2 Future Plans

Additional data are needed to measure and model the formation of eskolaite in representative Hanford HLW glasses. These data will be collected along with eskolaite accumulation rate data as an extension of the efforts to manage spinel in the melter, as described in Section 2.2.

2.5 Viscosity

The viscosity of waste glass melts should be maintained between roughly 2 and 8 Pa·s (20 to 80 P) at the melting temperature (nominally 1150°C) for ideal processing. Perez (2006) summarizes this need as follows.

> *Joule-heated ceramic melters (JHCM) have been under development and application by DOE and internationally for the production of borosilicate glass in radioactive environments. As operating conditions, glass formulations, and materials of construction have been assessed the practical limits of glass viscosity have been established. For melters operating at a nominal bulk tank temperature of 1150°C, waste glass composition have been tailored to achieve a glass viscosity of between 20 and 80 Poise. The lower limit of 20 Poise has its roots in the following historical considerations; 1) limiting refractory and metal alloy corrosion of the melter components in contact with the molten glass, 2) limiting glass penetration through the refractory lining and 3) minimizing the potential for an energetic water-glass reaction (the so-called steam explosion) and 4) achieving acceptable pouring of the glass over the pour tip of the discharge trough. These considerations when combined with providing a reasonable range for glass formulations that also have acceptable electrical conductivity and durability (leach resistance) result in the 20 Poise value for a lower viscosity limit.*
>
> *The upper limit of 80 Poise is based on the following considerations; 1) obtaining an acceptable convective heat transfer rate between the bulk glass and the cold cap solids, 2) minimizing the stability and accumulation of foam caused by gases formed during the melting process, 3) acceptable transfer of glass from the tank through the riser/discharge using the airlift transfer system, and 4) acceptable filling of the canister, i.e., no voids near the canister wall. Again when these considerations are combined with providing a reasonable range for glass formulations that also have acceptable electrical conductivity result in the 80 Poise value for an upper viscosity limit.*

Although the acceptable range of η_{1150} is 2 to 8 Pa·s, current glass formulations and optimal performance are centered closer to 5 Pa·s. Therefore, a narrower viscosity range of $4 \le \eta_{1150} \le 6$ Pa·s is recommended for estimating loading of HLW (and LAW) in glass.

Sufficient new viscosity data for HLW glasses have been generated since the HTWOS 2009 and WTP Baseline glass property models were developed to justify a new viscosity model. Several approaches have been used to model the temperature and composition effects on viscosity in the past. For the current purpose, the effect of composition on the viscosity at 1150°C is of most interest. LMMs and PQMMs for the natural logarithm of viscosity data at 1150°C were investigated. The LMM has the form

$$\ln(\eta_{1150}, \text{Pa-s}) = \sum_{i=1}^{q} a_i g_i \ , \tag{2.22}$$

while the PQMM has the form

$$\ln(\eta_{1150}, \text{Pa-s}) = \sum_{i=1}^{q} a_i g_i + \text{Selected}\left\{ \sum_{i=1}^{q} a_{ii} g_i^2 + \sum_{i=1}^{q-1} \sum_{j=i+1}^{q} a_{ij} g_i g_j \right\}, \quad (2.23)$$

where

q = number of HLW glass components in the model

a_i = model coefficient for the i^{th} HLW glass component

g_i = mass fraction of the i^{th} HLW glass component, so that $g_1 + \ldots + g_{q=\text{Others}} = 1.0$

a_{ii} = coefficient for the squared term of the i^{th} HLW glass component

a_{ij} = coefficient of the crossproduct term involving the i^{th} and j^{th} HLW glass components.

Only selected quadratic terms in Equation (2.23) can be chosen because of the constraint $g_1 + \ldots + g_{q=\text{Others}} = 1.0$. See Piepel et al. (2002) for more discussion of PQMMs.

2.5.1 Viscosity Data for HLW Glasses

Data from several different sets of HLW and LAW glasses were combined to create the dataset used for modeling η_{1150} of HLW glasses. The datasets included the following

- ***Set 1***: EM07 glasses (Schweiger et al. 2011)
- ***Set 2***: HTWOS HLW models; filename (Vienna et al. 2009)
- ***Set 3***: VSL ORP HLW dataset 2012 (Muller et al. 2012)
- ***Set 4***: VSL-15T3800-1 (Kot et al. 2015)
- ***Set 5***: EWG dataset (Chou et al. 2016)
- ***Set 6***: VSL-15R3250-1 Rev. 0 (Matlack et al. 2015b)
- ***Set 7***: VSL-15R3420-1 Rev. 0 (Gan et al. 2015)
- ***Set 8***: VSL-15R3440-1, Rev. 0 (Matlack et al. 2015a)
- ***Set 9***: DWPF Startup Frit (Crum et al. 2012)
- ***Set 10***: LAW dataset (see Table 3.8)

The combined dataset includes 725 LAW and 785 HLW glasses with η_{1150} data ranging from 0.47 to 99.4 Pa·s (LAW) and 0.279 to 245.5 Pa·s (HLW). The major component concentration ranges are given in Table 2.15 and the pairwise distributions of glass compositions are shown in a scatterplot matrix in Figure 2.18.

Table 2.15. Component Concentration Ranges (mass fractions) in the η_{1150} Modeling Dataset Including HLW and LAW Glasses

	HLW		LAW	
Component	Min	Max	Min	Max
Al_2O_3	0	0.3000	0.0350	0.1821
B_2O_3	0	0.2200	0	0.1380
Bi_2O_3	0	0.1641	0	0.0002
CaO	0	0.1820	0	0.1273
Cr_2O_3	0	0.0300	0	0.0060
F	0	0.0281	0	0.0130
Fe_2O_3	0	0.2639	0	0.1198
K_2O	0	0.0899	0	0.0809
LN_2O_3[(a)]	0	0.1127	0	0.0489
Li_2O	0	0.0788	0	0.0633
MgO	0	0.0801	0	0.0815
MnO	0	0.1360	0	0.0006
Na_2O	0.01	0.3000	0.0245	0.3500
NiO	0	0.0851	0	0.0017
P_2O_5	0	0.0702	0	0.0403
SiO_2	0.1944	0.6002	0.3350	0.6278
SnO_2	0	0.0068	0	0.0503
SO_3	0	0.0128	0.0002	0.0246
SrO	0	0.2990	0	0.0788
ThO_2	0	0.0601	0	0
TiO_2	0	0.0171	0	0.0399
UO_3	0	0.1255	0	0
V_2O_5	0	0.0250	0	0.0570
ZnO	0	0.0400	0	0.0978
ZrO_2	0	0.1548	0	0.0675

(a) LN_2O_3 is the combined mass fractions of Y_2O_3 and all the rare-earth oxides (which are all assumed to be in the trivalent state).

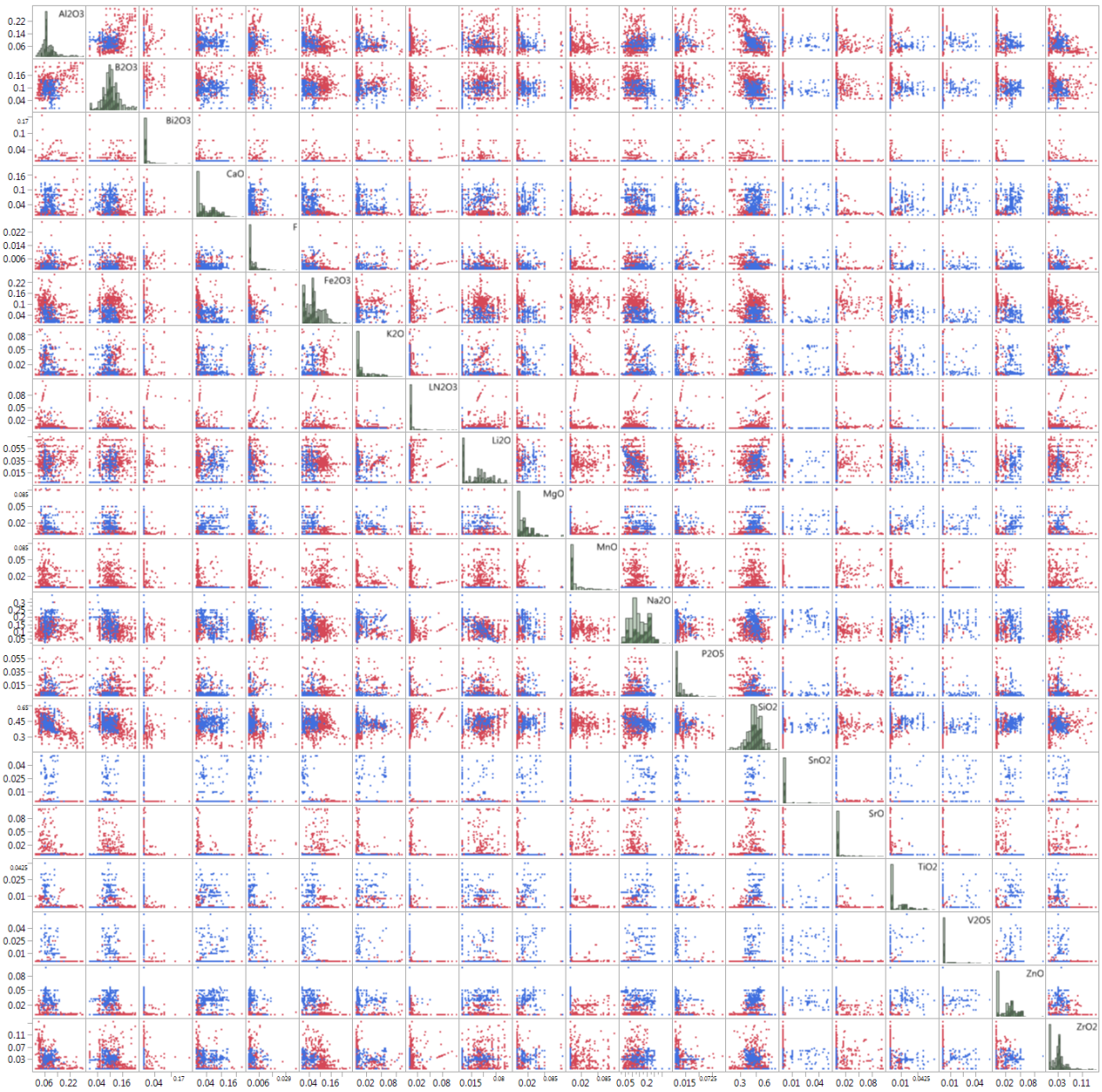

Figure 2.18. Scatterplot Matrix of Glass Compositions (mass fractions) in the Modeling Dataset for Viscosity at 1150°C. Red points represent HLW glasses, while blue points represent LAW glasses.

After the HLW and LAW glass datasets were assembled separately, they were carefully combined into a single spreadsheet. Each data point (each separate Glass ID) was labeled with a "HLW" or "LAW" tag to designate each type of glass. Additionally, the rare-earths were grouped into a single component called "LN_2O_3" so that the combined effect of rare-earths could be investigated during model development.

The HLW and LAW data were fit to several LMMs and a PQMM to identify components having significant effects on η_{1150}. A LMM for the combined HLW and LAW glasses was the first model attempted, followed by a LMM with HLW glasses only. Finally, a PQMM was developed with both

HLW and LAW glasses included. These models are discussed in Sections 2.5.2, 2.5.3, and 2.5.4, respectively. The LMM with LAW glasses only is discussed in Section 3.4.

2.5.2 Model #1 – Linear Mixture Model for Viscosity at 1150ºC Fit to Data for HLW and LAW Glasses

A LMM was fit to the combined HLW and LAW dataset. The coefficients and summary statistics for this LMM are listed in Table 2.16. The R^2 = 0.9107 indicates the model fits very well. The R^2_{Adj} = 0.9097 value being very close to the R^2 value indicates that there are not several unneeded terms in the model. The R^2_{Pred} and R^2_{Val} values are also very close to the model fit R^2. This suggests that across the breadth of the combined LAW and HLW glass composition and viscosity data, the LMM accounts for roughly 90% of the variation in data both used to fit the model and not used to fit the model. The RMSE = 0.2405 in ln(Pa·s) indicates an %RSD = 24.04 for "measured" η_{1150} values. This %RSD value is larger than the experimental and measurement uncertainty in the process of measuring viscosity at temperature data, fitting a Voget-Fulcher-Tammann (VFT) equation, and calculating the η_{1150} for a given glass. Hence, the RMSE value indicates that the model has some LOF.

Table 2.16. Model Coefficients and Selected Statistics for a Linear Mixture Model of the Natural Logarithm of Viscosity at 1150ºC Fit to All HLW and LAW Glasses

Model Term	Coefficient, ln(η_{1150}, Pa·s)	Statistic	Value
Al_2O_3	12.415516	# of glasses	1510
B_2O_3	-7.801257	Average ln(η1150, Pa·s)	1.589
CaO	-7.522078	RMSE, ln(η1150, Pa·s)	0.2405
F	-12.809553	R^2	0.9107
K_2O	-3.277962	R^2_{Adj}	0.9097
LN_2O_3	2.0426415	R^2_{Pred}	0.9068
Li_2O	-34.591303	R^2_{Val}	0.9075
MnO	-6.016994		
Na_2O	-9.469464		
P_2O_5	5.1318727		
SiO_2	9.0203141		
SnO_2	3.4888111		
SrO	-5.737294		
TiO_2	-6.633455		
UO_3	1.9888519		
ZnO	-3.649457		
ZrO_2	6.367637		
Others	-0.807473		

Figure 2.19 shows a plot of predicted vs. measured ln(η_{1150}) values with 90% PIs for the 1510 HLW and LAW glasses used to fit the LMM in Table 2.16. If a 90% PI overlaps the 45º line, then the predicted and measured values are not statistically different (with 90% confidence) after accounting for data and model uncertainties. The 90% PIs for 1415 of the 1510 glasses (93.7%) in Figure 2.19 overlap the 45º line. Thus, the predicted ln(η_{1150}) values are generally within prediction uncertainties of the measured ln(η_{1150}) values. Ignoring the PIs, Figure 2.19 shows the LMM has a tendency to underpredict ln(η_{1150}) below approximately -0.5 and above approximately 4.0. In η_{1150} units of Pa·s, these values are 0.6 and 54.6, respectively. These are well outside the constraint limits for η_{1150} of 4 to 6 Pa·s. Hence, the LMM in Table 2.16 predicts η_{1150} without substantive bias within the limiting range of 4 to 6 Pa·s.

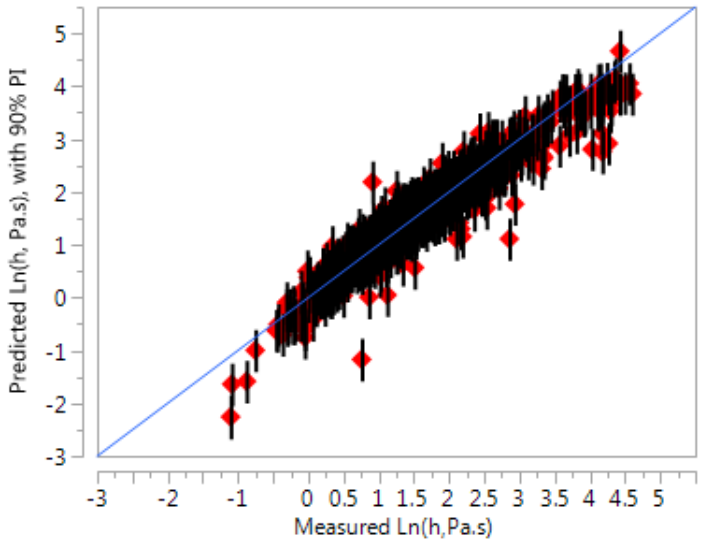

Figure 2.19. Predicted vs. Measured Plot of ln(η_{1150}) Values with 90% Prediction Intervals Using the Linear Mixture Model Fit to Data from HLW and LAW Glasses

2.5.3 Model #2 – Linear Mixture Model for Viscosity at 1150ºC Fit to Data from HLW Glasses Only

A LMM was fit to the HLW-only dataset of compositions and η_{1150} values for 785 HLW glasses. The major component concentration ranges for these glasses are given in Table 2.15. The coefficients and summary statistics for this LMM are listed in Table 2.17. The model fits quite well with R^2 = 0.9027, and the R^2_{Adj}, R^2_{Pred} and R^2_{Val} values are only slightly smaller. Hence, this suggests that across the HLW glass composition and viscosity data, the LMM accounts for roughly 90% of the variation in data both used to fit the model and not used to fit the model. Interestingly, the R^2 values are slightly lower (and RMSE value slightly higher) for the HLW-only model than the combined LAW and HLW model. This is likely due to the HLW-only data covering a smaller glass composition region with a smaller range of η_{1150} values.

Table 2.17. Model Coefficients and Selected Statistics for a Linear Mixture Model of the Natural Logarithm of Viscosity at 1150ºC Fit to All HLW Glasses

Model Term	Coefficient, $\ln(\eta_{1150}$, Pa·s)	Statistic	Value
Al_2O_3	12.093093	# of glasses	785
B_2O_3	-6.968649	Average ln(Pa·s)	1.527
CaO	-7.867327	RMSE, ln(Pa·s)	0.2685
Cr_2O_3	10.263034	R^2	0.9027
F	-18.405435	R^2_{Adj}	0.9007
LN_2O_3	3.5927373	R^2_{Pred}	0.8930
Li_2O	-34.656075	R^2_{Val}	0.8954
MnO	-6.137735		
Na_2O	-9.383399		
NiO	4.1828203		
P_2O_5	2.8993337		
SiO_2	8.7348186		
SrO	-5.661461		
TiO_2	-9.632734		
UO_3	2.4199882		
ZrO_2	6.1936719		
Others	-0.982565		

The LMM in Table 2.17 has RMSE = 0.2685 in ln(Pa·s), which indicates an %RSD = 26.85 for "measured" η_{1150} values. This %RSD value is larger than the experimental and measurement uncertainty in the process of measuring viscosity at temperature data, fitting a VFT equation, and calculating the η_{1150} for a given glass. Hence, the RMSE value indicates that the model has some LOF.

Figure 2.20 shows a plot of predicted vs. measured $\ln(\eta_{1150})$ values with 90% PIs for the 785 LAW glasses used to fit the LMM in Table 2.17. If a 90% PI overlaps the 45º line, then the predicted and measured values are not statistically different (with 90% confidence) after accounting for data and model uncertainties. The 90% PIs for 736 of the 785 glasses (93.8%) in Figure 2.20 overlap the 45º line. Thus, the predicted $\ln(\eta_{1150})$ values are generally within prediction uncertainties of the measured $\ln(\eta_{1150})$ values. Ignoring the PIs, Figure 2.20 shows the LMM has a tendency to underpredict $\ln(\eta_{1150})$ below approximately -0.5 and above approximately 3.5. In η_{1150} units of Pa·s, these values are 0.6 and 33.1, respectively. These are well outside the constraint limits for η_{1150} of 4 to 6 Pa·s. Hence, the LMM in Table 2.17 predicts η_{1150} without substantive bias within the limiting range of 4 to 6 Pa·s.

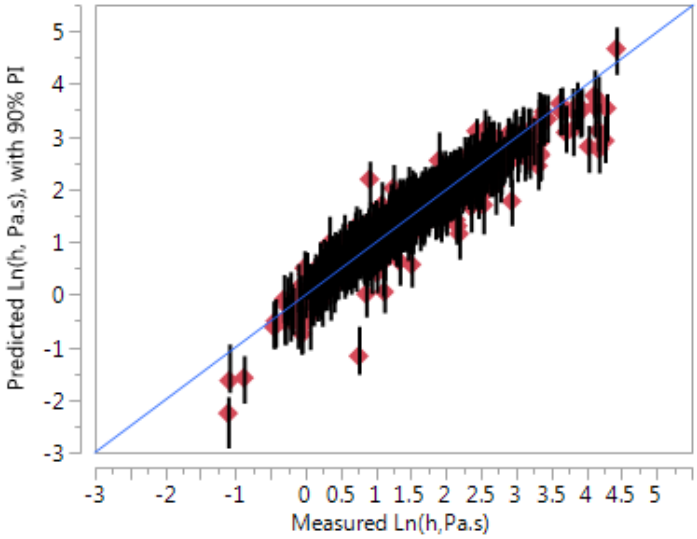

Figure 2.20. Predicted vs. Measured ln(η_{1150}) Values with 90% Prediction Intervals [ln(η_{1150})] Using the Linear Mixture Model Fit to Data from HLW Glasses

2.5.4 Model #3 – Partial Quadratic Mixture Model for Viscosity at 1150ºC Fit to Data from HLW and LAW Glasses

In the third model developed, the LMM was augmented by a limited number of quadratic terms (three) to form a PQMM (Piepel et al. 2002). This model was fit to the combined data from LAW and HLW glasses. The coefficients and summary statistics for this model are listed in Table 2.18. The model fit is improved by the addition of the three quadratic terms, which result in R^2 = 0.9253. The R^2_{Adj}, R^2_{Pred} and R^2_{Val} values are only slightly smaller. This suggests that across the combined LAW and HLW composition and viscosity data, the PQMM is able to account for roughly 92% in the variation in data both used to fit the model and not used to fit the model.

Figure 2.21 shows a plot of predicted vs. measured ln(η_{1150}) values with 90% PIs for the 1510 HLW and LAW glasses used to fit the PQMM in Table 2.18. If a 90% PI overlaps the 45º line, then the predicted and measured values are not statistically different (with 90% confidence) after accounting for data and model uncertainties. The 90% PIs for 1408 of the 1510 glasses (93.2%) in Figure 2.21 overlap the 45º line. Thus, the predicted ln(η_{1150}) values are generally within prediction uncertainties of the measured ln(η_{1150}) values. Ignoring the PIs, Figure 2.21 shows the PQMM has a tendency to underpredict ln(η_{1150}) below approximately -0.5 and above approximately 3.5. In η_{1150} units of Pa·s, these values are 0.6 and 33.1, respectively. These are well outside the constraint limits for η_{1150} of 4 to 6 Pa·s. Hence, the LMM in Table 2.18 predicts η_{1150} without substantive bias within the limiting range of 4 to 6 Pa·s.

Table 2.18. Model Coefficients and Selected Statistics for a Partial Quadratic Mixture Model of the Natural Logarithm of Viscosity at 1150ºC Fit to All HLW and LAW Glasses

Model Term	Coefficient, $\ln(\eta_{1150}$, Pa·s)	Statistic	Value
Al_2O_3	12.34002	# of glasses	1510
B_2O_3	-8.136744	Average ln(Pa·s)	1.589
CaO	-7.540488	RMSE, ln(Pa·s)	0.2203
Cr_2O_3	8.8445457	R^2	0.9253
F	-18.217558	R^2_{Adj}	0.9243
K_2O	-3.697342	R^2_{Pred}	0.9208
Li_2O	-34.400958	R^2_{Val}	0.9218
MnO	-5.91489		
Na_2O	-9.675683		
NiO	3.8137787		
P_2O_5	4.3595093		
SiO_2	8.9079268		
SnO_2	4.2538858		
SrO	-5.932515		
TiO_2	-3.20823		
UO_3	1.9226832		
ZnO	-2.798958		
ZrO_2	6.5218116		
Others	-0.660038		
$B_2O_3 \times B_2O_3$	24.99695		
$Al_2O_3 \times Na_2O$	26.937827		
$B_2O_3 \times Na_2O$	-24.314018		

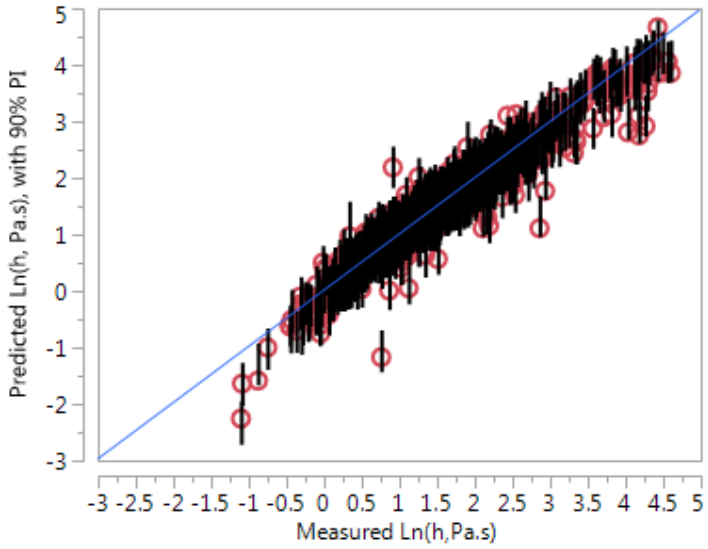

Figure 2.21. Predicted vs. Measured ln(η_{1150}) Values for the Partial Quadratic Mixture Model Fit to Data from LAW and HLW Glasses

2.5.5 Summary and Recommended Model for Viscosity at 1150ºC

For each model, the signs (positive or negative) of the individual components were the same, but with different magnitudes. The following components had an increasing effect on viscosity: Al_2O_3, Cr_2O_3, LN_2O_3, NiO, P_2O_5, SiO_2, SnO_2, UO_3, and ZrO_2. The following components had a decreasing effect on viscosity: B_2O_3, CaO, F, K_2O, Li_2O, MnO, Na_2O, SrO, TiO_2, ZnO, and Others. Figure 2.22 shows a comparison of the LMM coefficients for the LAW-only (Section 3.4), HLW-only (Section 2.5.3), and HLW+LAW (Section 2.5.2) datasets. It is clear from the figure that the models generally have similar coefficients for each component.

Although the combined HLW+LAW model has improved R^2 over the HLW-only model, the R^2 for HLW-only data calculated using the combined HLW+LAW model is actually lower than the HLW-only model (0.898 vs 0.903). In addition, the LAW-only model presented in Section 3.4 shows improved fit statistics compared to the combined HLW+LAW model given here. It is therefore recommended that Model 2 (HLW-only, LMM) be used for predicting ln(η_{1150}) of HLW glasses.

The data and models are not fully QA compliant and therefore are not intended to be used in quality-affecting activities or decisions (e.g., design basis input, plant operations, waste form compliance). Instead the models and constraints are intended for use in mission planning activities.

.

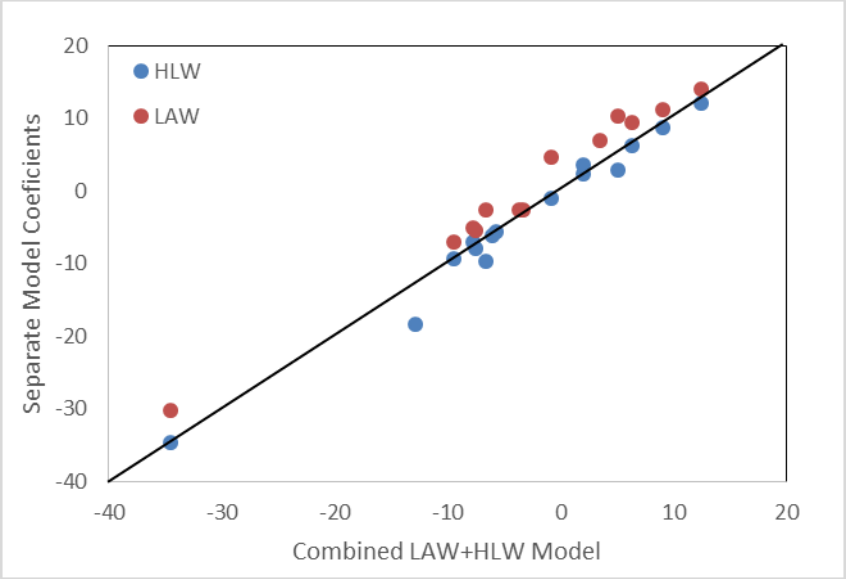

Figure 2.22. Comparison of LMM Coefficients for ln(η_{1150}) Fit to LAW-Only, HLW-Only, and Combined HLW+LAW Datasets

2.5.6 Future Plans

Viscosity models will need to be developed for plant operation. While models predicting the ln(η_{1150}) are sufficient for glass mass estimation, models that predict the temperature impact of viscosity will be useful for many plant operating applications (including meeting design constraints at 1100 and 1200°C). Therefore, as additional HLW glass property testing continues, the measurement of viscosity will continue to be performed over a range of temperatures. When plant operating models are needed, these viscosity data will be fitted to functions of both composition and temperature.

2.6 Product Consistency Test

The WTP contract (DOE 2000), the Waste Acceptance Product Specifications (DOE 1996), and the Waste Acceptance System Requirements Document (OCRWM 2008) all require the PCT responses of HLW glasses to meet the standard, with sufficient confidence, and be reported during production. The standard is that the PCT responses of B, Li, and Na, normalized to their concentration in the glass, be below those of the DWPF Environmental Assessment (EA) glass (Jantzen et al. 1993).

The latest existing PCT model (Vienna et al. 2013) was evaluated to determine if it adequately predicted the PCT responses of new enhanced HLW glasses that were not used to fit the model. Vienna et al. (2013) clearly demonstrated that Al_2O_3 has a nonlinear impact on PCT response that was fitted using higher-order polynomial terms for Al_2O_3 (2^{nd}, 3^{rd}, and 4^{th} order Al_2O_3 terms). This model more accurately estimated the PCT response when Al_2O_3 was at low (0 – 6 wt%), moderate (6 – 20 wt%) and high (> 20 wt%) concentrations that were used to fit the model. However, the model still did not accurately predict the PCT response for very high Al_2O_3 glasses (> 25 wt%) that were not used to fit the model. This was expected because of the lack of data in the high and very high Al_2O_3 region. There are also other possible reasons for the poor prediction performance such as nonlinear blending effects of components

(i.e., curvature and interaction effects, which are partially confounded). Nonlinear blending effects of components are likely variable within the large composition space of this global model. In an attempt to find additional nonlinear effects a few different modeling approaches were examined besides the approach previously taken by Vienna et al. (2013). These approaches are discussed in Section 2.6.2.

2.6.1 Product Consistency Test Data for HLW Glasses

A dataset of 2758 HLW glasses was compiled to model the PCT response of quenched glasses over the composition region of interest for HLW at Hanford, see Table 2.19. The multivalent components were normalized to a consistent valance state (for example, FeO, Fe_2O_3, and Fe_3O_4 were converted to Fe_2O_3) after which the compositions (in mass fractions) were renormalized to a total of one to prepare them for modeling.

Table 2.19. Data for PCT Modeling of HLW Glasses

# Data	Dataset/study	Reference
1283	Existing data 2013 model	Vienna et al. 2013
1302	SRNL dataset	Taylor et al. 2004
50	EWG study	Chou et al. 2016
31	Nepheline matrix study	Kroll et al. 2016
20	CCIM study	Smith et al. 2014
72	VSL studies	Kot et al. 2015

The database was trimmed down to 1712 data points by excluding glasses with extreme concentrations to achieve desirable component distributions (as an example, one or a few glasses with a concentration ≥ 12 wt% for a certain component are removed if all other glasses had a reasonable distribution up to 8 wt%). The resulting model validity range and ranges of PCT responses are given in Table 2.20. The components that were trimmed included F, BaO, CaO, Fe_2O_3, K_2O, Li_2O, MgO, MnO, Nd_2O_3, P_2O_5, SrO, SO_3, ThO_2, TiO_2, UO_3, ZnO, ZrO_2, and "Others". HLW glasses designed for Idaho waste streams (calcine and sodium bearing waste) were excluded based on historical LOF evidence for PCT models applicable to Hanford. Twenty one additional data points were removed from the dataset as outliers because they did not fit any of the models generated: 5 and 24 (Oksoy et al. 1994), PEI (Feng et al. 1996), NP-B-1 (Li et al. 1996), SRL-202-G and -P (Shade 1991), HLW98-27B, -31, -51R, -52R, -56, -58, -60, 62, -77, and -77CG (VSL-07R1240-04), SB5NEPH-25, -33, and -37 (SRNL WSRC-STI-2007-00659), and EWG-OL-2463 (PNNL). Three additional data points were found to be outliers in the PCT-Li model and were excluded; DG-WV29 and 30 (Brouns et al. 1988a) and HLW98-94 (VSL-07R1240-04).

Table 2.20. PCT (g/m^2), ln(PCT, g/m^2), and Component (mass fraction) Ranges of the Dataset Used to Model the PCT Response of HLW Glasses

Property or Component	Min	Max
PCT-B (g/m^2)	0.045	43.82
PCT-Na (g/m^2)	0.032	35.52
ln(PCT-B, g/m^2)	-3.10	3.78
ln(PCT-Na, g/m^2)	-3.44	3.57
Al_2O_3	0.0000	0.3600
B_2O_3	0.0392	0.2200
F	0.0000	0.0083
Fe_2O_3	0.0000	0.2065
Li_2O	0.0000	0.0747
MgO	0.0000	0.0500
Na_2O	0.0389	0.2390
SiO_2	0.2000	0.6235
TiO_2	0.0000	0.0499
ZnO	0.0000	0.0486
ZrO_2	0.0000	0.1300
Components Combined into Others Component		
BaO	0.0000	0.0118
CaO	0.0000	0.1001
CdO	0.0000	0.0147
K_2O	0.0000	0.0723
MnO	0.0000	0.0488
Nd_2O_3	0.0000	0.0284
P_2O_5	0.0000	0.0351
SO_3	0.0000	0.0143
SrO	0.0000	0.0488
ThO_2	0.0000	0.0495
UO_3	0.0000	0.0431
Sum of Others	0.0000	0.0498

A scatterplot matrix of the 1712 glasses in Figure 2.23 graphically shows the scatter of the data for each component relative to other components that were modeled, as well as a histogram for each component. Highly correlated components hinder accurate regression analysis; namely, separation of individual component effects. The most correlated components were Al_2O_3 to SiO_2 (-0.7409), followed by SiO_2 to B_2O_3 (-0.4945), UO_3 to B_2O_3 and B_2O_3 to Fe_2O_3 (-0.4736), and Al_2O_3 to Fe_2O_3 (-0.4682). It was

not surprising to see these were components negatively correlated because they were major components that were typically varied at the expense of one another to optimize key properties. However, the negative correlation between Al_2O_3 to SiO_2 is large enough that model fitting methods may not be able to correctly separate the (i) linear effects of Al_2O_3 and SiO_2 and (ii) nonlinear blending effects involving these two components. If this problem occurs, the resulting models should still have predictive ability commensurate with the goodness of fit of the model. However, it will be necessary to exercise caution in interpreting the effects of Al_2O_3 and SiO_2 based on the fitted models.

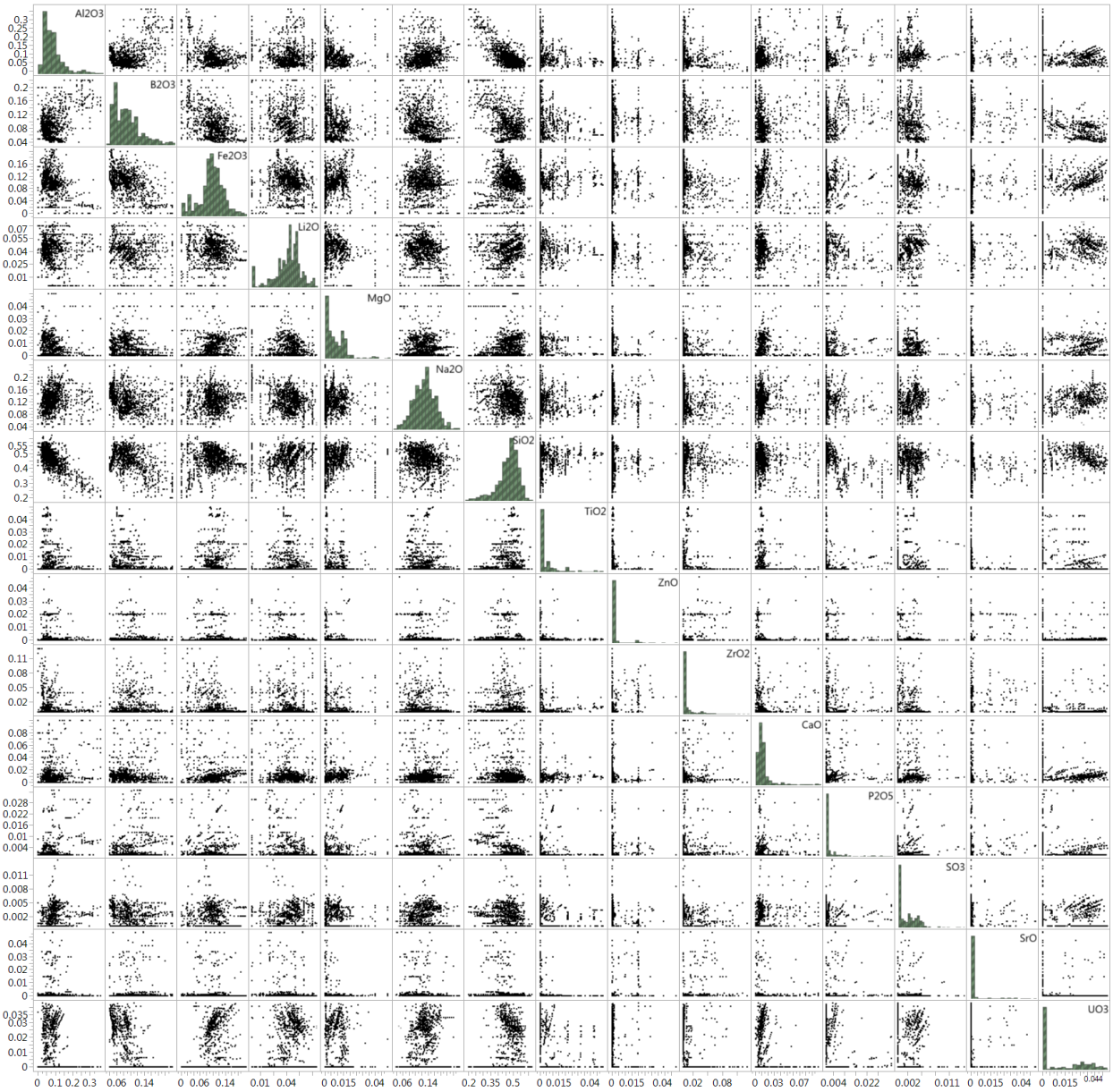

Figure 2.23. Scatterplot Matrix and Histograms for Compositions (mass fractions) of 1712 HLW Glasses

2.6.2 Product Consistency Test Models for HLW Glasses

Three modeling approaches were investigated to identify the best approach to model the PCT response over the large HLW glass composition space. With a large composition space the HLW glass structure changes significantly, possibly resulting in nonlinear blending effects (curvature and/or interactions, which are partially confounded) for some components. As previously mentioned, Vienna et al. (2013) found that Al_2O_3 has significant nonlinear curvature effects. It was possible that other major components such as SiO_2, Alkali, B_2O_3, also have significant nonlinear blending effects. Models that were attempted included (i) global PQMMs in mass fraction oxides (like Vienna et al 2013), (ii) global nonlinear regression models with a non-bridging oxygen, Q3, Q4, N3 and N4 components along with mole fraction oxides for other major components of the glass, and (iii) separate LMMs or PQMMs for each of three subregions determined by the mass fraction of Al_2O_3. The results of these investigations determined that the approach taken by Vienna et al. (2013) provides the best overall model for the PCT response of HLW glasses. The other approaches attempted provide equally predictive models, however they are more difficult to implement. For example, significant calculations are required to determine the NBO, Q3, Q4, N3, and N4 values and the overall fits are similar to the global mixture model. The approach with three separate LMMs or PQMMs for subranges of Al_2O_3 concentrations result in discontinuities (i.e., abrupt changes in PCT response at the Al_2O_3 boundaries), making it difficult to implement this model for glass formulation. Because these alternative models were more complex and did not offer a significant improvement, they were abandoned and a global PQMM, using mass fraction oxides, was chosen like the one used by Vienna et al. (2013)

$$\ln[\mathrm{PCT}] = \sum_{i=1}^{q} b_i g_i + \mathrm{Selected}\left\{ \sum_{i=1}^{q} b_{ii} g_i^2 + \sum_{i=1}^{q-1} \sum_{j=i+1}^{q} b_{ij} g_i g_j \right\} + b2_{Al_2O_3} g_{Al_2O_3}^2 + b3_{Al_2O_3} g_{Al_2O_3}^3 + b4_{Al_2O_3} g_{Al_2O_3}^4 + \ldots, \qquad (2.24)$$

where

$\ln[\mathrm{PCT}]$ = PCT response, either ln[PCT-B, g/m^2], ln[PCT-Na, g/m^2], or ln[PCT-Li, g/m^2]

b_i = coefficient for the i^{th} HLW glass component,

b_{ij} = coefficient for the crossproduct of the i^{th} and j^{th} HLW glass components, where a squared term results when $i = j$

g_i, g_j = mass fraction of the i^{th} and j^{th} HLW glass components

$b2_{Al_2O_3}$, $b3_{Al_2O_3}$, $b4_{Al_2O_3}$ = coefficients for higher-order Al_2O_3 mass fraction terms.

During the modeling effort, both the model-fit and validation statistics improved with the higher-order Al_2O_3 terms, as was expected. Squared and crossproduct terms for other components were considered, but were not found to significantly improve the fit using the R^2_{Pred} metric (see Table 2.21). R^2_{Pred}, R^2_{Val}, and validation residuals were used to decide which first-order terms and how many higher-order Al_2O_3 terms to include.

Table 2.21. R^2 and R^2_{Pred} for Various Numbers of Nonlinear Terms Included in the Model for ln[PCT-B] with HLW Glasses

Nonlinear Term	# of Nonlinear Terms Included	R^2	R^2_{Pred}	$R^2 - R^2_{Pred}$
None	0	0.6397	0.6292	0.0104
$(Al_2O_3)^2$	1	0.7823	0.7755	0.0068
$(Al_2O_3)^3$	2	0.7841	0.7754	0.0086
$(Al_2O_3)^4$	**3**	**0.8117**	**0.8043**	**0.0073**
$(B_2O_3)^2$	4	0.8226	0.8152	0.0074
$Al_2O_3 \times B_2O_3$	5	0.8268	0.8186	0.0082
$Al_2O_3 \times MgO$	6	0.8315	0.8232	0.0083
$Al_2O_3 \times Na_2O$	7	0.8345	0.8258	0.0087
$B_2O_3 \times Na_2O$	8	0.8381	0.8285	0.0096
$Al_2O_3 \times Li_2O$	9	0.8409	0.8304	0.0105
$Li_2O \times Na_2O$	10	0.8423	0.8316	0.0130
$(SiO_2)^2$	11	0.8440	0.8329	0.0111
$B_2O_3 \times Li_2O$	12	0.8455	0.8337	0.0119
$(TiO_2)^2$	13	0.8469	0.8350	0.0119
$SiO_2 \times Fe_2O_3$	14	0.8481	0.8357	0.0123
$B_2O_3 \times Fe_2O_3$	15	0.8484	0.8354	0.0130
$(Na_2O)^2$	16	0.8487	0.8351	0.0136

The final model terms and fit statistics are summarized in Table 2.22. The R^2 values range from 0.7611 for the ln(PCT-Li) model to 0.8117 for the ln(PCT-Na) model. The data-splitting approach described in Section 1.4 was used to validate the models, with the average of the five R^2_{Val} values reported in Table 2.22. The R^2_{Adj}, R^2_{Pred} and R^2_{Val} values are only slightly smaller than the R^2 values for each of the three models in Table 2.22, which indicate no problems with overfitted models or highly influential data points. The RMSE values in ln(PCT, g/m^2) units range from 0.4086 (PCT-Li) to 0.4781 (PCT-B). Because of the natural log transformation, these RMSE (standard deviation) values can be interpreted as %RSD values ranging from 40.86 to 47.81%. The experimental and measurement uncertainty in PCT responses are much smaller than this, which indicates that the models have some LOFs. This is likely a result of nonlinear blending effects (and possibly linear blending effects) of HLW components on PCT responses not being constant over the whole HLW glass composition region for which data were available and used for modeling. However, the models in Table 2.22 account for a high enough proportion of the variation of PCT responses in the data sets to be useful for the intended purposes of models in this report.

Table 2.22. Summary of ln[PCT, g/m^2] Response Model Coefficients and Fit Statistics for HLW Glasses

Model Term	ln[PCT-B] Coefficient	ln[PCT-Na] Coefficient	ln[PCT-Li] Coefficient
Al_2O_3	-78.7836	-71.6595	-63.9519
B_2O_3	11.8314	7.5035	9.7161
CaO	-4.2608	0.1647	-1.5756
Fe_2O_3	-0.1367	-1.2469	-1.5209
Li_2O	26.6872	23.9739	21.5220
MgO	22.2708	19.8924	16.0853
Na_2O	18.0511	20.0074	13.5925
P_2O_5	-10.1336	-10.0559	-6.3595
SiO_2	-4.5104	-4.5442	-3.3104
SO_3	18.6514	17.5527	16.7191
TiO_2	-7.3229	-7.9836	-4.6582
UO_3	-8.6123	-7.9687	-6.6933
ZnO	-7.3998	-12.3124	-9.9948
ZrO_2	-8.8810	-9.7138	-8.0739
Other	2.9184	3.9227	1.9047
$(Al_2O_3)^2$	638.3727	594.5920	523.1351
$(Al_2O_3)^3$	-2360.5420	-2330.9850	-1983.3580
$(Al_2O_3)^4$	3174.4550	3321.4927	2738.6894
Summaries of Model Fits			
# Observations	1712	1710	1635
Mean of ln[PCT]	-0.5532	-0.6016	-0.5466
RMSE	0.4781	0.4173	0.4086
R^2	0.7875	0.8117	0.7611
R^2_{Adj}	0.7854	0.8098	0.7586
R^2_{Pred}	0.7805	0.8043	0.7516
R^2_{Val}	0.7786	0.8005	0.7500

The fits of the three models are shown graphically as overlaid predicted vs. measured plots in Figures 2.24, 2.25, and 2.26. Generally speaking, there is slightly less scatter for the ln(PCT-Na) model than for the ln(PCT-B) model, and the ln(PCT-Li) model has slightly more scatter than either of the models. However, all of the models have very similar fits to their data. The models tend to underpredict ln(PCT) values: (i) less than approximately -2.6 (0.074 g/m^2) and (ii) and between approximately 1.0 (2.72 g/m^2) and 1.5 (4.48 g/m^2). The models also tend to overpredict ln(PCT) values greater than approximately 2.2 (9.03 g/m^2). Because the limit for PCT responses is 4 g/m^2, the above discussion indicates the models may underpredict PCT responses below the limit. However, as noted previously, the models can be used for the intended purpose, recognizing that there is some uncertainty in the model predictions.

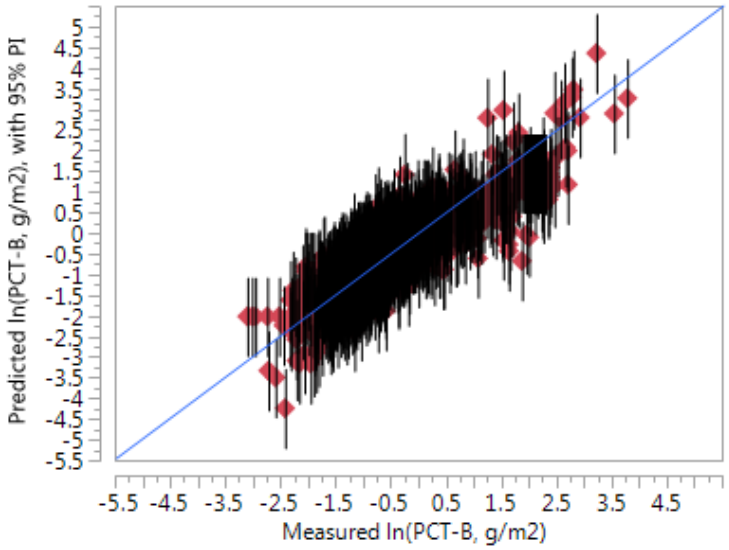

Figure 2.24. Predicted vs. Measured Plot of ln(PCT-B) Values and 95% Prediction Intervals [ln(g/m^2)] Using the Model in Table 2.22 Fit to HLW and LAW Glasses

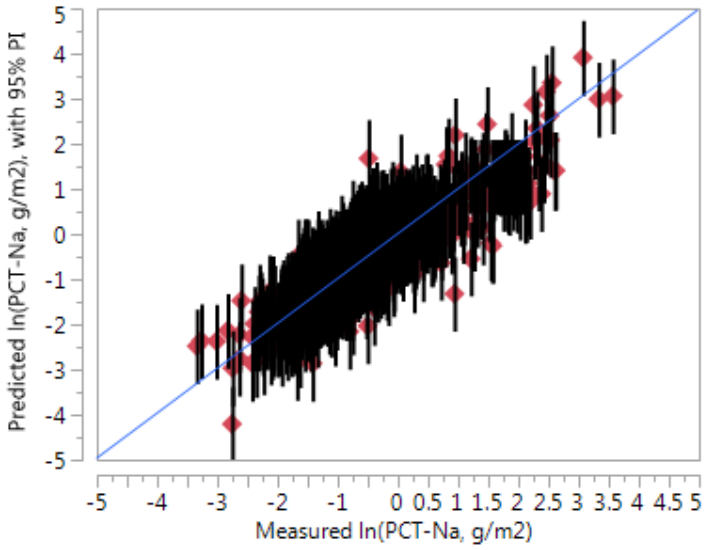

Figure 2.25. Predicted vs. Measured Plot of ln(PCT-Na) Values and 95% Prediction Intervals [ln(g/m^2)] Using the Model in Table 2.22 Fit to HLW and LAW Glasses

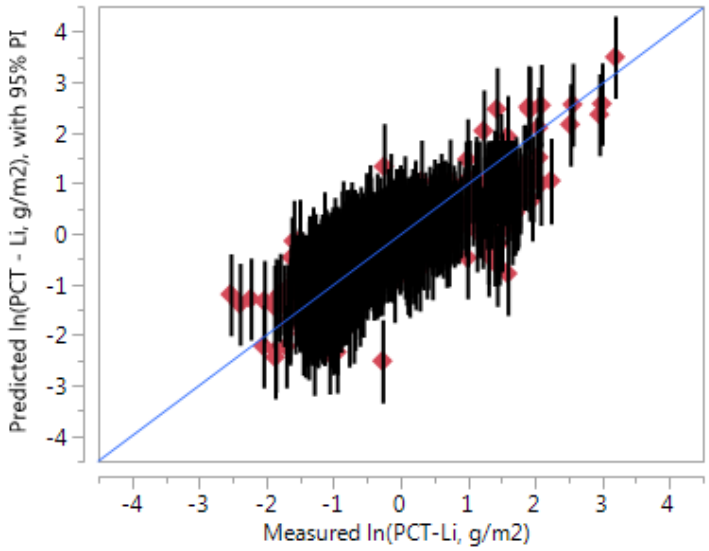

Figure 2.26. Predicted vs. Measured Plot of ln(PCT-Li) Values and 95% Prediction Intervals [ln(g/m^2)] Using the Model in Table 2.22 Fit to HLW and LAW Glasses

The prediction profile plots in Figure 2.27 show the predicted impact of each component on the ln(PCT-B) responses based on individual changes (solid black lines) from the composition denoted by the red dashed lines in the plots. The blue dashed lines estimate the uncertainty in the prediction profiles as a function of concentration for each component. The uncertainty appears to be larger at higher Al_2O_3 concentrations as would be expected, because less data are in this region to support the model fits. Note that Figure 2.27 is an example showing the model-predicted effects of varying each component from its value in a particular starting HLW glass composition.[1] If the starting composition is altered from the current location (red dashed lines), the plots (solid black lines) all change somewhat relative to what is shown. The Al_2O_3 plot shows the combined impact of the second-, third-, and fourth-order terms. The effect of Al_2O_3 dramatically reduces the PCT response below 5 wt% Al_2O_3, moderately reduces the response between 5 and 26 wt% Al_2O_3, and dramatically increases the response above 28 wt% Al_2O_3.

[1] Because the mass fractions of a glass composition sum to 1.0, it is not possible to vary a single component without offsetting changes in that component with changes in one or more other components. The prediction profile plots offset the changes in one component so as to keep all remaining components in the same relative proportions as the starting composition.

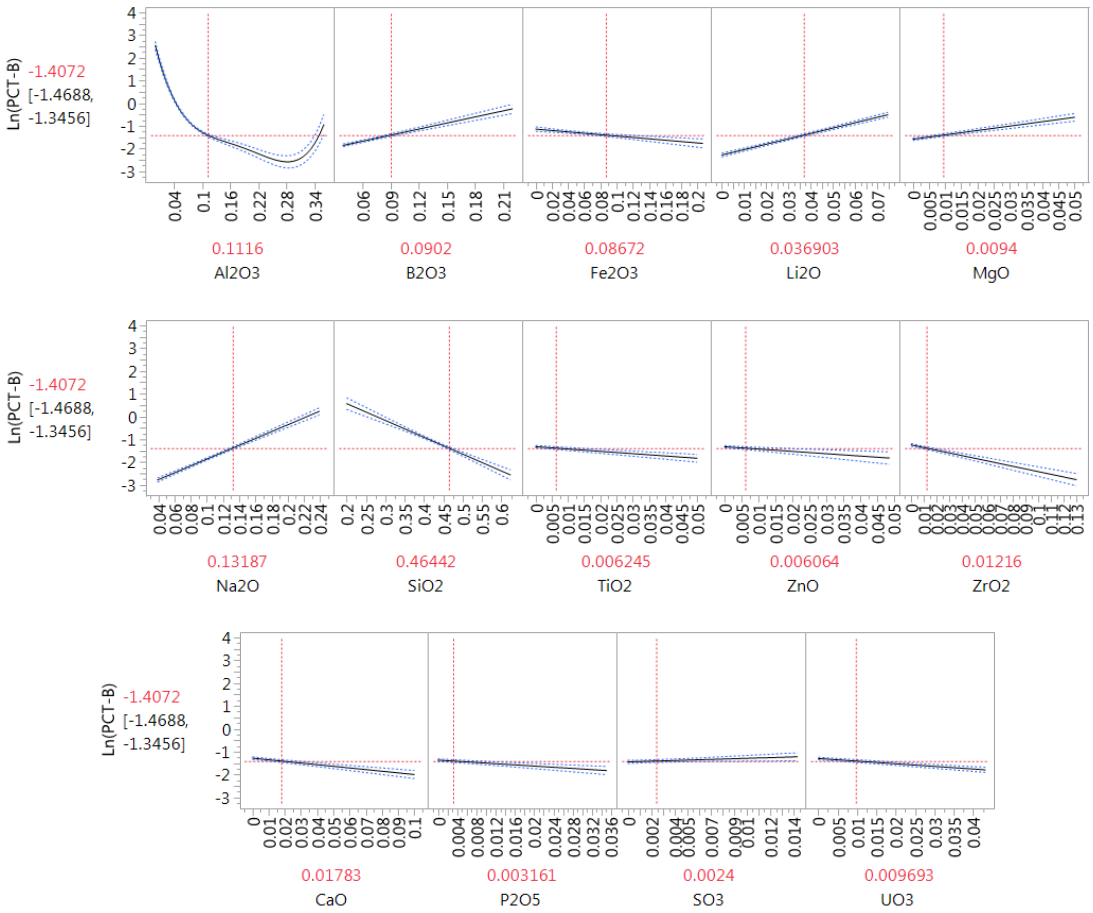

Figure 2.27. Component Effects Profiles for the HLW PCT-Boron Model

To validate the two models, the dataset was split into five groups and each group (20% of the data) was separately excluded from the model fitting. Then the excluded data were used to determine the R^2_{Val}. This resulted in five different R^2_{Val} for the five separate groups. The mean of these five R^2_{Val} is given in Table 2.22 for PCT models. Similar to previous models, the R^2_{Val} for the two models were very close to the R^2 of the models, indicating the models can predict future data well overall. Additionally, the R^2_{Pred} for each of the models was calculated and they also were close to the R^2 providing further evidence the models will predict well overall.

The PCT response models in Table 2.22 may have difficulty predicting the PCT response for HLW glasses with Al_2O_3 > 0.25 mass fraction, because of the small number of data points above that value. For this reason, the individual data points were examined by plotting the residuals of the validation models (80% datasets) versus the residuals of the fitted model (100% dataset) to identify poor fitting data points. Figure 2.28 shows the plots for the PCT-B and PCT-Na responses. Generally speaking, all of the data points have similar residuals versus validation residuals, resulting in an excellent linear relationship. However, three HLW glasses with Al_2O_3 > 0.36 mass fraction (C36-9, C36-20 and C36-21) significantly deviate from the linear relationship. These data points illustrate likelihood of less accurate and/or precise predictions of PCT responses for HLW glasses with Al_2O_3 concentrations > 0.36. As each of these data

points were removed during the validation process, the models no longer accurately predicted these glasses. The data points were also plotted in Figure 2.29 with $|(R-R_V)|$ from the ln(PCT-B) model versus Al_2O_3 concentration in glass, where R = residual and R_V = validation residual. Figure 2.29 shows that (i) the vast majority of glasses are below an Al_2O_3 mass fraction of 0.20, (ii) there is clearly a lack of data above an Al_2O_3 mass fraction of 0.25, and (iii) the model stops predicting well above an Al_2O_3 mass fraction of 0.30.

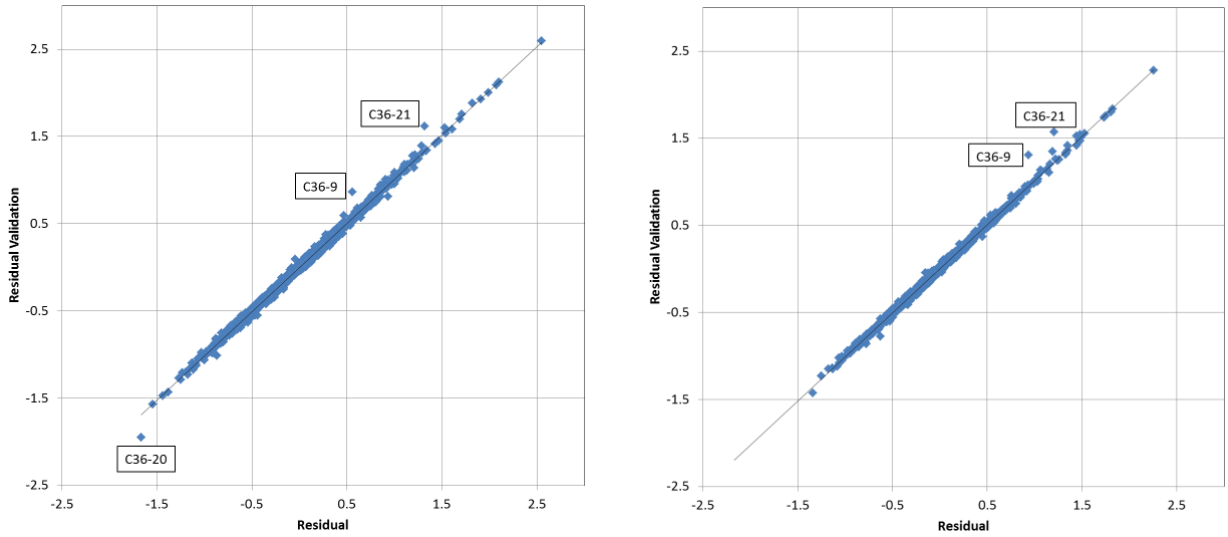

Figure 2.28. Residuals vs. Validation Residuals: left ln(PCT-B), right ln(PCT-Na), in g/m^2

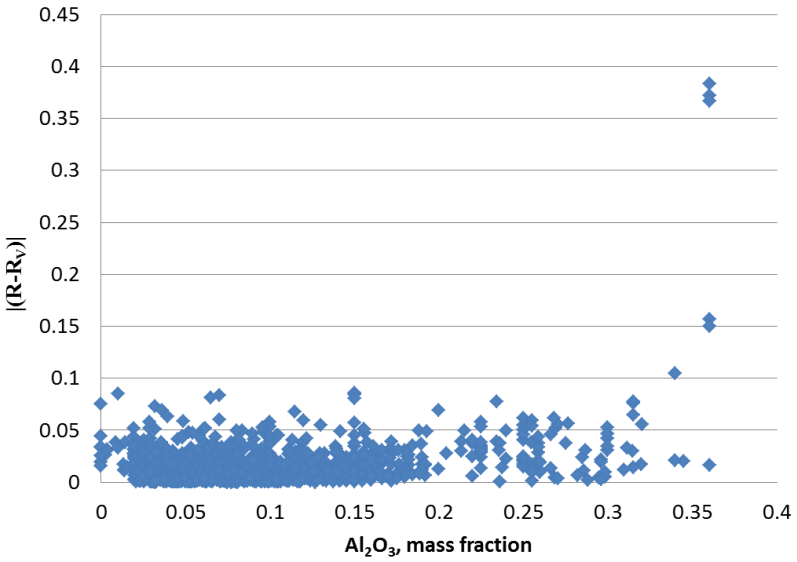

Figure 2.29. $|(R-R_V)|$ for the ln(PCT-B) Model versus Al_2O_3 Concentration, where R = Residual and R_V = Validation Residual

2.6.3 Future Plans

Given the difficulty with pretreatment, for example Al-dissolution may not be available at the time, the waste received at the WTP HLW melters may be high Al_2O_3 for at least a portion of the mission. Hence, such glasses will be limited by high concentrations of Al_2O_3 that tends to promote crystallization of nepheline and spinel. It is vital to expand the glass dataset and PCT-composition models to higher Al_2O_3 concentrations to accommodate glass formulations for these high Al_2O_3 waste streams. The major improvement of the PCT models in this report relative to the 2013 models was the expansion to higher Al_2O_3 concentrations. The models now can predict glasses up to an Al_2O_3 mass fraction of 0.30. However, Figure 2.28 and Figure 2.29 point out the need for more high-Al_2O_3 glasses to improve the predictability in the high-Al_2O_3 region. A high-Al_2O_3 test matrix with systematic changes of major glass components is needed to provide enough data to adequately support refitting the PCT models with nonlinear Al_2O_3 terms. Additionally, these new glasses should be designed for melting temperatures inside a joule heated melter (~ 1150°C). Current high-Al_2O_3 glasses above 0.30 mass fraction were designed for higher-temperature melters. Also note, the data and models are not NQA-1 compliant and therefore are not intended to be used in quality-affecting activities or decisions. Additional fully NQA-1 compliant data and models are needed for implementation in plant process control.

2.7 Zirconium-Containing Phases

The recommended T_L model for zirconium-containing phases is discussed in Section 2.7.1. Future plans are discussed in Section 2.7.2.

2.7.1 Model for Liquidus Temperature of Zirconium-Containing Phases

Enhanced glass formulation efforts have not yet focused on expanding the range of glasses containing significant concentrations of zirconium. Therefore, there is little basis for changing the zirconium-containing phase T_L model or limit. It is recommended that the HTWOS 2009 model and constraints (Vienna et al. 2009) be used for the present (2016) enhanced glass formulations until additional data are developed and this model can be updated or validated for higher zirconium based glasses.

This model is of the following form

$$T_L\text{-Zr} = \sum_{i=1}^{q} t_i g_i \ , \tag{2.25}$$

where T_L is the liquidus temperature (in °C), t_i is the coefficient of the i^{th} HLW glass component, and g_i is the mass fraction of the i^{th} HLW glass component. This model (coefficients and select statistical parameters) is summarized in Table 2.23. Similar to the other models, the HLW glass composition is in mass fractions. This model was shown to validate well and be predictive as long as the glasses were sufficiently high in ZrO_2 concentration (Vienna et al. 2009). The minimum g_{ZrO_2} for which the model is valid is 0.04 mass fraction (i.e., 4 wt%). This model should not be applied to glasses with lower g_{ZrO_2}, which are assumed not to form zirconium-containing phase.

The data and models are not fully QA compliant and therefore are not intended to be used in quality-affecting activities or decisions (e.g., design basis input, plant operations, waste form compliance). Instead the models and constraints are intended for use in mission planning activities.

Table 2.23. T_L-Zr Linear Mixture Model Coefficients and Selected Fit Statistics

Model Term	Coefficient, °C	Statistic	Value
Al_2O_3	3193.3628	# data points	69
B_2O_3	651.39721	Mean	1079
LN_2O_3[(a)]	2156.4074	RMSE	26.2
Li_2O	-1904.417	R^2	0.9069
Na_2O	-1947.711	R^2_{Adj}	0.8962
SrO	13011.909	R^2_{Pred}	0.8693
ZrO_2	3747.4241	R^2_{Val}	0.8718
Others	1259.2233		

(a) LN_2O_3 is the combination of Y_2O_3 and all the rare-earth oxides (which are all assumed to be in the trivalent state).

2.7.2 Future Plans

Several Hanford tank wastes will be rich in ZrO_2, ThO_2, and other components that tend to crystalized at high concentrations in glass. Additional crystal fraction-temperature-composition data for melts in these composition regions will be developed and used to fit models. If evaluations show sufficient impacts of these constraints on glass mass, then models for crystal accumulation will be developed as is currently underway for melts in the spinel primary phase field as described in Section 2.2.

2.8 Phosphate Limits

Section 2.8.1 discusses phosphate limits and a liquidus temperature model for phosphate-containing phases. Section 2.8.1 discusses future plans.

2.8.1 Phosphate Constraints and a Liquidus Temperature Model for Phosphate-Containing Phases

Vienna and Kim (2008) evaluated a broad range of high phosphate glasses ($0.01 \leq g_{P_2O_5} \leq 0.065$). They found that the following rules effectively excluded glasses that showed deleterious effects of phosphorous on glass processing properties (scum formation that can lead to a frozen cold cap) and product-quality-related properties (potential amorphous phase separation that can increase PCT release):

$$, g_{P_2O_5} \leq 0.045 \tag{2.26}$$

$$g_{CaO} \times g_{P_2O_5} \leq 6.5 \times 10^{-4}, \text{ and} \tag{2.27}$$

$$g_{Li_2O} \leq 0.06, \tag{2.28}$$

where g_i is the mass fraction of the i^{th} oxide in HLW glass. However, the model-validity constraints for some properties were found to be lower than the $g_{P2O5} \leq 0.045$ limit because of a lack of data coverage at higher concentrations of P_2O_5. McCloy and Vienna (2010) further evaluated the impact of P_2O_5 concentrations on various key properties of HLW glasses and recommended

> *…that additional data with P_2O_5 concentrations extending to 4.5 wt% and above be collected and used to revise glass property models, including T_L, $T_{1\%}$, PCT-Li, and N_{TCLP}. While these data are being developed, there is a low risk of using the existing models, reported by Vienna et al. (2009), for glasses with phosphate concentrations up to 4.5 wt%.*

Recent efforts by Gan et al. (2015) fabricated and measured the liquidus temperature of 86 glasses precipitating one of many phosphate containing phases. They fit a PQMM to the data of the form

$$T_L = \sum_{i=1}^{q} t_i g_i + \text{Selected}\left\{ \sum_{i=1}^{q} t_{ii} g_i^2 + \sum_{i=1}^{q-1} \sum_{j=i+1}^{q} t_{ij} g_i g_j \right\}, \tag{2.29}$$

where T_L is the liquidus temperature (in °C), t_i is the coefficient of the i^{th} HLW glass component, g_i is the mass fraction of the i^{th} HLW glass component, and t_{ij} is the coefficient of the crossproduct of the i^{th} and j^{th} components (where a squared term results when $i = j$). Table 2.24 summarizes the coefficients and fit statistics for this model.

Table 2.24. Partial Quadratic Mixture Model for T_L of Phosphate Containing Phases in HLW Glasses (Gan et al. 2015)

Model Term	Coefficient	Statistic	Value
Al_2O_3	1469.935	# data points	86
CaO	2260.14	# model terms	12
Li_2O	-2981.33	RMSE	46.83
Na_2O	-538.42	R^2	0.742
P_2O_5	8588.551	R^2_{Adj}	0.704
SiO_2	1702.605	R^2_{Pred}	0.619
SrO	-2317.75		
ZrO_2	4034.096		
Others	458.373		
$P_2O_5 \times SiO_2$	-17591.4		
$Li_2O \times SrO$	123679.1		
$Li_2O \times ZrO_2$	-83403.6		

The dataset used to fit this model was evaluated using the three constraints developed by Vienna and Kim (2008), as listed in Equations (2.26) to (2.28). It was found that the rules did exclude most of the glasses with T_L > 1000°C and all but one glass with T_L > 1050°C (HWI-Al-16). It was also found that the T_L model would be less restrictive than the rules, particularly the $CaO \times P_2O_5$ rule. Since that rule is in place primarily to avoid a frozen cold-cap (e.g., *killer scum*) rather than T_L, we recommend the following:

- adopt the Vienna and Kim (2008) phosphate limits for future system planning efforts and
- conduct a study of additional high-phosphate (e.g., $0.01 \leq g_{P_2O_5} \leq 0.065$) glasses to refine the limits and ensure that phase-separated glasses and frozen cold-caps are avoided.

2.8.2 Future Plans

Additional data for HLW glasses rich in phosphate are needed. These data should include measurement of the current set of controlling properties and also scaled melter tests. The data for property measurements are needed simply to expand the region of model validity and for modeling. However, phosphate has the potential to significantly impact some properties such as immiscible liquid separation, crystallization of phosphate containing phases, cold cap melting, and salt accumulation. These latter two properties require significant scaled melter test data to understand and model.

2.9 Summary of Property Models and Component Concentration Limits for HLW Glasses

Table 2.25 lists the commonly applied limits for HLW glass and melt properties. Table 2.25 also compares the limits and models used in the WTP formulation algorithm (Vienna and Kim 2008), the HTWOS model (Vienna et al. 2009), the updated HTWOS model (McCloy and Vienna 2010), and those recommended for enhanced HLW glass mass estimation. These constraints have evolved in consecutive steps. Constraints that changed from the previous step are highlighted in red in Table 2.25.

With new models come new model-validity constraints on HLW glass compositions. Table 2.26 summarizes the single component constraints, primarily due to model-validity ranges. These constraints have evolved over time in consecutive steps. Constraints that changed from the previous step are highlighted in red in Table 2.25. Between the HTWOS 2010 constraints and the enhanced constraints, there have been a number of changes (listed below).

- **Maximum $g_{Al_2O_3}$ was increased to 0.30.** This value represents the upper limit of data used in the nepheline, viscosity, PCT, and spinel models. The upper limits of $g_{Al_2O_3}$ for the SO_3 solubility model was 0.24 and for the T_L-Zr model was 0.172. Hence, those models will need to be extrapolated up to $g_{Al_2O_3}$ of 0.30. This extrapolation is not expected to be a problem because the high-alumina wastes are typically limited by spinel and nepheline in the glass, not by the other properties. The PCT model has a maximum $g_{Al_2O_3}$ of 0.36 while the nepheline model has a maximum of 0.39. It is the viscosity and $T_{2\%}$ models that drive the new proposed limit.
- **Maximum g_{CaO} was increased to 0.1.** This value represents the validity limit for all HLW property models except for SO_3 solubility, which has a maximum g_{CaO} of 0.0856. This slight extrapolation is not expected to make a significant impact.
- **Maximum $g_{Cr_2O_3}$ was decreased to 0.03.** Although the $T_{2\%}$ and eskolaite constraints suggest a $g_{Cr_2O_3}$ of 0.045 is possible, the viscosity, PCT, and nepheline models are all valid only to 0.03. Only the SO_3 solubility model will need to be extrapolated, which poses some risk because it is valid only up to 0.01.
- **Maximum g_{MnO} was increased to 0.08.** This value represents the upper limit of data used in the $T_{2\%}$, SO_3 solubility, and viscosity models. The nepheline model contained data with g_{MnO} up to 0.06, and the PCT model up to 0.05. That is, these models need to be extrapolated, which may not pose a high risk as spinel precipitation is the process of most concern with high MnO concentrations.
- **Maximum g_{Na_2O} was increased to 0.24.** This value represents the range of data used in the PCT models and is below the maximum values in the $T_{2\%}$, nepheline, and viscosity models. The SO_3 solubility and T_L-Zr models will need to be extrapolated from g_{Na_2O} values of 0.20 and 0.15, respectively.
- **The g_{SiO_2} lower bound was decreased to 0.22**. The lower limit is above the range of data used in the $T_{2\%}$, nepheline, viscosity, and PCT models, which are thought to be most impacted by SiO_2.

Recent experience has suggested that for g_{SiO_2} below 0.22, the composition region over which acceptable glasses are formed is relatively small (Chou et al. 2016). An additional constraint on combined $g_{SiO_2} + g_{B_2O_3} \geq 0.32$ (see Table 2.25) should also be used to reduce the likelihood of unacceptable glasses. The SO_3 solubility and T_L-Zr models will need to be extrapolated from g_{SiO_2} values of 0.27 and 0.397, respectively.

- **Maximum g_{TiO_2} was increased to 0.05.** This value represents the upper limit of data used in the $T_{2\%}$ and PCT models, which are most likely to be impacted by TiO_2. The nepheline, SO_3 solubility, and viscosity models will need to be extrapolated from g_{TiO_2} values of 0.0212, 0.01, and 0.0399, respectively.

The revised set of constraints in Tables 2.25 and 2.26, and the enhanced HLW glass formulation models recommended in Section 2, are proposed for assessing their potential impacts on the likely mass of HLW glass to be produced at Hanford.

Table 2.25. Comparison of HLW Melt and Glass Constraints Used in HLW Glass Mass Estimation

	WTP		HTWOS 2009		HTWOS 2010		Enhanced-2013		Enhanced-2016	
	Model	Value	Model	Value	Model	Value	Model	Value	Model	Value
PCT-B	WTP	<16.7 g/L[b]	**2009 rpt**	**<4 g/m^2**	2009 rpt	<4 g/m^2			**New PCT-B**	<4 g/m^2
PCT-Na	WTP	<13.35 g/L	**2009 rpt**	**<4 g/m^2**	2009 rpt	<4 g/m^2	**2013 PQMM**	<4 g/m^2	**New PCT-Na**	<4 g/m^2
PCT-Li	WTP	<9.57 g/L	**2009 rpt**	**<4 g/m^2**	2009 rpt	<4 g/m^2			**New PCT-Li**	<4 g/m^2
Nepheline	*NSi*	>0.62	*NSi*	>0.62	*NSi* **OB**	>0.62 **<0.575**	**2013 NN**	**<0.27 prob**	**New LR-SM**	**<0.3 prob**
TCLP [a]	WTP	<0.48 mg/L	**n/a**	**n/a**	n/a	n/a	n/a	n/a	n/a	n/a
$T_{1\%}$ Spinel	WTP	<950°C	**2009 rpt**	<950°C	2009 rpt	<950°C	**2013 c_T LMM**	**2 vol%, 950°C**	**New $T_{2\%}$ PQMM**	950°C
Nonspinel	Al+Th+Zr Th+Zr Zr	<18% <13% <9.5%	**T_L-Zr, 2009 rpt**	**<1050°C if ZrO_2>4%**	T_L-Zr, 2009 rpt	<1050°C if ZrO_2>4%	T_L-Zr, 2009 rpt	<1050°C if ZrO_2>4%	T_L-Zr, 2009 rpt	<1050°C if ZrO_2>4%
Low η_{1150}	WTP	>2 Pa·s	**2009 rpt**	**>4 Pa·s**	2009 rpt	>4 Pa·s	2009 rpt	>4 Pa·s	**New ln[η_{1150}] PQMM**	>4 Pa·s
High η_{1150}	WTP	<8 Pa·s	**2009 rpt**	**<6 Pa·s**	2009 rpt	<6 Pa·s	2009 rpt	<6 Pa·s	**New ln[η_{1150}] PQMM**	<6 Pa·s
High η_{1100}	WTP	<15 Pa·s	**n/a**	**n/a**	n/a	n/a	n/a	n/a	n/a	n/a
Low ε_{1100}	WTP	>0.1 S/cm	**n/a**	**n/a**	n/a	n/a	n/a	n/a	n/a	n/a
High ε_{1200}	WTP	<0.7 S/cm	**n/a**	**n/a**	n/a	n/a	n/a	n/a	n/a	n/a
$CaO{\times}P_2O_5$[c]	$CaO{\times}P_2O_5$	<6.5 wt%^{2}	$CaO{\times}P_2O_5$	<6.5 wt%^{2}	$CaO{\times}P_2O_5$	<6.5 wt%^{2}	$CaO{\times}P_2O_5$	<6.5 wt%^{2}	$CaO{\times}P_2O_5$	<6.5 wt%^{2}
Salt	SO_3	<0.44 wt%	SO_3	**<0.5 wt%**	SO_3	**<0.6 wt%**	**2013 SO_3 PQMM**	**SO_3 limit**	**New SO_3 PQMM**	SO_3 limit
Noble Metal	Pd+Ru+Rh	<0.25 wt%	Pd+Ru+Rh	<0.25 wt%	Pd+Ru+Rh	<0.25 wt%	Pd+Ru+Rh	<0.25 wt%	Pd+Ru+Rh	<0.25 wt%
Glass Former	n/a	n/a	n/a	n/a	n/a	n/a	n/a	n/a	**SiO_2+B_2O_3**	**>32 wt%**

(a) TCLP = Toxicity Characteristic Leaching Procedure. This constraint is only active for one waste tank with high CdO concentrations and it has been repeatedly shown not to significantly influence glass masses.

(b) PCT responses may be normalized to component concentration in glass and reported in units of $g_{glass}/L_{solution}$ or normalized to both component concentration in glass and glass surface area and reported in units of g_{glass}/m^2_{glass} surface. If the glass has a density of roughly 2.65 g/cm^3 (as these glasses do) and a surface area to solution volume of 2000 m^{-1} is used for the test (as it was) then 1 g/L is equivalent to 0.5 g/m^2.
Note: Red font denotes entries that changed since the previous iteration.

(c) The other two phosphate limits, $g_{P2O5} \leq 0.045$ and $g_{Li2O} \leq 0.06$, discussed in Section 2.8 were not included – they do not limit waste loading because the model validity constraints have lower concentration limits.

Table 2.26. Summary of Single Component Model-Validity Constraints (mass fractions) for HLW Glasses

Comp-onent	WTP[(a)]		HTWOS 2009		HTWOS 2010		Enhanced-2013		Enhanced-2016	
	Min	Max	Min	Max	Min	Max	Min	Max	Min	Max
Al_2O_3	0.018 [0.019]	0.13 [0.085]	0.019	**0.20**	0.019	0.20	0.019	**0.29**	0.019	**0.30**
B_2O_3	0.045	0.15	0.04	**0.20**	0.04	0.20	0.04	0.20	0.04	**0.22**
Bi_2O_3	0	In Others	0	0.032	0	**0.07**	0	0.07	0	0.07
CaO	0	0.01	0	**0.07**	0	0.07	0	0.07	0	**0.10**
CdO	0	0.001 [0.016]	0	0.015	0	0.015	0	0.015	0	0.015
Cr_2O_3	0	0.006 [0.005]	0	**0.012**	0	0.012	0	**0.04**	0	**0.03**
F	0	0.0044	0	**0.02**	0	0.02	0	**0.025**	0	0.025
Fe_2O_3	0.014 [0.019]	0.15 [0.14]	**0.04**	**0.174**	0.04	0.174	**0**	**0.20**	0	0.20
K_2O	0	0.016	0	**0.06**	0	0.06	0	0.06	0	0.06
Li_2O	0 [0.019]	0.06	0	0.06	0	0.06	0	0.06	0	0.06
MgO	0	0.012	0	**0.06**	0	0.06	0	0.06	0	0.06
MnO	0	0.08 [0.07]	0	0.07	0	0.07	0	0.07	0	**0.08**
Na_2O	0.039	0.20 [0.15]	0.041	**0.214**	0.041	0.214	0.041	**0.23**	0.041	**0.24**
NiO	0	0.01	0	**0.03**	0	0.03	0	0.03	0	0.03
P_2O_5	0	0.045	0	**0.025**	0	**0.045**	0	0.045	0	0.045
PbO	0	0.01	0	-	0	-	0	-	0	-
SiO_2	0.35	0.53	**0.303**	0.53	0.303	0.53	0.303	0.53	**0.22**	0.53
SrO	0	0.10	0	0.101	0	0.101	0	0.101	0	0.101
ThO_2	0	0.06	0	0.06	0	0.06	0	0.06	0	0.06
TiO_2	0	0.01	0	**0.031**	0	0.031	0	0.031	0	**0.05**
UO_3	0	0.065 [0.063]	0	0.063	0	0.063	0	0.063	0	0.063
ZnO	0	0.04	0	0.04	0	0.04	0	0.04	0	0.04
ZrO_2	0	0.096 [0.091]	0	**0.135**	0	0.135	0	0.135	0	0.135

(a) WTP model-validity constraints are different depending on whether the Toxicity Characteristic Leaching Procedure (TCLP) model is used. TCLP model-validity constraints are given in square brackets for those components with differences. This model is used for glasses with $g_{CdO} > 0.001$.

Note: Red font denotes entries that changed since the previous iteration.

2.10 Example Calculations for HLW Glasses

Two examples are given for use in determining if application and coding of the HLW models are correct. To make these examples, two hypothetical wastes, based loosely on real projected Hanford HLW feeds, were used in glass optimization calculations. The glass formulations were optimized for maximum waste loading while maintaining component concentrations and property values within the limits described in Section 2.9. Current glass forming chemicals include mined minerals (kyanite, borax, wollastonite, olivine, silica, zincite, and zircon) and processed chemicals (boric acid, hematite, sodium carbonate, lithium carbonate, rutile, and sucrose) which are sources of Al_2O_3, B_2O_3, CaO, Fe_2O_3, Li_2O, MgO, Na_2O, SiO_2, ZnO, and ZrO_2. For the purposes of example calculations the pure oxides (without impurities) of Al_2O_3, B_2O_3, CaO, Li_2O, MgO, Na_2O, SiO_2, V_2O_5, ZnO, and ZrO_2 were selected (V_2O_5 replacing Fe_2O_3) and their concentrations adjusted along with waste loading until a maximum waste loading was obtained. Only B_2O_3, Li_2O, Na_2O, and SiO_2 were selected for inclusion. The details are summarized in Table 2.27.

Example 1 is a high-alumina waste. It was optimized until it met five constraints with five additives (all the degrees of freedom being used up). The limits obtained were CaO and SiO_2 concentrations, upper viscosity, nepheline probability, and PCT-Na responses. The additives were B_2O_3, CaO, Li_2O, SiO_2, and ZrO_2. The resulting waste loading of 45.30 wt% was obtained. Note that the predicted T_L-Zr value for the glass is above the 1050°C limit, but, that limit is only enforced with $g_{ZrO_2} > 0.04$ in the glass.

Example 2 is a high-iron waste. It was optimized until it met three constraints with three additives (all the degrees of freedom being used up). The limits obtained were lower viscosity, $T_{2\%}$, and nepheline probability. The additives were B_2O_3, Na_2O, and SiO_2. The resulting waste loading of 54.19 wt% was obtained.

Table 2.27. Summary of Example Calculation Results. All compositions are in mass fractions

	Limits		Example 1			Example 2		
Oxide	Lower	Upper	Waste	Add	Glass	Waste	Add	Glass
Al_2O_3	0.019	0.30	0.60	-	0.2718	0.17	-	0.0921
B_2O_3	0.04	0.22	-	0.3482	0.1904	-	0.1888	0.0865
Bi_2O_3	0	0.07	0.02	-	0.0091	0.02	-	0.0108
CaO	0	0.10	0.01	0.1745	**0.1000**	0.03	-	0.0163
Cr_2O_3	0	0.03	0.02	-	0.0091	0.01	-	0.0054
Fe_2O_3	0	0.20	0.04	-	0.0181	0.30	-	0.1626
Li_2O	0	0.06	-	0.0427	0.0233	-	0.00	0.00
MnO	0	0.08	0.02	-	0.0091	0.03	-	0.0163
Na_2O	0.041	0.24	0.19	-	0.0861	0.22	0.1900	0.2062
NiO	0	0.03	0.005	-	0.0023	0.022	-	0.0108
P_2O_5	0	0.045	0.01	-	0.0045	0.015	-	0.0081
SiO_2	0.22	0.53	0.045	0.3649	**0.2200**	0.08	0.6212	0.3279
UO_3	0	0.063	0.04	-	0.0181	0.065	-	0.00
ZrO_2	0	0.135	-	0.0697	0.0381	0.04	-	0.0217
Loading (wt%)	-	-	45.30	54.70	0.4530	54.19	45.81	
Property								
η_{1150}, Pa·s	4	6	-	-	**6.00**	-	-	**4.00**
T_L-Zrs, °C	-	1050	-	-	1414	-	-	777
$CaO \times P_2O_5$, wt%^{2}	-	6.5	-	-	4.53	-	-	1.32
$T_{2\%}$, Spinel, °C	-	950	-	-	944	-	-	**950**
Nepheline Probability	-	0.3	-	-	**0.30**	-	-	**0.30**
SO_3 limit, wt%	-	w_{SO_3}	-	-	1.589	-	-	0.714
PCT-B, g/m^2	-	4	-	-	2.912	-	-	0.984
PCT-Na, g/m^2	-	4	-	-	**4.000**	-	-	1.075
PCT-Li, g/m^2	-	4	-	-	3.095	-	-	0.723

Note: Values in boldface denote the limiting factors for formulating the HLW glass.

3.0 Low-Activity Waste Glass Models and Constraints

Section 3.0 describes the models to be used in estimating LAW glass properties including: sulfur limits (Section 3.1), PCT response (Section 3.2), VHT response (Section 3.3), viscosity (Section 3.4), glass formulation approach (Section 3.5), and other property models and component concentration limits (Section 3.6), followed by example calculations in Section 3.7.

The data and models are not fully QA compliant and therefore are not intended to be used in quality-affecting activities or decisions (e.g., design basis input, plant operations, waste form compliance). Instead the models and constraints are intended for use in mission planning activities.

3.1 Sulfur Tolerance

Salt accumulation in the melter will increase the corrosion rates of melter components in contact with the salt, increase volatility, and potentially supersaturate the melt with salt that will separate into a water-soluble phase when the glass is canister-cooled. Therefore, constraints must be put in place to avoid the accumulation of salt in the melter. SO_3 tolerance models were developed for HLW glasses in Section 2.3. A previous study developed a similar model for LAW glasses (Vienna et al. 2014). The model from this previous study is briefly summarized in Section 3.1.1 and is recommended for use in enhanced LAW glass formulation. Section 3.1.2 discusses future plans.

3.1.1 SO_3 Solubility Model for LAW Glasses

Crucible-scale sulfur solubility for 253 LAW glasses was measured by super-saturation and bubbling methods. In addition, the maximum sulfur tolerance was measured for 13 base glass compositions in scaled melter tests. The crucible-scale bubbling method results were found to correlate directly to the melter data while there was a systematic offset in the crucible super-saturation data. Therefore, the super-saturation data was adjusted by the fixed offset of 0.2115 wt% SO_3 and combined with the crucible-scale bubbling data to form the modeling dataset. An empirical PQMM was fitted to the data with the form

$$w_{SO_3}^{Limit} = \sum_{i=1}^{q} s_i n_i + \text{Selected}\left\{ \sum_{i=1}^{q} s_{ii} n_i^2 + \sum_{i=1}^{q-1} \sum_{j=i+1}^{q} s_{ij} n_i n_j \right\}, \quad (3.1)$$

where

$w_{SO_3}^{Limit}$ = sulfur tolerance limit (in wt%)

s_i = coefficient of the i^{th} component

n_i = mass fraction of the i^{th} component normalized after removing SO_3, so that $n_1 + \ldots + n_{q=\text{Others}} = 1.0$

s_{ij} = coefficient of the product of the i^{th} and j^{th} components (note that $i = j$ for a squared term).

The coefficients determined for the model are given in Table 3.1 along with the single component concentration ranges of the data.

Since the development of the LAW SO_3 tolerance model by Vienna et al. (2014), a study was performed by VSL to better understand the impacts of SO_3, Cl, Cr_2O_3, and P_2O_5 on salt accumulation (Matlack et al. 2014). A total of 29 melter tests were performed using four base glasses (ORPLE12, ORPLD6, ORPLA38-1, and ORPLG27) with systematic variations in SO_3, Cl, Cr_2O_3, and P_2O_5. For each test the presence (15 tests) or absence (14 tests) of salt was determined. The melter results were used to validate the model in Table 3.1. Figure 3.1 compares the predicted SO_3 solubility with 90% PIs to the measured SO_3 concentrations in the LAW glasses. If a 90% PI overlaps the 45º line, then the predicted SO_3 solubility and measured SO_3 values are not statistically different (with 90% confidence) after accounting for data and model uncertainties. Figure 3.1 uses two symbols to show the presence or absence of salt in the melter tests.

Table 3.1. SO_3 Solubility Partial Quadratic Mixture Model Coefficients and Component Validity Ranges (mass fractions) for LAW Glasses

		Concentration Range	
Model Term	Coefficient	Min	Max
Al_2O_3	-2.0919	0.0553	0.1395
B_2O_3	3.044075	0.0398	0.1606
CaO	4.442289	0	0.1294
Cl	-22.6535	0	0.0117
Cr_2O_3	-13.1414	0.0001	0.01
K_2O	0.615785	0.0011	0.0834
Li_2O	2.473926	0	0.0586
Na_2O	2.897209	0.0248	0.2605
P_2O_5	4.606083	0	0.0308
SiO_2	0.240729	0.3005	0.5064
SnO_2	-1.77533	0	0.0501
V_2O_5	7.534548	0	0.0439
ZrO_2	-1.87192	0.0262	0.0902
Others	-0.28027	0.0253	0.1777
$(Li_2O)^2$	260.203		
# data points	253		
Mean value, SO_3 wt%	1.004		
RMSE	0.115		
R^2	0.891		
R^2_{Adj}	0.885		
R^2_{Pred}	0.874		
R^2_{Val}	0.869		

When 90% PIs were applied, SO_3 solubility was overpredicted for one glass (1.473 vs. 1.5 wt% SO_3) and underpredicted for one glass (0.900 vs. 0.903 wt% SO_3). This gives a 2 out of 29 misclassification rate (~7%) which is quite reasonable for a 90% PI (10% anticipated), which further validates the model. The SO_3 solubility model by Vienna et al. (2014), given in Table 3.1, is recommended for use in enhanced LAW glass formulation.

The data and models are not fully QA compliant and therefore are not intended to be used in quality-affecting activities or decisions (e.g., design basis input, plant operations, waste form compliance). Instead the models and constraints are intended for use in mission planning activities.

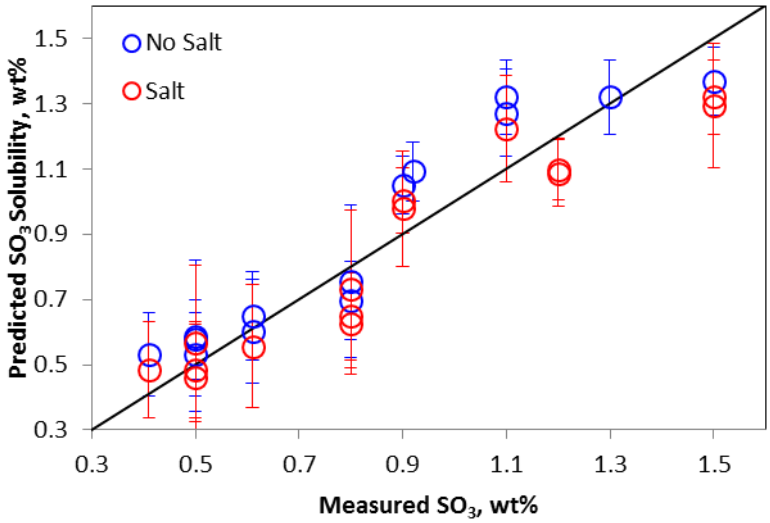

Figure 3.1. Predicted vs. Measured Plot of SO_3 Solubility Values with 90% Prediction Intervals (wt%) for Melter Test Data on 29 LAW Glasses Used to Validate the Model by Vienna et al. (2014)

3.1.2 Sulfur Retention in the Melter

Estimates of sulfur retention in the melter for WTP baseline formulations showed increasing loss with increasing target w_{SO_3} as shown in Figure 3.2. Extrapolation of that trend to 1.5 wt% SO_3 (or higher) would suggest significant loss and associated recycle concentrations of SO_3 in the melter feed. This prompted an examination of the retention of SO_3 for the advanced formulations to see if this reported trend continues at higher SO_3 concentrations. Data were gathered from those reported in Vienna et al. 2014 (12 tests, none with accumulated salt) and Matlack et al. 2014 (29 tests, 15 with salt accumulated). The target (feed) concentration of SO_3 is compared to the analyzed (glass) concentration in Figure 3.3. The effect of w_{SO_3} on sulfur retention is not as dramatic as would be predicted by the trend in Jenkins et al. (2013) as shown in Figure 3.4. All retention values for these advanced glasses are above 76% and the general trend suggest a retention near 93%, although there is a slight downward trend as shown in Figure 3.4. The presence of accumulated salts in the melter tests from Matlack et al. (2014) do not appear to significantly alter the fraction of SO_3 retained in the glass, although taken to the extreme that trend couldn't continue to higher target w_{SO_3}. It is recommended that the sulfur retention used in system planning models be examined for consistency with these results.

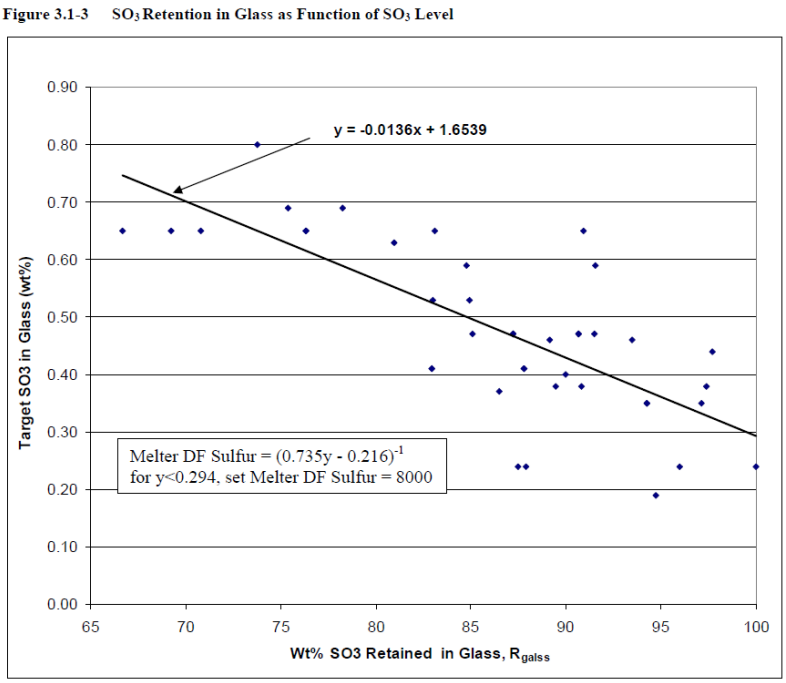

Figure 3.2. SO_3 retention (wt%) as a Function of Target w_{SO_3} for WTP Baseline Formulations (Figure 3.1-3 from Jenkins et al. 2013)

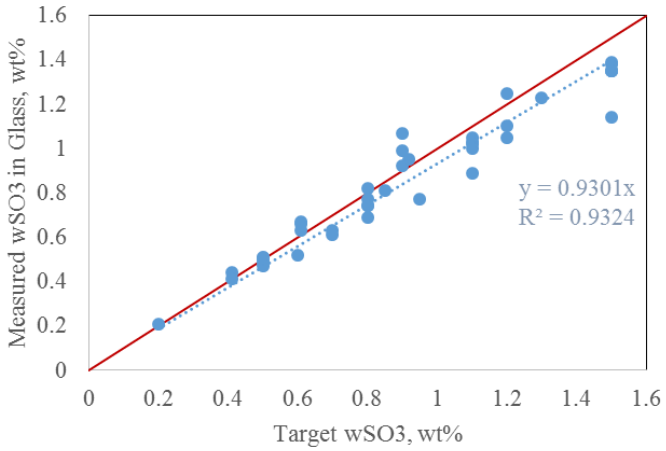

Figure 3.3. Comparison of Target and Final Measured w_{SO_3} from Melter Tests Performed with Advanced Glass Formulations at VSL, in wt%

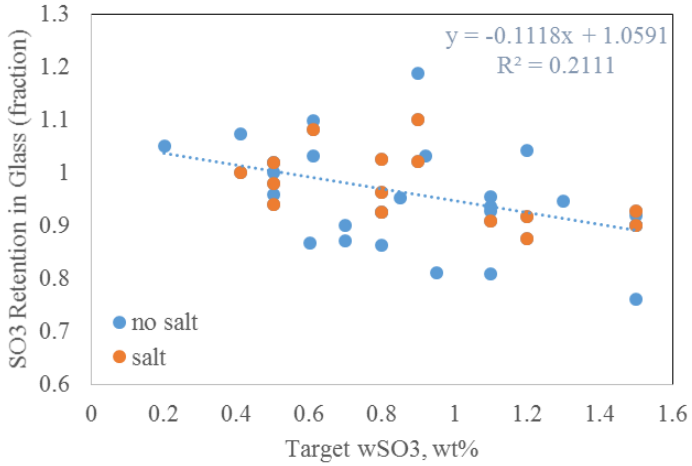

Figure 3.4. Calculated SO_3 Retention in the Melt as a Function of Target w_{SO_3}

3.1.3 Future Plans

Additional crucible and melter scale testing of sulfate solubility (and tolerance) is needed to resolve issues related to impacts of volatiles (e.g., Cl, F, Cr, NO_3) on sulfate salt accumulation and also the optimization of Cr_2O_3 content in the melts. As data are collected, new models will be fitted for use in WTP operations.

3.2 Product Consistency Test Response

The WTP contract requires glasses to have 7-d normalized PCT-Na, -B, and -Si responses below 2 g/m^2 (equivalent to 4 g/L) (DOE 2000):

> *2.2.2.17.2 Product Consistency Test: The normalized mass loss of sodium, silicon, and boron shall be measured using a seven day product consistency test run at 90°C as defined in ASTM C1285-98. The test shall be conducted with a glass to water ratio of 1 gram of glass (-100 to +200 mesh) per 10 milliliters of water. The normalized mass loss shall be less than 2.0 grams/m^2. Qualification testing shall include glass samples subjected to representative waste form cooling curves. The product consistency test shall be conducted on waste form samples that are statistically representative of the production glass.*

Section 3.2.1 discusses the data compiled to fit a model for PCT responses, as well as the model that was developed. Section 3.2.2 discusses future plans.

3.2.1 Data and Model for PCT Response of LAW Glasses

A dataset of LAW glasses was compiled to model their PCT responses. These data include crucible-scale tests with simulants, melter tests with simulants, and crucible-scale tests with actual LAW. Table 3.2 summarizes the PCT dataset of 804 glasses compiled for modeling and model validation. The database excluded 38 glasses out of 842 initially collected: four VSL-WTP glasses with outlying single component concentrations, one HLP and 23 ICV glasses with B_2O_3 concentration below 4 wt%, and 10 highly crystallized HLP glasses. It should be noted that the current VSL-WTP subset in Table 3.2 includes newly added glasses that were previously excluded from the WTP Baseline model dataset (Piepel et al. 2007) because of lack of measured SO_3 concentration. Initial modeling efforts with all 804 glasses suggested that there are significant biases in PCT responses between glasses designed for WTP operation and those formulated for other purposes. Therefore only the first four subsets (VSL-WTP, VSL-ORP-A, VSL-ORP-M, and PNNL-M1) specifically designed for WTP containing a total of 581 glasses were used for model development. The remaining 223 glasses were reserved for model validation.

As discussed in a previous report (Vienna et al. 2013), the PCT normalized silicon responses fall well below those of sodium and boron while generally sodium and boron responses are nearly the same. Therefore, there is no need to model *NL*(Si), and the models for *NL*(B) and *NL*(Na) should be developed separately and used to control LAW glass composition during operation. Rather than fit *NL*(B) and *NL*(Na) separately, it was decided to average the natural logarithms (ln) of the two values for each glass and use the average {(ln[*NL*(B)] + ln[*NL*(Na)])}/2 as a measure of the PCT response of LAW glasses. This quantity is denoted ln(*NL*) subsequently. Although not intended to replace individual *NL*(B) and *NL*(Na) models for plant operation, the ln[*NL*] model will give a reasonable constraint to estimate waste loading.

Table 3.2. Summary of PCT Dataset for LAW Glasses

Dataset[a]	# of Data Points	Reference	Comments
VSL-WTP	330	Muller et al. 2001 Muller and Pegg 2003a Muller and Pegg 2003b Muller and Pegg 2003c Rielley et al. 2004 Muller et al. 2004 Muller et al. 2005 Muller et al. 2006a Muller et al. 2006b Matlack et al. 2006c Piepel et al. 2007	Data used to develop WTP LAW glass models and additional glasses that were excluded in the original WTP models (see text)
VSL-ORP-A	174	Muller et al. 2012	Enhanced glass formulations with high waste loading (actively designed)
VSL-ORP-M	41	Muller et al. 2014	Enhanced glass formulations with high waste loading (test matrix)
PNNL-M	36	Russell et al. 2016[b]	Enhanced glass formulations with high waste loading (test matrix)
HLP	62	Vienna et al. 2001a	Study glasses used to set the contract limits for LAW glass performance
ICV	15	Kim et al. 2003	Glasses formulated to demonstrate in-container vitrification technology
POSTECH	146	Farooqi and Hrma 2016[c]	Simple 7-component (Al_2O_3, B_2O_3, CaO, Li_2O, Na_2O, SiO_2, and ZrO_2) glasses designed to systematically study component effects on PCT of LAW glasses

(a) HLP: Hanford LAW product acceptance, ICV: in-container vitrification, POSTECH: Pohang University of Science and Technology

(b) Russell RL et al. 2016 (Draft). Enhanced Hanford Low-Activity Waste Glass Property Data Development: Phase I. EWG-RPT-009, Pacific Northwest National Laboratory, Richland, Washington.

(c) Farooqi, RU and P Hrma. 2016 (draft). Effect of Na_2O on aqueous dissolution of nuclear waste glasses. In preparation.

Glasses with high-alkali content tend to challenge the PCT constraint. Figure 3.5 plots PCT normalized responses of 581 glasses for model development as a function of a *NAlk*, defined as $Na_2O + 0.66K_2O + 2.07\ Li_2O$ (mass fraction). Figure 3.5 shows a general trend of increasing PCT response with increasing *NAlk*. However, there are four glasses (marked by circles in Figure 3.5) that are outliers to the general trend. These four glasses were excluded and the resulting 577 glasses were used for model development.

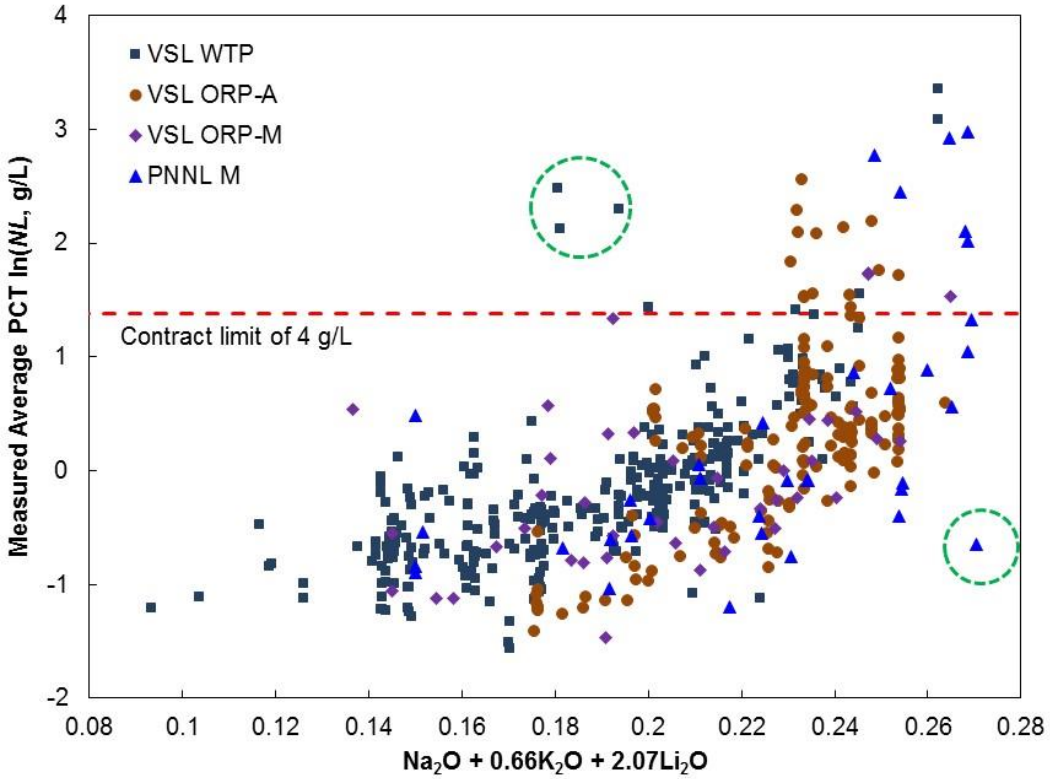

Figure 3.5. PCT Normalized Responses versus *NAlk* ($Na_2O + 0.66K_2O + 2.07\ Li_2O$ in mass fraction) of LAW Glasses Reserved for Model Development (four glasses marked in circles were excluded from modeling)

Evaluation of LAW glasses for modeling identified 15 components that have reasonable concentration distributions for consideration as model components: Al_2O_3, B_2O_3, CaO, Fe_2O_3, K_2O, Li_2O, MgO, Na_2O, P_2O_5, SiO_2, SnO_2, TiO_2, V_2O_5, ZnO, and ZrO_2. The sum of concentrations of all other components were combined into an Others component resulting in 16 candidate model components. It should be noted that if a reduced number of components is used for modeling, the new Others included those components that were removed as separate model terms. Initial modeling efforts used the LMM

$$\ln(NL,\ \text{g/L}) = \sum_{i=1}^{q} b_i g_i \qquad (3.2)$$

to model the natural logarithm of *NL* (g/L) as a function of LAW glass composition, where

- q = number of LAW glass components in the model
- b_i = model coefficient for the i^{th} LAW glass component
- g_i = mass fraction of the i^{th} LAW glass component, so that $g_1 + \ldots + g_{q=\text{Others}} = 1.0$.

This model was used to identify the LAW glass components that had significant effects on PCT response.

Out of 16 components (including Others) evaluated as PCT model components, a step-by-step removal of components that did not have significant effects on PCT response was performed. This identified three components that were removed from modeling without affecting the performance of the

model, Fe_2O_3, V_2O_5, and ZnO. Removing the three components from modeling of 577 glasses resulted in negligible changes of R^2 (from 0.752 to 0.751) and RMSE statistics (0.3837 to 0.3830). The concentration ranges for the final PCT model components are listed in Table 3.3 and the scatterplot matrix is in Figure 3.6.

Table 3.3. Component Concentration Ranges (in Mass Fraction) for PCT Model Data on LAW Glasses

Component	Min	Max
Al_2O_3	0.035	0.1476
B_2O_3	0.05	0.1515
CaO	0	0.1281
K_2O	0	0.0591
Li_2O	0	0.0633
MgO	0	0.0994
Na_2O	0.0245	0.2601
P_2O_5	0	0.0475
SiO_2	0.2983	0.5591
SnO_2	0	0.0503
TiO_2	0	0.0399
ZrO_2	0	0.0675
Others[(a)]	0	0.1754
Limits on Selected Components Included in Others		
Fe_2O_3	0	0.10
V_2O_5	0	0.04
ZnO	0	0.0581

(a) Sum of all components not specifically listed above.

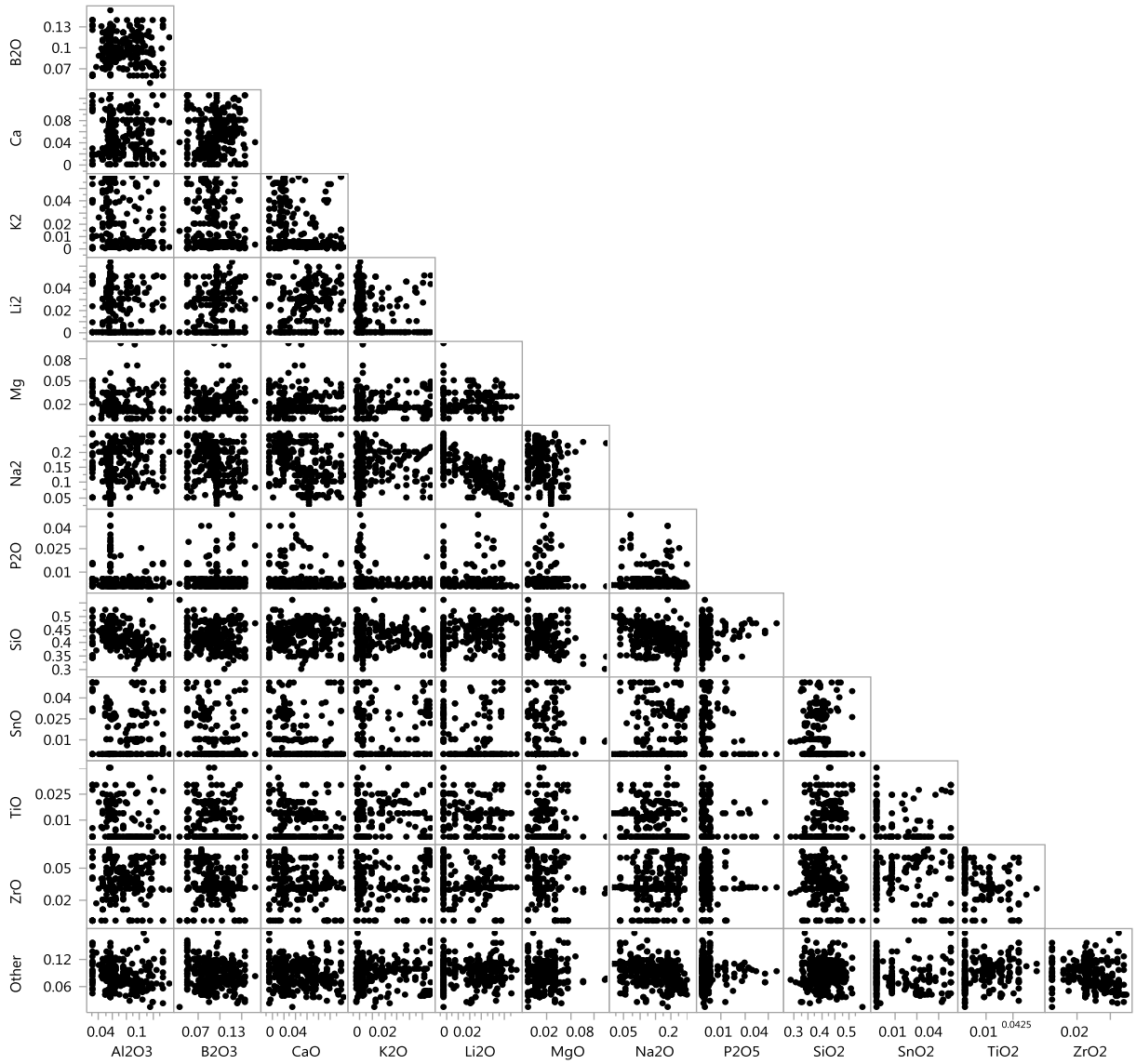

Figure 3.6. Scatterplot Matrix of PCT Model Data for LAW Glasses

As with the previous efforts (Piepel et al. 2007, Vienna et al. 2009, Muller et al. 2014) to model PCT responses, PQMMs were considered in an attempt to obtain a better fit to the data than provided by the LMM. The PQMM is given by

$$\ln\left(NL,\ \mathrm{g/L}\right) = \sum_{i=1}^{q} b_i g_i + \text{Selected}\left\{\sum_{i=1}^{q} b_{ii} g_i^2 + \sum_{i=1}^{q-1}\sum_{j=i+1}^{q} b_{ij} g_i g_j\right\}, \tag{3.3}$$

where

q = number of LAW glass components in the model

b_i = model coefficient for the i^{th} LAW glass component

g_i = mass fraction of the i^{th} LAW glass component, so that $g_1 + \ldots + g_{\text{q=Others}} = 1.0$

b_{ij} = coefficient of the product of the i^{th} and j^{th} components (note that $i = j$ for a squared term).

In general, adding quadratic terms improves the model-fit statistics, but too many quadratic terms increase the probability of overfitting and can result in poor model validation statistics. To maximize the model-fit statistics while minimizing the risk of overfitting, the following approach was applied. Candidate models were developed for different total number of model terms (13 linear terms plus selected quadratic terms). Various methods for selecting model terms were used to determine the quadratic terms that resulted in the best model-fit statistics. Validation statistics for all candidate models were calculated based on two separate methods: (i) using the subset of glasses reserved for model validation and (ii) using a data-splitting approach. Out of 223 glasses reserved for model validation (HLP, ICV, and POSTECH subsets), 129 glass compositions were within the component ranges of the glasses for model development (Table 3.3) and were used for validation. For the data-splitting approach, all 577 points in the modeling dataset were sorted by their ln(*NL*) values and then the data-splitting approach described in Section 1.4 was implemented.

The model-fit and validation statistics as a function of number of model terms are shown in Figure 3.7. The model-fit and validation statistics continuously improve as the number of model terms increases (i.e., R^2 increases and RMSE decreases). However, the model validation statistics initially improve, but reach a maximum (for R^2) or a minimum (RMSE) and further increasing the number of quadratic terms does not improve these statistics. The 21-term model (13 linear terms, 8 quadratic terms) has the best validation statistics for 129 validation glasses. The 22-term model (13 linear terms, 9 quadratic terms) is best based on data-splitting validation statistics. The 22-term model was selected taking into consideration that data-splitting validation approach is likely more reliable than the validation with 129 glasses that showed biased PCT results.

Table 3.4 summarizes the final 22-term PQMM and the model-fit statistics for the PCT ln(*NL*) response of LAW glasses. The $R^2 = 0.8411$ indicates the model accounts for over 84% of the variation in ln(*NL*) responses. The R^2_{Adj} and R^2_{Pred} values are only slightly smaller than the R^2 value, which indicates, respectively, that (i) the model does not contain many statistically nonsignificant terms, and (ii) there are no highly influential data points. The subset data-splitting validation R^2_{Val} value of 0.823 is slightly below the model fit R^2 so we can anticipate that roughly 82% of the variation in new data in the appropriate composition region. The $R^2_{Val129} = 0.5494$ value indicates that the model did not account for as high a fraction of the variation in the ln(*NL*) responses for the separate validation set of 129 LAW glasses from other studies. However, as discussed previously, these glasses were not formulated for WTP, and previous work has shown that the PCT responses are biased compared to PCT responses of LAW glasses designed for WTP.

The RMSE = 0.3086 in Table 3.4 is an estimate of the experimental and measurement standard deviation [in ln(NL, g/L) units] if the model adequately fits the data. The RMSE corresponds to a %RSD = 30.86 value for measured PCT (g/L) responses. This %RSD value is significantly larger than the experimental and measurement uncertainties in determining PCT responses of LAW glasses. Hence, the RMSE value indicates the model has some LOF.

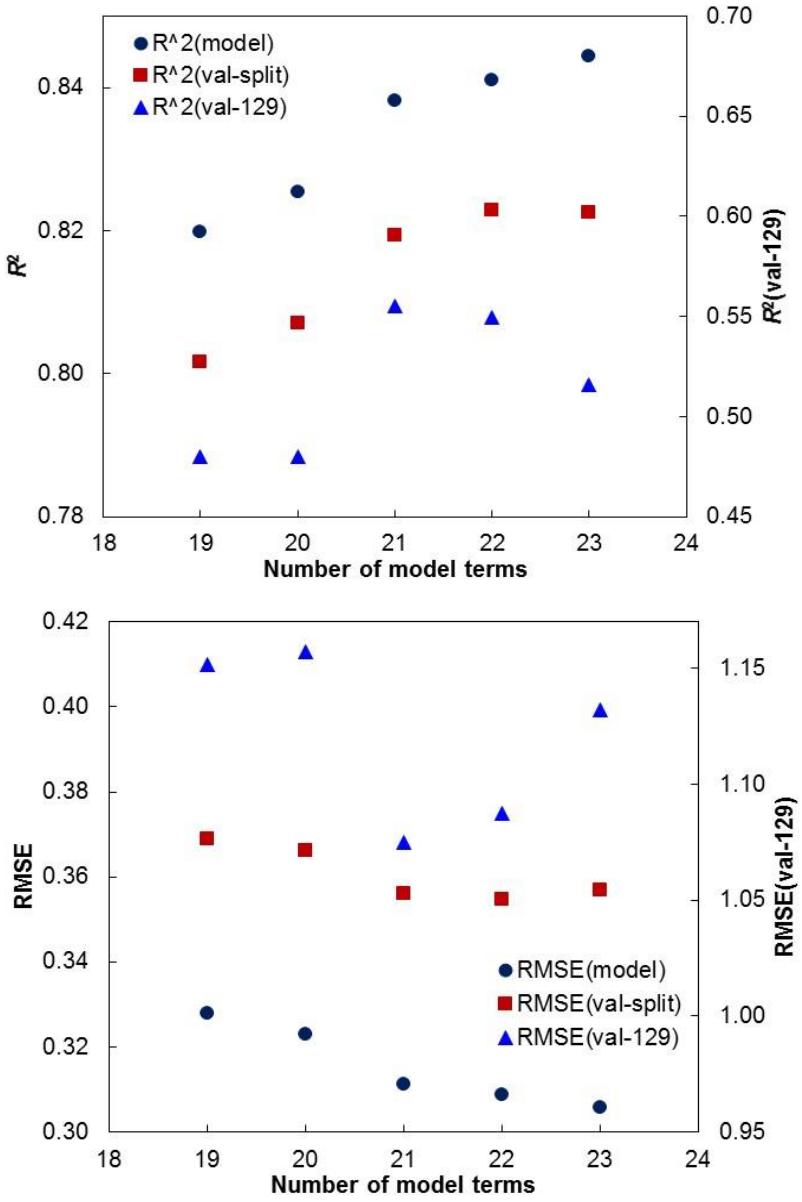

Figure 3.7. Model and Validation Statistics for PCT ln(*NL*) Models on LAW Glasses versus Number of Model Terms. Notation in parenthesis: "model" for model-fit, "val-split" for data-splitting validation, and "val-129" for 129 validation glasses. Left y-axes are for "model" and "val-split" statistics and right for "val-129" statistics.

Table 3.4. PCT Response Model Coefficients and Fit Statistics for the 22-Term Partial Quadratic Mixture Model for LAW Glasses, ln(*NL*, g/L)

Model Term	Coefficient	Statistic	Value
Al_2O_3	-4.7932	# of data points	577
B_2O_3	-31.2612	Mean of response, ln(g/L)	-0.0313
CaO	3.8636	RMSE	0.3086
K_2O	-13.5298	R^2	0.8411
Li_2O	-16.6826	R^2_{Adj}	0.8351
MgO	21.4263	R^2_{Pred}	0.8217
Na_2O	-25.2993	R^2_{Val129}	0.5494
P_2O_5	-5.1242	R^2_{Val}	0.8230
SiO_2	0.3093		
SnO_2	-4.4031		
TiO_2	-1.7604		
ZrO_2	3.8966		
Others	6.2375		
$B_2O_3 \times B_2O_3$	157.3873		
$K_2O \times K_2O$	201.4790		
$Al_2O_3 \times Li_2O$	-255.4098		
$CaO \times Li_2O$	-128.0130		
$Li_2O \times Li_2O$	474.3082		
$B_2O_3 \times Na_2O$	81.1682		
$K_2O \times Na_2O$	120.3814		
$Li_2O \times Na_2O$	391.5456		
$Na_2O \times Na_2O$	97.6643		

Figure 3.8 shows a plot of the predicted vs. measured ln(PCT *NL*, g/L) values with 95% PIs for the 577 LAW glasses used to fit the PQMM in Table 3.4. If a 95% PI overlaps the 45º line, then the predicted and measured values are not statistically different (with 95% confidence) after accounting for data and model uncertainties. The 95% PIs for 548 of the 577 glasses (95%) in Figure 3.8 overlap the 45º line. Thus, the predicted ln(*NL*) values are generally within prediction uncertainties of the measured ln(*NL*) values. Ignoring the PIs, Figure 3.8 shows the PQMM has a tendency to underpredict ln(*NL*, g/L) above approximately 2, which corresponds to a *NL* of 7.39 g/L. This is well above the constraint upper limit of 4 g/L. Hence, the PQMM in Table 3.4 predicts PCT *NL* without substantive bias below the limit of 4 g/L. Therefore, the 22-term PCT model given in Table 3.4 is recommended for use in enhanced LAW glass formulation.

The data and models are not fully QA compliant and therefore are not intended to be used in quality-affecting activities or decisions (e.g., design basis input, plant operations, waste form compliance). Instead the models and constraints are intended for use in mission planning activities.

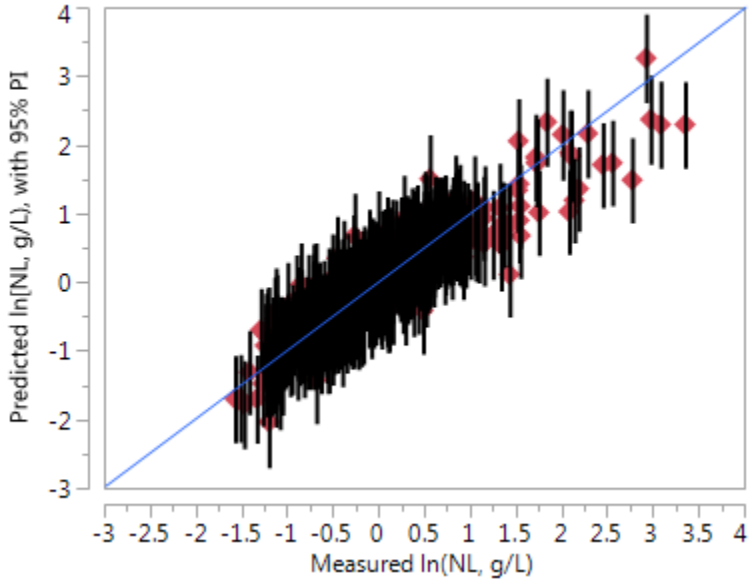

Figure 3.8. Predicted vs. Measured Plot of Average (ln[NL]) Values with 95% Prediction Intervals Using the Partial Quadratic Mixture Model for LAW Glasses

3.2.2 Future Plans

Future plans fall into two general categories: (i) develop additional data and models to predict PCT response and (ii) develop alternative approaches to demonstrate the performance of LAW glasses in the Integrated Disposal Facility (IDF) environment. Very little data exists for the LAW glasses with PCT responses at or above the 4 g/L contract limit. Additional studies are needed to measure PCT data focused on the high-alkali region that have PCT responses at or above 4 g/L. These data will be collected and modeled to predict the PCT response. These data and models will be developed under the appropriate QA so the models can be implemented in plant operations. Additional effort is needed to correlate the

response of PCT to performance in the IDF, or to develop a different criterion (or set of criteria) for controlling the performance of LAW glasses produced at WTP.

3.3 Vapor Hydration Test Response

The WTP contract requires glasses to have VHT responses below 50 g/(m^2 d) (DOE 2000):

> *2.2.2.17.3 Vapor Hydration Test: The glass corrosion rate shall be measured using at least a seven (7)-day vapor hydration test run at 200°C as defined in the DOE-concurred upon ILAW Product Compliance Plan. The measured glass alteration rate shall be less than 50 grams/(m^2 day). Qualification testing shall include glass samples subjected to representative waste form cooling curves. The vapor hydration test shall be conducted on waste form samples that are representative of the production glass.*

For glasses with typical densities near the reference value of 2.65 g/cm^3, the 50 g/(m^2 d) translates to alteration thickness (D) of 453 μm during the 24-d test period (Piepel et al. 2007).

Section 3.3.1 discusses the data compiled to fit a model for the VHT response, as well as the model that was developed. Section 3.3.2 discusses future plans.

3.3.1 Data and Model for VHT Response of LAW Glasses

A dataset of LAW glasses was compiled to model their VHT responses. These data include crucible-scale tests with simulants, melter tests with simulants, and crucible-scale tests with actual LAW. Table 3.5 summarizes the VHT dataset of 468 glasses compiled for modeling. The dataset excluded 57 glasses out of 525 initially collected: five VSL-WTP glasses with outlying single component concentrations and 52 glasses that either had the alteration thickness outside the measurement range (VSL datasets) or were tested for 7-d (PNNL-M dataset). Similar to PCT modeling, the VHT responses of HLP and ICV glasses were also collected for model validation. However, the initial modeling efforts with combined dataset revealed extreme bias between the VHT results of these glasses (HLP and ICV) and those of the glasses designed for WTP application (VSL-WTP, VSL-ORP-A, VSL-ORP-M, and PNNL-M), resulting in negative model R^2 values. Therefore it was decided that HLP and ICV glasses cannot be used for VHT model validation. It should be noted that the current VSL-WTP subset includes newly added glasses, which were previously excluded because of lack of measured SO_3 concentration.

Glasses with high alkali content tend to challenge the VHT constraint. Figure 3.9 shows a general trend of increasing VHT alteration depth with increasing *NAlk*. Because initial modeling efforts with all 577 glasses resulted in very poor model-fit statistics, various attempts were made to improve the model. It was found that using the reduced number of glasses after removing the glasses with *NAlk*. < 0.18 (the number chosen based on several model calculations varying cutoff values) improves the model fit (see the vertical line at *NAlk* = 0.18 in Figure 3.9). In addition, the ten glasses that deviate from the general trend were excluded, assuming that these glasses likely had experimental errors that may not be easily identified, leaving 330 glasses for modeling (inside the dotted line in Figure 3.9).

Table 3.5. Summary of VHT 24-Day Datasets for LAW Glasses

Dataset	# of Data Points[(a)]	Reference	Comments
VSL-WTP	234 (9)	Muller et al. 2001 Muller and Pegg 2003a Muller and Pegg 2003b Muller and Pegg 2003c Rielley et al. 2004 Muller et al. 2004 Muller et al. 2005 Muller et al. 2006a Muller et al. 2006b Matlack et al. 2006c Piepel et al. 2007	Data used to develop WTP LAW glass models and additional glasses that were excluded in the original WTP models (see text)
VSL-ORP-A	175 (28)	Muller et al. 2012	Enhanced glass formulations with high waste loading (actively designed)
VSL-ORP-M	38 (2)	Muller et al. 2014	Enhanced glass formulations with high waste loading (test matrix)
PNNL-M	21 (13)	Russell et al. 2016	Enhanced glass formulations with high waste loading (test matrix)

(a) The numbers in parenthesis represents the number of glasses that were tested for VHT but were removed form dataset. These glasses had alteration thickness values outside the measurement range (VSL datasets) or were tested for 7-d (PNNL-M dataset).

Evaluation of LAW glasses for modeling identified 15 components that have reasonable concentration distributions for consideration as model components: Al_2O_3, B_2O_3, CaO, Fe_2O_3, K_2O, Li_2O, MgO, Na_2O, P_2O_5, SiO_2, SnO_2, TiO_2, V_2O_5, ZnO, and ZrO_2. The sum of concentrations of all other components were combined into an Others component resulting in 16 candidate model components. It should be noted that if a reduced number of components is used for modeling, the new Others included those components that were removed as separate model terms. Initial modeling efforts used the LMM

$$\ln(D, \mu m) = \sum_{i=1}^{q} b_i g_i \tag{3.4}$$

to model the natural logarithm of the VHT response (D, μm) as a function of LAW glass composition, where

q = number of LAW glass components in the model

b_i = model coefficient for the i^{th} LAW glass component

g_i = mass fraction of the i^{th} LAW glass component, so that $g_1 + \ldots + g_{q=Others} = 1.0$.

This model was used to identify the LAW glass components that had significant effects on VHT response.

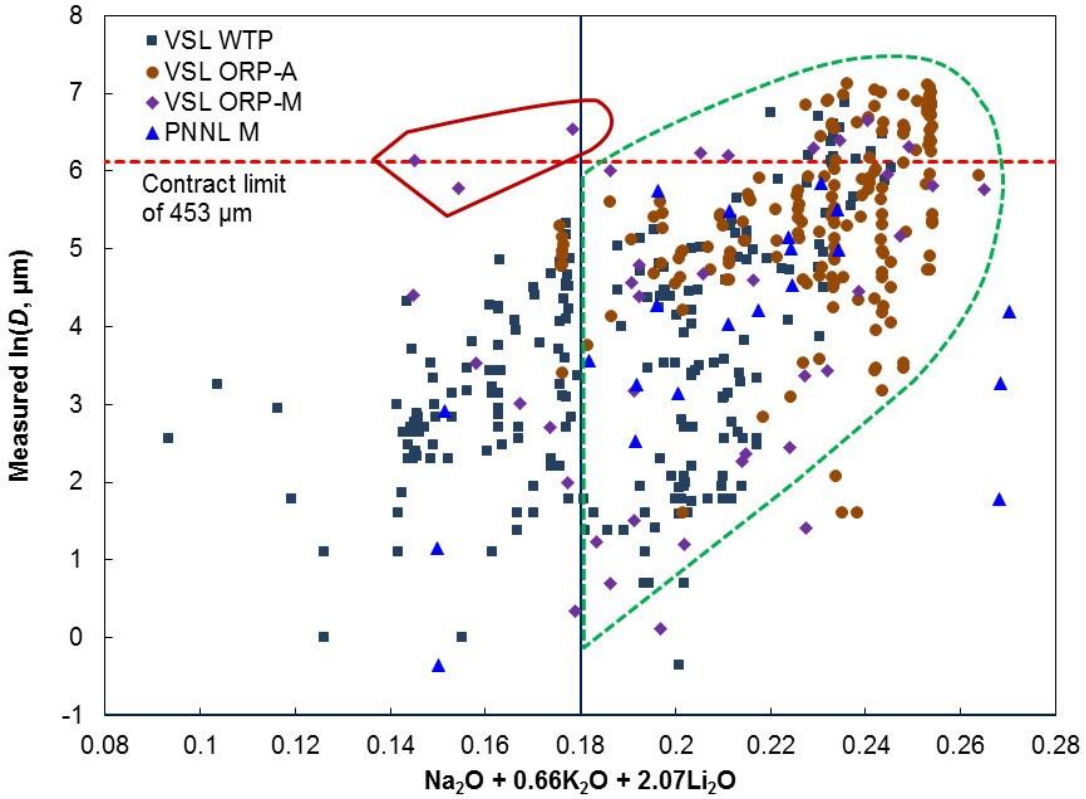

Figure 3.9. VHT 24-d Test Alteration Depth versus *NAlk* ($Na_2O + 0.66K_2O + 2.07\ Li_2O$ in mass fraction) of LAW Glasses. Glasses in dotted green line were used for model development.

Out of 16 components (including Others) evaluated as potential VHT model components, a step-by-step removal of components that did not have significant effects on VHT response was performed. This process identified four components (MgO, P_2O_5, V_2O_5 and ZnO) that were removed from the model without affecting the performance of the model. Removing these four components from the VHT model fit to data for 330 LAW glasses resulted in negligible changes to the R^2 (from 0.631 to 0.627) and RMSE statistics (0.9875 to 0.9867). Note that the four removed components become part of the Others component. The concentration ranges for the final VHT model components are listed in Table 3.6 and the scatterplot matrix is in Figure 3.10.

Table 3.6. Component Concentration Ranges (in Mass Fractions) for VHT Model Data on LAW Glasses

Component	Min	Max
Al_2O_3	0.035	0.1476
B_2O_3	0.05	0.1377
CaO	0	0.1227
Fe_2O_3	0	0.0998
K_2O	0	0.0591
Li_2O	0	0.0503
Na_2O	0.0245	0.2601
SiO_2	0.2983	0.5215
SnO_2	0	0.0502
TiO_2	0	0.0342
ZrO_2	0	0.0675
Others[(a)]	0.0195	0.1659
Selected Components Included in Others		
MgO	0	0.099
P_2O_5	0	0.034
V_2O_5	0	0.04
ZnO	0	0.058

(a) Sum of all components not specifically listed above.

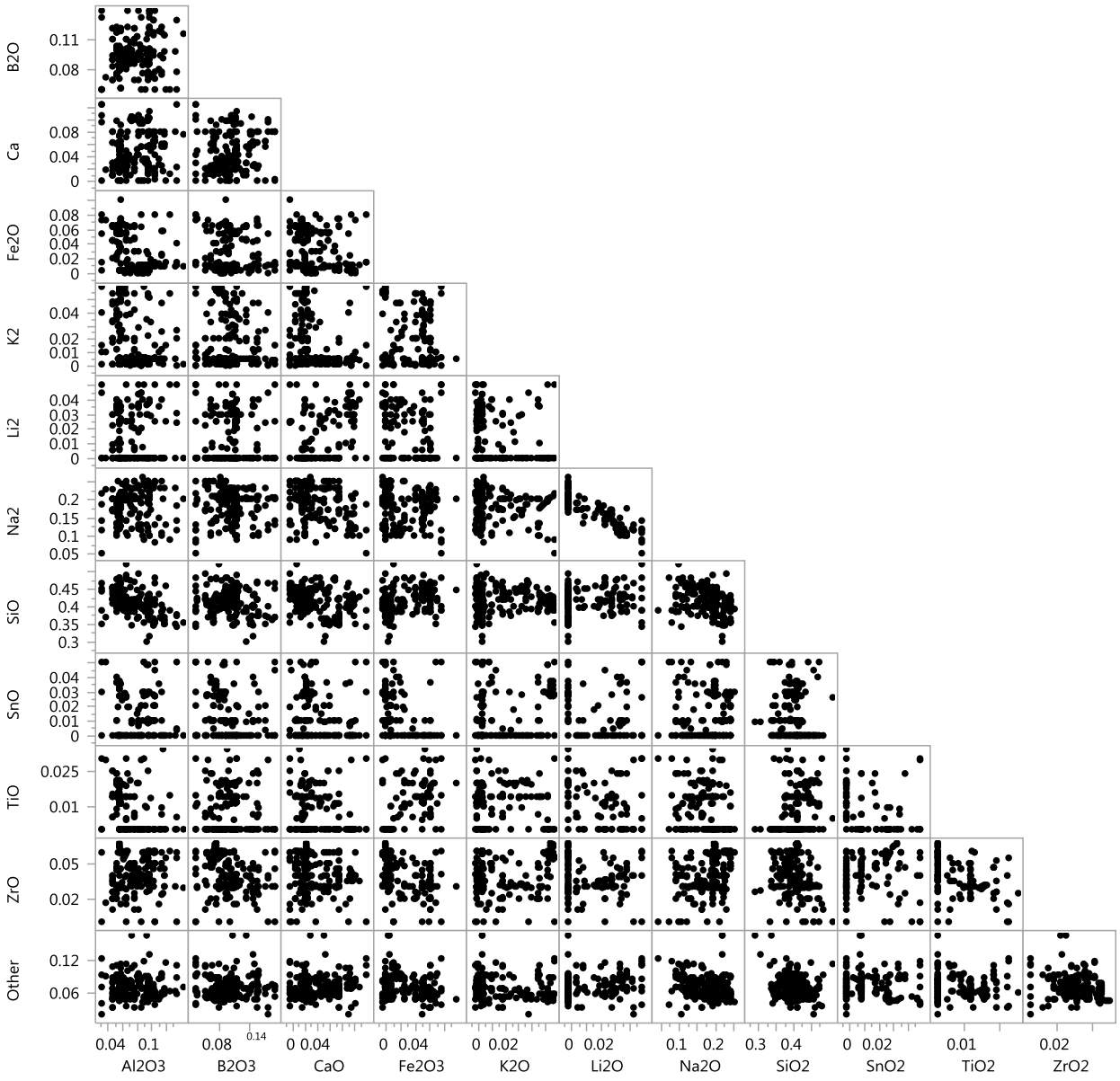

Figure 3.10. Scatterplot Matrix of VHT Model Data

As with the previous efforts (Piepel et al. 2007, Muller et al. 2008, Muller et al. 2014) to model the natural logarithm of the VHT response (D, μm), PQMMs were considered in an attempt to obtain a better fit to the data than provided by the LMM. The PQMM is given by

$$\ln(D,\ \mu\text{m}) = \sum_{i=1}^{q} b_i g_i + \text{Selected}\left\{ \sum_{i=1}^{q} b_{ii} g_i^2 + \sum_{i=1}^{q-1} \sum_{j=i+1}^{q} b_{ij} g_i g_j \right\}, \tag{3.5}$$

where

q = number of LAW glass components in the model

b_i = model coefficient for the i^{th} LAW glass component

g_i = mass fraction of the i^{th} LAW glass component, so that $g_1 + \ldots + g_{q=\text{Others}} = 1.0$

b_{ij} = coefficient of the product of the i^{th} and j^{th} components (note that $i = j$ for a squared term)

A similar approach to developing a PQMM for the PCT response was used for the VHT response (see the text in Section 3.2 following Figure 3.6). Briefly, 12 linear terms for the components listed in Table 3.6 were included in every model, and then models with increasing numbers of quadratic (crossproduct or squared) terms having statistically significant effects were added to the model using statistical modeling methods.

The model-fit and validation statistics as a function of number of model terms are shown in Figure 3.11. The model-fit and validation statistics continuously improve as the number of model terms increases (i.e., R^2 increases and RMSE decreases). However, the model validation statistics initially improve, but nearly reach a plateau (R^2) or minimum (RMSE) and further increasing the number of quadratic terms does not improve these statistics. Therefore, the 19-term model that had a minimum validation RMSE value was selected.

Table 3.7 summarizes the final 19-term PQMM and the model-fit statistics for the ln(D) VHT response for LAW glasses. The $R^2 = 0.7400$ indicates that the model accounts for 74% of the variation in ln(D) responses. The $R^2_{Adj} = 0.7249$ value is not much less than the R^2 value, which indicates that there are not several unneeded terms in the model. The R^2_{Pred} and R^2_{Val} values (0.7041 and 0.6930) are not substantially less than the R^2 and R^2_{Adj} values, which indicates there are not any excessively influential data points. The RMSE = 0.8329 is an estimate of the experimental and measurement standard deviation [in ln(D, μm) units] if the model adequately fits the data. The RMSE corresponds to a %RSD = 83.29 value for measured VHT (D, μm) responses. This %RSD value is significantly larger than the experimental and measurement uncertainties in determining VHT responses of LAW glasses. Hence, the RMSE value indicates the model has some LOF.

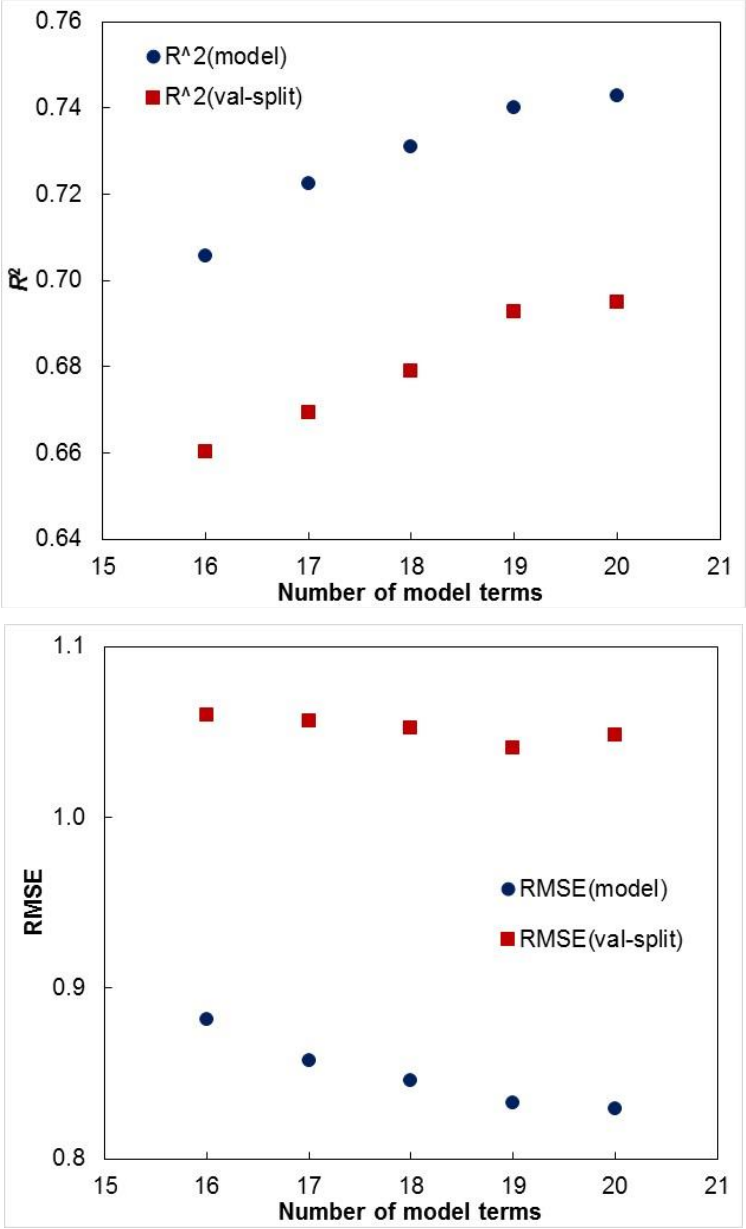

Figure 3.11. Model and Validation Statistics for VHT ln(*D*) Models on LAW Glasses versus Number of Model Terms. Notation in parenthesis: "model" for model-fit and "val-split" for data-splitting validation.

Table 3.7. VHT Model Coefficients and Fit Statistics for the 19-Term Partial Quadratic Mixture Model for LAW Glasses, ln(*D*, μm)

Model Term	Coefficient	Statistic	Value
Al_2O_3	-3.1247	# of data points	330
B_2O_3	9.0537	Mean of response, ln(*D*, μm)	4.685
CaO	-165.0264	RMSE	0.8329
Fe_2O_3	-9.3359	R^2	0.7400
K_2O	-68.6719	R^2_{Adj}	0.7249
Li_2O	308.9919	R^2_{Pred}	0.7041
Na_2O	75.8436	R^2_{Val}	0.6930
SiO_2	-22.5420		
SnO_2	-28.5312		
TiO_2	-27.0704		
ZrO_2	-48.6944		
Others	2.5197		
CaO×CaO	452.8308		
Li_2O×Li_2O	-3040.2579		
K_2O×Na_2O	433.9384		
Li_2O×Na_2O	-1273.4629		
CaO×SiO_2	267.5427		
K_2O×K_2O	724.3290		
Li_2O×SiO_2	361.8056		

Figure 3.12 shows a plot of the predicted vs. measured VHT ln(*D*, μm) values with 95% PIs for the 330 LAW glasses used to fit the PQQM in Table 3.7. If a 95% PI overlaps the 45º line, then the predicted and measured values are not statistically different (with 95% confidence) after accounting for data and model uncertainties. The 95% PIs for 318 of the 330 glasses (96.4%) in Figure 3.12 overlap the 45º line. This number is large because of the relatively large model prediction uncertainties. Still, the predicted VHT ln(*D*) values are generally within prediction uncertainties of the measured ln(*NL*) values. Ignoring the PIs, Figure 3.12 shows the PQMM has a tendency to over-predict ln(*D*, μm) below approximately 3, which corresponds to a *D* of approximately 20.1 μm. This is well below (i.e., inside) the constraint upper limit of 453 μm. However, as seen in Figure 3.12, the degree of over-prediction when $D < 20.1$ is not large enough to predict *D* is above the 453 μm limit when it is not. Hence, the PQMM in Table 3.8 can be used to predict the VHT *D* values of LAW glasses for comparison to the 453 μm limit, with the expectation that the PQMM will not mistakenly predict that glasses will fail the limit. Therefore, the 19-term VHT model given in Table 3.7 is recommended for use in enhanced LAW glass formulation.

The data and models are not fully QA compliant and therefore are not intended to be used in quality-affecting activities or decisions (e.g., design basis input, plant operations, waste form compliance). Instead the models and constraints are intended for use in mission planning activities.

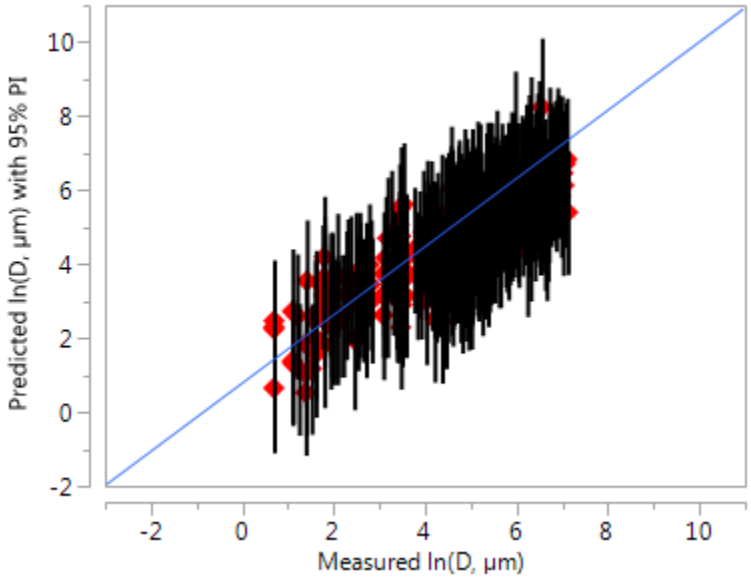

Figure 3.12. Predicted vs. Measured Plot of VHT ln(Alteration Depth) Values with 95% Prediction Intervals [ln(µm)] Using the Partial Quadratic Mixture Model for LAW Glasses

3.3.2 Future Plans

Future plans fall into two general categories: (i) develop additional data and models to predict VHT response and (ii) develop alternative approaches to demonstrate the performance of LAW glasses in the IDF environment. Very little data exists for the LAW glasses with VHT responses at or above the 50 $g/m^2/d$ contract limit. This is partially due to the fact that a large fraction of the glasses that exceed the limit result in unquantifiable VHT responses (e.g., less than values) that are not useful in modeling. Additional studies are needed to measure VHT data focused on the high-alkali region that have VHT responses at or above 50 $g/m^2/d$, while below the value of complete corrosion during the test duration. These data will be collected and modeled to predict the VHT response. These data and models will be developed under the appropriate QA for implementation in plant operations. Additional effort is needed to correlate the response of VHT to performance in the IDF or to develop a different criterion or set of criteria for controlling the performance of LAW glasses produced at WTP.

3.4 Viscosity

During operation of the LAW glass facility, it will be necessary to control glass compositions to have the viscosity of the glass melt within a desirable range. For LAW glasses melting at 1150ºC, an appropriate viscosity ranges from 2 to 8 Pa·s (as described in Section 2.5). However, optimal performance is typically found for viscosities in the range of 4 to 6 Pa·s. Because this doesn't strongly influence waste

loading, but, can improve melting performance, the tighter limits are recommended. A model for the natural logarithm of viscosity at 1150ºC as function of composition can be used for this purpose.

Section 3.4.1 discusses the data compiled for viscosity modeling, as well as the model for the natural logarithm of viscosity at 1150ºC that was developed. Section 3.4.2 discusses future plans.

3.4.1 Data and Model for Viscosity at 1150ºC of LAW Glasses

A database of 429 LAW glasses with viscosity measured at several temperatures (1990 data points total) was compiled and used to develop viscosity models. These data include simulated LAW glasses from both crucible-scale and melter tests. Table 3.8 summarizes the dataset of 429 LAW glasses compiled for modeling and model validation. The database excluded 6 glasses out of 435 for which data were initially compiled because of extreme concentrations of certain components.

The viscosity at 1150ºC (η_{1150}) value for each of the 429 LAW glasses was calculated by fitting either the VFT equation or the Arrhenius equation to the viscosity at temperature data for each LAW glass. The Arrhenius equation was fit only for one LAW glass for which the available data did not adequately support fitting a VFT equation. Then, the fitted VFT or Arrhenius equations were used to calculate the η_{1150} for each LAW glass.

Table 3.8. Summary of Viscosity Datasets for LAW Glasses

Dataset	# of Data Points	Reference	Comments
VSL-WTP	243	Muller et al. 2001 Muller and Pegg 2003a Muller and Pegg 2003b Muller and Pegg 2003c Rielley et al. 2004 Muller et al. 2004 Muller et al. 2005 Muller et al. 2006a Muller et al. 2006b Matlack et al. 2006c Piepel et al. 2007	Data used to develop WTP LAW glass models and additional glasses that were excluded in the original WTP models (see text)
VSL-ORP-A	122	Muller et al. 2012	Enhanced glass formulations with high waste loading (actively designed)
VSL-ORP-M	34	Muller et al. 2014	Enhanced glass formulations with high waste loading (test matrix)
PNNL-M	36	Russell et al. 2016	Enhanced glass formulations with high waste loading (test matrix)

A LMM was used to model the natural logarithm of η_{1150} (Pa·s) as a function of LAW glass composition. The LMM form is given by

$$\ln(\eta_{1150}, \text{Pa} \cdot \text{s}) = \sum_{i=1}^{q} b_i g_i \tag{3.6}$$

where

q = number of LAW glass components in the model

b_i = model coefficient for the i^{th} LAW glass component

g_i = mass fraction of the i^{th} LAW glass component, where $g_1 + \ldots + g_{\text{q=Others}} = 1.0$.

The LAW glass components included in the LMM were those that had sufficient ranges and distributions of values to support estimating the corresponding model coefficients. The sum of the mass fractions of all remaining LAW glass components is denoted as the Others component.

Equation (3.6) was fitted to the data consisting of the 429 LAW glass compositions and the corresponding calculated values of η_{1150}. The fitted model coefficients and several statistics related to the model fit are given in Table 3.9. The $R^2 = 0.9303$ indicates the model accounts for over 93% of the variation in $\ln(\eta_{1150})$ responses. The R^2_{Adj} and R^2_{Pred} values are only slightly smaller than the R^2 value, which indicates, respectively, that (i) the model does not contain many statistically nonsignificant terms, and (ii) there are no highly influential data points.

The RMSE = 0.1476 is an estimate of the experimental and measurement standard deviation [in $\ln(\eta_{1150}$, Pa·s) units] if the model adequately fits the data. The RMSE corresponds to a %RSD = 14.76 value for "measured" η_{1150} (Pa·s) values. This %RSD value is marginally larger than the experimental and measurement uncertainties in determining η_{1150} values of LAW glasses. Hence, the RMSE value indicates the model may have some LOF.

Table 3.9. Coefficients and Selected Fit Statistics of the Linear Mixture Model for Viscosity at 1150ºC Fitted to Data from 429 LAW Glasses.

Model Term	Coefficient, ln(η_{1150}, Pa·s)	Statistic	Value
Al_2O_3	11.67007	# of glasses	429
B_2O_3	-7.44665	Average ln($\boldsymbol{\eta_{1150}}$, Pa·s)	1.4584
CaO	-7.60545	RMSE, ln(Pa·s)	0.1476
Fe_2O_3	-0.11082	R^2	0.9303
K_2O	-4.65558	R^2_{Adj}	0.9277
Li_2O	-32.67344	R^2_{Pred}	0.9241
MgO	-4.26291		
Na_2O	-9.30809		
P_2O_5	7.94147		
SiO_2	8.88092		
SnO_2	4.73082		
TiO_2	-4.93294		
V_2O_5	-2.64858		
ZnO	-4.51330		
ZrO_2	6.91854		
Others	2.74032		

Figure 3.13 shows a plot of the predicted vs. measured[1] ln(η_{1150}, Pa·s) values with 90% PIs for the 429 LAW glasses used to fit the LMM in Table 3.9. If a 90% PI overlaps the 45º line, then the predicted and measured values are not statistically different (with 90% confidence) after accounting for data and model uncertainties. The 90% PIs for 395 of the 429 glasses (92.1%) in Figure 3.13 overlap the 45º line. Thus, the predicted ln(η_{1150}) values are generally within prediction uncertainties of the "measured" ln(η_{1150}) values. Ignoring the PIs, Figure 3.13 shows the LMM has a tendency to underpredict (i) below ln(η_{1150}) ~ 0.5 (i.e., η_{1150} ~ 1.65 Pa·s) and (ii) above ln(η_{1150}) ~ 2.2 (i.e., η_{1150} ~ 9.03 Pa·s). These ranges of underprediction with the LMM are outside the η_{1150} constraints of 4 to 6 Pa·s for LAW glasses. Hence, the LMM for viscosity at 1150ºC given in Table 3.9 is recommended for use in enhanced LAW glass formulation.

[1] This type of plot is traditionally referred to as a "predicted versus measured" plot. In this case, the "measured" η_{1150} values are actually values calculated from a fitted VFT or Arrhenius equation for each LAW glass, as discussed previously.

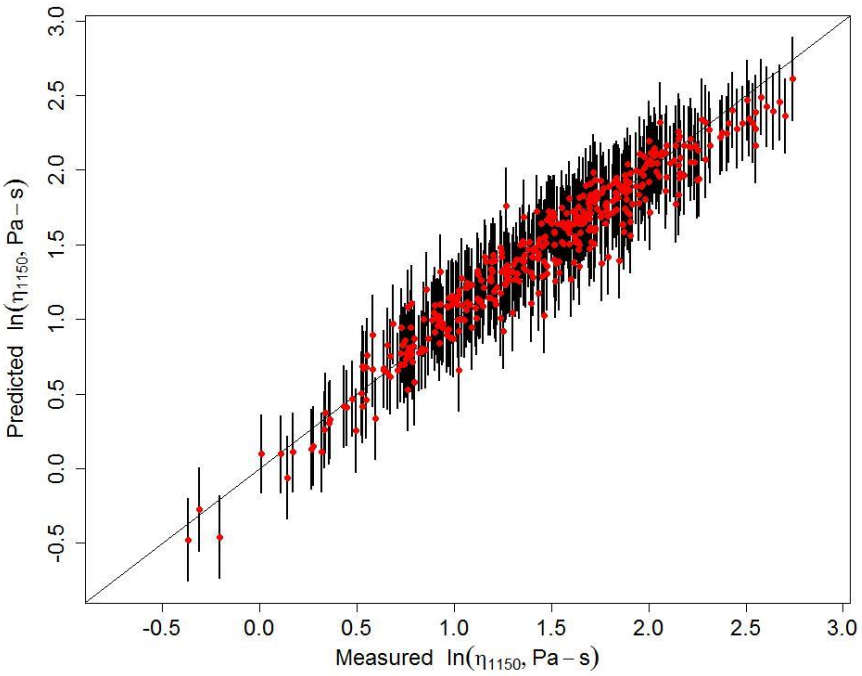

Figure 3.13. Predicted vs. Measured Plot of ln(η_{1150}) Values with 90% Prediction Intervals for the Linear Mixture Model for LAW Glasses.

The data and models are not fully QA compliant and therefore are not intended to be used in quality-affecting activities or decisions (e.g., design basis input, plant operations, waste form compliance). Instead the models and constraints are intended for use in mission planning activities.

3.4.2 Future Plans

Viscosity models will need to be developed for plant operation. While models predicting the ln(η_{1150}) are sufficient for glass mass estimation, models that predict the temperature impact of viscosity will be useful for many plant operating applications (including meeting design constraints at 1100 and 1200°C). Therefore, as additional LAW glass property testing continues, the measurement of viscosity will continue to be performed over a range of temperatures. When plant operating models are needed, these viscosity data will be fitted to functions of both composition and temperature.

3.5 Refractory Corrosion

LAW melts with high-alkali content are known to be corrosive to the melter materials of construction such as Inconel 690 and Monofrax K3 refractories (Gan et al. 2001). This concern has become more prevalent as waste loading has increased in the enhanced glass formulations, particularly for melts with higher alkali contents. Muller et al. (2015b) gathered available data for LAW glass composition effects on K3 corrosion and developed a preliminary model for its prediction. Based on melter operating experience, and review of melter design and operation, they recommend a corrosion depth limit of 0.040 inches per

6-day test at 1208°C.

Section 3.5.1 discusses a model for refractory corrosion as a function of LAW glass composition. Section 3.5.2 discusses future plans.

3.5.1 Model for Refractory Corrosion of LAW Glasses

A 24-term PQMM was recommended by Muller et al. (2015b) to predict the natural logarithm of neck loss on a 6-day K-3 refractory coupon corrosion test at 1208°C as a function of LAW glass composition using a dataset of 261 WTP-LAW and ORP-LAW glasses. The model is of the form

$$\ln(k_{1208}) = \sum_{i=1}^{q} k_i g_i + \text{Selected}\left\{ \sum_{i=1}^{q} k_{ii} g_i^2 + \sum_{i=1}^{q-1} \sum_{j=i+1}^{q} k_{ij} g_i g_j \right\}, \quad (3.7)$$

where

k_{1208} = neck corrosion distance in 6-day test at 1208°C (in inches)

k_i = coefficient of the i^{th} component in LAW glass

g_i = mass fraction of the i^{th} component in LAW glass

k_{ij} = coefficient of the product of the mass fractions in LAW glass of the i^{th} and j^{th} components (where a squared terms occurs when $i = j$).

The coefficients and component concentration ranges are listed in Table 3.10. The 24-term model for K-3 corrosion given in Table 3.10 is recommended for use in enhanced LAW glass formulation.

The data and models are not fully QA compliant and therefore are not intended to be used in quality-affecting activities or decisions (e.g., design basis input, plant operations, waste form compliance). Instead the models and constraints are intended for use in mission planning activities.

3.5.2 Future Plans

Refractory and metal (bubbler, thermowell, level measurement, electrode, etc.) corrosion in LAW glass melts may be significant, particularly for high-alkali glasses. The model in Section 3.5.1 represents the first attempt at modeling the composition effects on refractory corrosion (see Muller et al. 2015b). The data used to fit this model need to be expanded significantly and new models will need to be developed and validated for both refractory and metal corrosion. A large set of glasses designed and tested for other properties are available and could be tested for electrode and refractory corrosion.

Table 3.10. K-3 Corrosion Model Coefficients and Component Concentration Ranges

Model Term	$\ln(k_{1208})$ Coefficient	Range (mass fraction) Min	Max
Al_2O_3	-23.696	0.049	0.137
B_2O_3	-0.965	0.042	0.137
CaO	6.590	0	0.106
Cr_2O_3	-85.437	0.0001	0.006
Fe_2O_3	-4.315	0	0.137
K_2O	7.997	0	0.081
Li_2O	44.748	0	0.059
MgO	-37.185	0	0.035
Na_2O	20.337	0.024	0.26
P_2O_5	117.297	0	0.034
SiO_2	-10.103	0.313	0.502
SnO_2	-38.779	0	0.037
TiO_2	90.238	0	0.05
V_2O_5	-114.733	0	0.05
ZnO	-12.560	0	0.054
ZrO_2	-11.150	0	0.075
Others	-20.952	0.001	0.055
$Li_2O \times P_2O_5$	-3092.687		
$(MgO)^2$	716.072		
$Na_2O \times P_2O_5$	-579.772		
$Na_2O \times V_2O_5$	335.374		
$SiO_2 \times TiO_2$	-241.722		
$SnO_2 \times$ Others	2880.688		
$V_2O_5 \times$ ZnO	1028.765		
# data points	261		
R^2	0.905		
R^2_{Adj}	0.896		
R^2_{Pred}	0.881		
RMSE	0.255		

3.6 Loading Rules

Two options are available to optimize LAW glass and determine the waste loading. The first is to perform a multi-attribute optimization maintaining all properties within their acceptable ranges as is described in Vienna and Kim (2014) for WTP Baseline HLW formulation. The second is to use loading rules aimed at interpolating between successful glasses as described in Kim and Vienna (2012), which were developed for WTP Baseline LAW formulations. This latter approach is recommended for purposes of estimating the amount of glass to be produced at Hanford over the mission life as described below.

The loading of LAW in glass can be determined by interpolating between successful high waste-loaded compositions, as was done by Vienna et al. (2013). Muller et al. (2010) developed a correlation for estimating LAW loading, as shown schematically in Figure 3.14. The data used to develop this plot are summarized in Table 3.11. This correlation leads to the following rules

$$w_{Na_2O} + 0.66\, w_{K_2O} \le 24, \text{ wt\%} \tag{3.8}$$

$$w_{Na_2O} + 0.66\ w_{K_2O} \le 33.94 - 11.69\ w_{SO_3}, \text{ wt\%} \tag{3.9}$$

$$w_{SO_3} \le 1.5, \text{ wt\%} \tag{3.10}$$

where w_i is the i^{th} oxide weight percent in LAW glass (i.e., $g_i \times 100$). These rules correspond to the solid blue line in Figure 3.14.

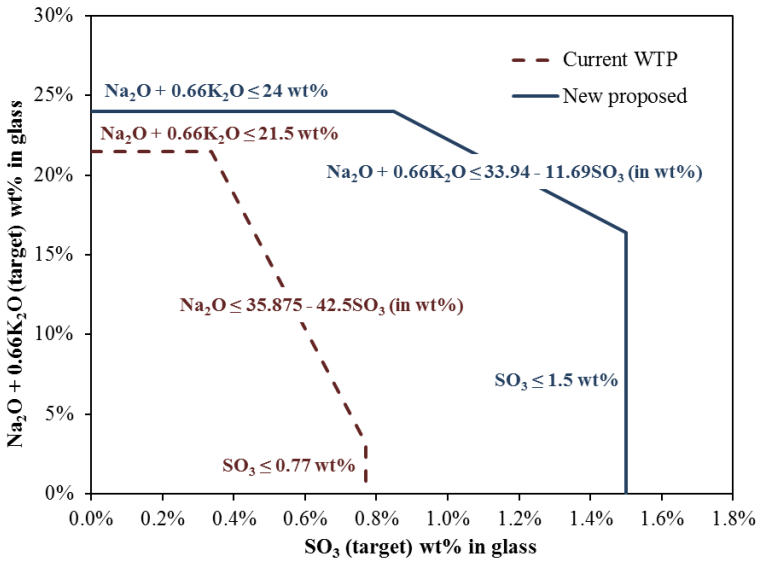

Figure 3.14. Overview of Waste Alkali Concentration ($d = w_{Na_2O} + 0.66\, w_{K_2O}$) and SO_3 Loadings for Advanced LAW Glasses (Vienna et al. 2013)

Table 3.11. Summary of Enhanced LAW Correlation Glasses (wt%)

Glass ID	Target w_{SO_3}	Measured w_{SO_3}	Target w_{Na_2O}	Target w_{K_2O}	d (w_{Na_2O} + 0.66 w_{K_2O})
ORPLG9	0.2	0.21	21.08	5.77	24.89
ORPLG27	0.5	-	21.08	5.77	24.89
ORPLA20	0.7	0.63	24.04	0.54	24.40
ORPLC5	0.7	0.61	23.69	0.54	24.05
ORPLA38-1	0.8	-	24.24	0.54	24.60
ORPLB4	0.85	0.81	24.12	0.11	24.20
LAWA187	0.95	0.77	23.17	0.51	23.51
LAWA161	1.0	-	20.70	0.44	20.99
LAWC100	1.1	1.05	20.24	0.15	20.34
ORPLD1	1.1	0.89	21.21	0.16	21.31
ORPLD6	1.2	1.25	22.22	0.17	22.34
LAWB99	1.5	1.14	10.08	0.41	10.35
ORPLE12	1.5	1.38	16.20	0.56	16.57
ORPLF7	1.5	1.35	12.24	0.51	12.57

Note: Glass compositions in this report are generally presented in mass fractions for consistency with the property models developed using mass fractions. However, this table presents the glass compositions in wt% for consistency with the rules and Figure 3.14 presented in this section.

Two methods (optimistic and conservative) were used to estimate the halide and chromate impacts in Vienna et al. (2013). These two methods added unnecessary confusion to the process of formulating glasses and the difference in glass mass estimated to be produced during mission life cycle was less than 3% between the two methods. A single approach should be developed and used in glass mass estimation rather than two. In addition, 29 melter test results have added to the understanding of Cr_2O_3, Cl, P_2O_5, F, and SO_3 impacts on salt formation (Matlack et al. 2014). Therefore, the impacts of halogen and chromium concentrations on the LAW glass loading limits were reevaluated.

The melter test data on enhanced LAW glasses from Vienna et al. (2013) and Matlack et al. (2014) were combined into a single set containing 55 distinct tests – 27 without accumulated salt and 28 with accumulated salt. A single parameter was calculated of the form

$$H = h_{Cl} g_{Cl} + h_{Cr} g_{Cr_2O_3} + h_P g_{P_2O_5} + h_F g_F + h_A \left(g_{Na_2O} + 0.66 g_{K_2O} \right), \tag{3.11}$$

where H is the halide parameter, h_i is the i^{th} component coefficient, and g_i is the i^{th} component target mass fraction in the glass. A line was drawn between SO_3 concentration and H in an attempt to separate compositions that accumulate a salt from those that don't (based only on components coming from waste). The slope and intercept of the line along with hi coefficients were then optimized to reduce the sum of squared differences between the composition and the line for only those glasses misclassified by the rule (e.g., glasses with salt above the line and glasses without a salt below the line). To add conservatism to the estimates, FNs (those compositions estimated not to accumulate a salt that actually do

accumulate a salt) were weighted by 10. The resulting optimized parameters are used to develop an additional SO_3 loading rule of

$$g_{SO_3} \le 0.01825 - 0.4936 \times \left(1.761 g_{Cl} + 2.971 g_{Cr_2O_3} - 0.1608 g_{P_2O_5}\right). \quad (3.12)$$

This method allows estimating the impacts of halide, chromate, and phosphate on the maximum sulfate loading in glass as shown in Figure 3.15. The uncertainty in the line is primarily due to the impacts of the glass-forming components on salt accumulation that are described in Section 3.1. The majority of the glasses tested and used to develop the rule in Equation (3.12) were not optimized for the concentrations of SO_3, halides, and Cr_2O_3 they contained. To develop a glass with the appropriate composition to tolerate that level of SO_3, Cl, Cr_2O_3, and P_2O_5 without accumulation of salt requires the optimization of the composition using the sulfate solubility model along with other constraints.

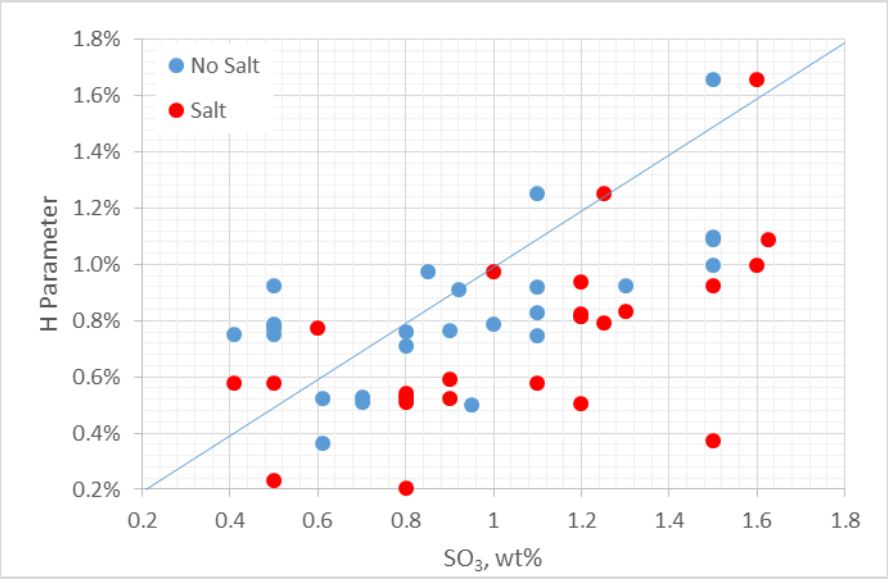

Figure 3.15. Plot of Prediction Parameter vs. W_{SO_3}

To determine the overall glass composition after the optimal waste loading is obtained, it is preferred to perform an optimization with glass property models described in this report. Alternatively, an advanced formulation correlation is underdevelopment similar to the WTP Baseline glass formulation correlation (see Muller et al. 2015a). If that becomes available, it may be preferable to apply it to design LAW glasses.

The data and models are not fully QA compliant and therefore are not intended to be used in quality-affecting activities or decisions (e.g., design basis input, plant operations, waste form compliance). Instead the models and constraints are intended for use in mission planning activities.

3.6.1 Future Plans

Enhanced waste glass loading rules and associated glass composition correlation rules are being developed (see for example Muller et al. 2015a). This approach to glass formulation will need to be completed and compared to the optimization technique that is currently used for HLW glass formulation. The most advantageous of the two approaches will be validated and incorporated into the LAW glass formulation algorithm for use in mission planning and plant operation.

3.7 Summary of Property Models and Component Concentration Limits for LAW Glasses

This subsection summarizes the LAW glass property constraints, models, and their associated validity ranges. Table 3.12 lists the model validity regions for each of the LAW glass property-composition models. However, these models, and the data used to produce them, are not fully QA compliant for plant operation and so should be used only as an estimation tool.

In addition to the model validity constraints, lessons learned from glass formulation work suggest more constraints should be added. Specifically, additional constraints are needed to avoid (i) secondary phase formation during processing and (ii) poor VHT performance. For example, Figure 3.16 shows a test glass that precipitated Cassiterite (SnO_2) during fabrication. Figure 3.17 shows a limited component scatterplot matrix highlighting the composition regions of concern for VHT failure and crystallization. From the plot, it is clear that LAW glasses with low CaO and high NAlk are prone to poor VHT performance. Further, the plot shows that LAW glasses with high Al_2O_3, SnO_2, and ZrO_2 are prone to crystallization. To address these concerns, two constraints have been added. First, a combined zirconia, tin, and alumina constraint

$$g_{ZrO_2} + g_{SnO_2} + g_{Al_2O_3} < 0.17 \tag{3.12}$$

was added to avoid crystallization. Second, an "alkali minus sum of zirconia, tin, and lime" constraint

$$g_{Na_2O} + 0.66 g_{K_2O} + 2.07 g_{Li_2O} - g_{ZrO_2} - g_{SnO_2} - g_{CaO} < 0.15 \tag{3.13}$$

was added to avoid poor VHT performance.

Table 3.12. Summary of LAW Glass Model Validity Constraints, mass fractions

	SO_3		PCT		VHT		Viscosity		K3		Overall	
Term	Min	Max	Min	Max	Min	Max	Min	Max	Min	Max	Min	Max
Al_2O_3	0.0553	0.1395	0.0305	0.1476	0.0350	0.1476	0.0350	0.1476	0.0490	0.1370	0.0553	0.1370
B_2O_3	0.0398	0.1606	0.0500	0.1515	0.0600	0.1377	0.0600	0.1380	0.0420	0.1370	0.0600	0.1370
CaO	0	0.1294	0	0.1281	0	0.1227	0	0.1273	0	0.1060	0	0.1060
Cl	0	0.0117	-	-	-	-	-	-	-	-	0	0.0117
Cr_2O_3	0.0001	0.01	-	-	-	-	-	-	0.0001	0.0060	0	0.0100
Fe_2O_3	-	-	-	-	0	0.0998	0	0.0998	0	0.1370	0	0.0997
K_2O	0.0011	0.0834	0	0.0591	0	0.0591	0	0.0589	0	0.0810	0	0.0589
Li_2O	0	0.0586	0	0.0633	0	0.0503	0	0.0633	0	0.0590	0	0.0503
MgO	-	-	0	0.0994	-	-	0	0.0502	0	0.0350	0	0.0350
Na_2O	0.0248	0.2605	0.0245	0.2601	0.05	0.2601	0.0245	0.2600	0.0240	0.2600	0.0248	0.2600
P_2O_5	0	0.0308	0	0.0475	-	-	0	0.0403	0	0.0340	0	0.0340
SiO_2	0.3005	0.5064	0.2983	0.5591	0.2983	0.5215	0.3350	0.5226	0.3130	0.5020	0.2983	0.5020
SnO_2	0	0.0501	0	0.0503	0	0.0502	0	0.0503	0	0.0370	0	0.0501
TiO_2	-	-	0	0.0399	0	0.0342	0	0.0399	0	0.0500	0	0.0341
V_2O_5	0	0.0439	-	-	-	-	0	0.0401	0	0.0500	0	0.0401
ZnO	-	-	-	-	-	-	0.0100	0.0581	0	0.0540	0	0.0540
ZrO_2	0.0262	0.0902	0	0.0675	0	0.0675	0	0.0675	0	0.0750	0	0.0675

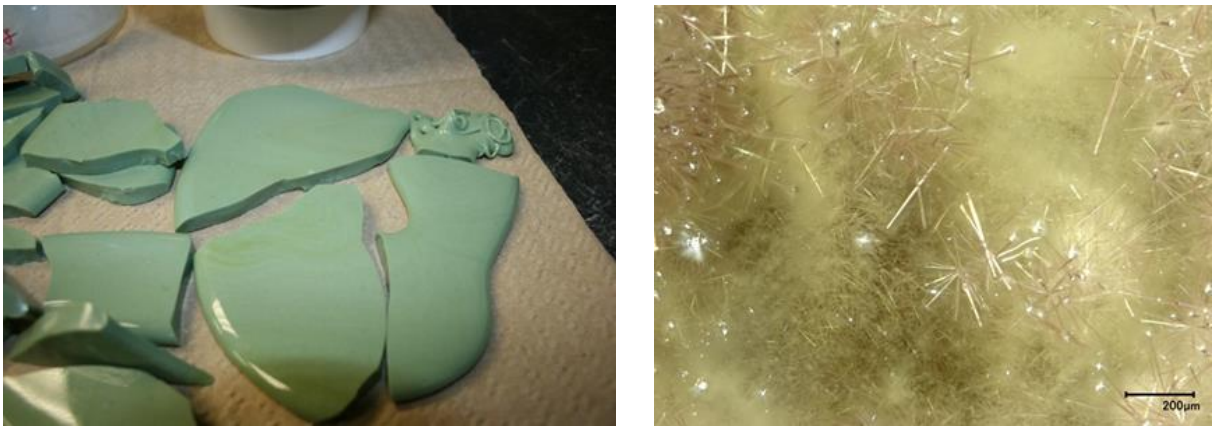

Figure 3.16. Example Crystallized LAW Glass Photograph of Pour-patty (left) and Optical Micrograph Showing Cassiterite (SnO_2) (right)

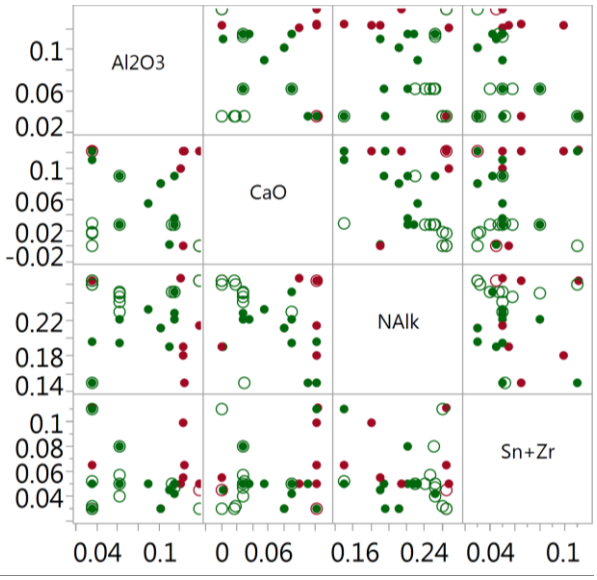

Figure 3.17. Scatterplot Matrix Showing Composition Region of Difficulties in LAW Glasses. Red dots form crystals and green open circles fail VHT. All values are mass fractions.

3.8 Calculation Examples

Examples are given to use in determining if the application and coding of the LAW models are correct. To create these examples, hypothetical wastes, based loosely on real projected Hanford LAW feeds, were used in glass optimization calculations. A set of waste compositions was selected to demonstrate the calculations and to provide an output file that can be used by others to make sure that they are using the models correctly. The waste estimates are from the LAW and secondary LAW vitrification feed, as estimated in Case 1 of System Plan revision 6 (Certa et al. 2011). The waste feeds were converted to mass fractions of reference oxides and halogens, and sorted by the ratios of Na_2O:SO_3, Na_2O:K_2O, and Na_2O:Cl. The waste with the minimum for each of the ratios was selected for the example calculations. Also, several other waste compositions that systematically varied the Na_2O:SO_3 ratio were selected. The selected waste compositions and associated component ratios are listed in Table 3.13.

Table 3.13. Selected Waste Compositions, mass fractions

Example #	1	2	3	4	5	6	7	8
Batch Date[(a)]	6/14/41	4/10/26	6/8/18	7/9/27	4/8/33	6/18/38	8/24/35	7/1/33
Batch #[(a)]	SLCP-937	LCP-391	LCP-1	SLCP-249	SLCP-539	LCP-1027	LCP-880	SLCP-551
Na_2O	0.5186	0.7672	0.7395	0.6952	0.7473	0.8086	0.7668	0.7882
SO_3	0.3511	0.0056	0.0135	0.0243	0.0743	0.0404	0.0511	0.0262
K_2O	0.0025	0.0655	0.1551	0.0223	0.0037	0.0028	0.0027	0.0030
Cl	0.0248	0.0148	0.0062	0.0532	0.0136	0.0059	0.0055	0.0050
F	0.0766	0.0060	0.0073	0.1263	0.0435	0.0087	0.0160	0.0112
P_2O_5	0.0066	0.0044	0.0060	0.0082	0.0201	0.0335	0.0589	0.0450
Cr_2O_3	0.0067	0.0012	0.0011	0.0061	0.0103	0.0044	0.0053	0.0071
Al_2O_3	0.0115	0.1317	0.0689	0.0595	0.0777	0.0868	0.0825	0.1034
SiO_2	0.0005	0.0016	0.0012	0.0018	0.0064	0.0072	0.0085	0.0079
SUM	0.9989	0.9981	0.9986	0.9968	0.9970	0.9983	0.9973	0.9969
Na_2O/SO_3	1	136	55	29	10	20	15	30
Na_2O/K_2O	204	12	5	31	202	293	281	265
Na_2O/Cl	21	52	120	13	55	137	140	158

(a) Batch date and # reflect the model projected date of delivery and numerical batch from the pretreatment facility concentrate storage vessel to the LAW vitrification facility concentrate receipt vessel.

As discussed in Section 1.2, two basic approaches are used to estimate loading of LAW in glass: (i) use of current loading rules described in Section 3.6 and (ii) numerical optimization of glass composition constrained by glass property models and constraints listed in this report (as is done for HLW in Section 2.10). Both approaches were applied to give examples of the calculations. The first approach was applied to each of the eight example waste compositions and the results are listed in Table 3.14. The optimization approach was also used to maximize waste loadings within property and component concentration constraints. Current glass forming chemicals include mined minerals (kyanite, wollastonite, olivine, silica, zincite, and zircon) and processed chemicals (boric acid, hematite, sodium carbonate, lithium carbonate, rutile, and sucrose) which are sources of Al_2O_3, B_2O_3, CaO, Fe_2O_3, Li_2O, MgO, Na_2O, SiO_2, ZnO, and ZrO_2. For the purposes of example calculations the pure oxides (without impurities) of Al_2O_3, B_2O_3, CaO, Cr_2O_3, Li_2O, MgO, SiO_2, SnO_2, V_2O_5, ZnO, and ZrO_2 were selected (adding Cr_2O_3, SnO_2, and V_2O_5; and removing Fe_2O_3 and Na_2O) and their concentrations adjusted along with waste loading until a maximum waste loading was obtained. The associated WL, additives, and constraints are listed in Table 3.14. Generally, the optimization routine will continue to change the additives and loading until all the degrees of freedom are used up (e.g., as many constraints are met as number of additives used) unless the loading is limited by a single waste component concentration limit. An exception to this is Example #7 for which six constraints were met with seven additives. It is not clear why the optimization for Example #7 achieved only 6 limits for 7 additives. Many unsuccessful attempts were made to remedy that problem. As anticipated, the optimization approach generally resulted in higher waste loadings (~15 relative% higher as a numeric average of the results) compared to the loading-rules approach.

Table 3.14. Waste Loading (wt%) and Liming Factor Results from Example Calculations

Example #	1	2	3	4	5	6	7	8
Waste Batch	SLCP-937	LCP-391	LCP-1	SLCP-249	SLCP-539	LCP-1027	LCP-880	SLCP-551
Loading rules								
Waste Loading	4.27%	29.61%	28.51%	23.16%	18.30%	26.46%	24.86%	30.37%
Limiting Factor[a]	S	NaK	NaS	H	H	NaS	NaS	NaK
Optimization								
Waste Loading	5.68%	33.62%	31.72%	21.99%	22.89%	32.15%	30.54%	32.99%
Properties								
PCT, g/L	0.275	1.856	2.165	0.643	3.395	2.455	1.112	1.870
VHT D, µm	453.0	453.0	453.0	4.4	82.9	453.0	453.0	453.0
K_3 corrosion, in	0.000	0.040	0.040	0.040	0.009	0.040	0.040	0.024
$ZrO_2+SnO_2+Al_2O_3$	0.097	0.170	0.170	0.170	0.123	0.120	0.091	0.127
Alk-(ZrO_2+SnO_2 +CaO)	-0.014	0.149	0.117	0.077	0.150	0.150	0.114	0.148
SO_3 limit, wt%	0.020	0.002	0.004	0.005	0.017	0.013	0.016	0.009
Viscosity, Pa·s	4.000	6.000	4.000	6.000	4.000	5.068	4.000	6.000
Additives								
Al_2O_3	5.79%	1.66%	4.90%	7.03%	4.87%	4.04%	4.33%	4.04%
B_2O_3	14.52%	9.04%	8.79%	7.69%	7.78%	8.84%	11.13%	8.95%
CaO	11.24%	1.30%	5.19%	5.15%	6.46%	6.75%	12.24%	6.92%
Cr_2O_3	0.00%	1.45%	1.41%	0.94%	0.00%	0.08%	0.00%	1.14%
Fe_2O_3	0.00%	0.00%	0.00%	0.00%	0.00%	0.00%	0.00%	0.00%
Li_2O	5.33%	0.00%	0.00%	3.93%	6.00%	0.00%	0.00%	0.00%
MgO	0.00%	1.02%	0.11%	0.11%	0.00%	1.98%	0.15%	0.15%
SiO_2	51.92%	61.53%	54.76%	52.96%	60.94%	62.43%	61.23%	62.93%
SnO_2	0.00%	7.11%	6.91%	4.44%	0.00%	0.00%	0.00%	0.00%
TiO_2	2.55%	5.14%	4.04%	4.18%	0.00%	0.39%	0.00%	0.00%
V_2O_5	4.25%	1.60%	4.01%	4.93%	5.20%	5.91%	5.77%	5.98%
ZrO_2	4.39%	10.17%	9.89%	8.65%	8.75%	9.58%	5.15%	9.88%
Limits[b]	8L/8A	Cr_2O_3	Cr_2O_3	Cl	7L/7A	Na_2O	6L/7A	Na_2O

(a) The limits for loading rules are: H = halide rule, NaK = Na_2O+K_2O, NaS = Na_2O and SO_3 equation, S = SO_3

(b) Limits for the optimization approach are denoted by #L/#A, which represent the number of limits reached and additives used in formulation. Cr_2O_3, Cl, and Na_2O represent single component concentration limits achieved.

4.0 Summary

Efforts are being made to increase the loading of Hanford tank wastes in glass while maintaining adequate processability, regulatory compliance, and product quality. These efforts have significantly expanded the composition regions and waste loadings of glasses beyond the point used in current project planning models. The effort documented in this report is aimed at evaluating the current glass formulation, property, and processing data, and to use the data to develop a non-conservative set of constraints and property models that can be used to estimate the amount of glass that would be produced at Hanford if the current enhanced waste glass formulation efforts were to be successfully completed according to current plans. This report presents a significant update of the Vienna et al. (2013) models report, incorporating new data and models, and addressing lessons learned from application of those models and constraints. However, the data used as well as the resulting models have not been reviewed, verified and validated; therefore, the information provided in this report cannot be used for quality-affecting activities or decisions.

An accurate method of estimating glass mass to be produced from Hanford tank waste is important for making informed decisions regarding the appropriate process options to pursue, as well as estimating the likely cost and schedule for tank waste cleanup mission completion. To help gain an accurate estimate of glass mass, glass property, processing, and composition, data have been gathered from literature including the results of the ongoing enhanced glass formulation program being led by ORP with support from PNNL and the VSL at the Catholic University of America along with other laboratories and universities. These data have been evaluated and used in the development of preliminary glass composition-property models as well as property and composition constraints. By combining these models and constraint sets, the reader can estimate the minimum amount of glass to be generated from Hanford tank waste with a given composition. Example calculations are supplied to ensure that the calculations are performed as intended. The models and constraints are only meant to give an indication of rough glass masses for information only and are not intended to be used in quality-affecting activities or decisions. A current research program is in place to develop the data, models, and uncertainty descriptions for that purpose.

Throughout this document, model coefficients and other values are reported with a higher number of figures than are significant. Ideally, the appropriate number of figures to report should be evaluated in detail. However, no such evaluation was performed. We therefore suggest using all reported figures in the model coefficients for consistency with example calculations supplied in this report.

4.1 HLW Glass Property Models

Models were developed to constrain the composition and loading of HLW glasses. These include models to control to following:

- The probability of nepheline formation during canister cooling of high-alumina glasses (Section 2.1). Avoiding nepheline allows for accurate prediction of PCT response while more detailed models for the PCT responses of slow cooled glasses is developed.

- The temperature at which 2 vol% of spinel is in equilibrium with the melt ($T_{2\%}$) (Section 2.2). Excessive crystallization in the melter may shorten melter lifetime. This $T_{2\%}$ model is a reasonable, yet somewhat arbitrary and conservative, method to minimize this risk while crystal accumulation models are developed.
- The sulfur tolerance of the melter feed using an SO_3 solubility model (Section 2.3). Separated salts may significantly increase corrosion of melter construction materials and this model and associated constraint are aimed at minimizing this risk.
- The viscosity of the melt at the 1150°C operating temperature (Section 2.5). Melt viscosity must be maintained in a range of 2 to 8 Pa·s for optimal operating. A slightly more restrictive range of 4 to 6 Pa·s is recommended for peak performance.
- The PCT of product glass using normalized B and Na release models (Section 2.6). The PCT responses are currently required to demonstrate compliance with disposal and contract requirements.
- The liquidus temperature (T_L) of zirconia-containing phases (Section 2.7). This model helps to reduce the risk of crystal accumulation in the melter for glasses with higher ZrO_2 concentrations.
- Also reported are component concentration limits for model validity, chromium tolerance, and phosphate tolerance. The recommended models are given, along with property and component concentration constraints. However, these models, and the data used to produce them, are not fully QA compliant for plant operation and so should be used only as an estimation tool.

4.2 LAW Glass Property Models

Models were developed to constrain the composition and loading of LAW glasses. These include models to control

- The sulfur tolerance of the melter feed using an SO_3 solubility model (Section 3.1). Separated salts may significantly increase corrosion of melter construction materials and this model and associated constraint are aimed at minimizing this risk.
- The PCT of product glass using normalized glass release model (Section 3.2). The PCT responses are currently required to demonstrate compliance with contract requirements.
- The VHT response of product glass using an alteration depth model (Section 3.3). The PCT responses are currently required to demonstrate compliance with contract requirements.
- The viscosity of the melt at the 1150°C operating temperature (Section 3.4). Melt viscosity must be maintained in a range of 2 to 8 Pa·s for optimal operating. A slightly more restrictive range of 4 to 6 Pa·s is recommended for peak performance.
- The K3 refractory corrosion (Section 3.6). This model helps to reduce the risk of excessive melter corrosion and shortened service life.
- Also reported are loading estimation rules and component concentration limits for model validity. The recommended models are given, along with property and component concentration constraints. However, these models, and the data used to produce them, are not fully QA compliant for plant operation and so should be used only as an estimation tool.

5.0 References

Allen GK, JD Belsher, TK Dhaliwal, RT Jasper, RA Kirkbride, LM Bergmann, and MN Wells. 2014. *Hanford Tank Waste Operations Simulator (HTWOS) Version 7.8 Model Design Document*. RPP-17152, Rev. 10, Washington River Protection Solutions, Richland, Washington.

Arakali VS, RC Chen, S Davis, Y Deng, MR Gross, R Gimpel, KD Jenkins, AS Klein, SC Orcutt, C Peredo, and IZ Stone. 2011. *Flowsheets Bases, Assumptions, and Requirements*, 24590-WTP-RPT-PT-02-005, Rev. 6, River Protection Project, Hanford Tank Waste Treatment and Immobilization Plant, Richland, Washington.

ASME. 2000. "Quality Assurance Requirements for Nuclear Facility Applications." ASME NQA-1-2000, American Society of Mechanical Engineers, New York.

Beal D. 2012. "Sample Size Determination for a Nonparametric Upper Tolerance Limit for any Order Statistic." *Proceedings of the Southeast SAS Users Group*, Paper SD-07. http://www.sesug.org/SESUG2012/

Belsher JD and FL Meinert. 2009. *High-Level Waste Glass Formulation Model Sensitivity Study 2009 Glass Formulation Model Versus 1996 Glass Formulation Model.* RPP-RPT-42649, Rev. 0, Washington River Protection Solutions, Richland, Washington.

Certa PJ, GK Allen, JD Belsher, PA Empey, JH Foster, TM Hohl, RT Jasper, RA Kirkbride, RL Lytle, FL Meinert, JA Shinabery, EB West, MN Wells, and LM Bergmann. 2010. *River Protection Project System Plan*. ORP-11242, Rev. 5, U.S. Department of Energy, Office of River Protection, Richland, Washington.

Certa PJ, GK Allen, TW Crawford, TM Hohl, KN Jordan, RA Kirkbride, and RL Lytle. 2008. *River Protection Project System Plan*. ORP-11242, Rev. 3, U.S. Department of Energy, Office of River Protection, Richland, Washington.

Certa PJ, GK Allen, TW Crawford, TM Hohl, KN Jordan, RA Kirkbride, and RL Lytle. 2008. *River Protection Project System Plan*. ORP-11242, Rev. 3A, U.S. Department of Energy, Office of River Protection, Richland, Washington.

Certa PJ, RD Adams, GK Allen, JD Belsher, PA Empey, JH Foster, TM Hohl, RT Jasper, RA Kirkbride, RL Lytle, FL Meinert, JS Ritari, RM Russell, KR Seniow, EB West, MN Wells, and LM Bergmann. 2011. *River Protection Project System Plan*. ORP-11242, Rev. 6, U.S. Department of Energy, Office of River Protection, Richland, Washington.

Certa PJ, RL Lytle, GK Allen, KN Jordan, TW Crawford, RA Kirkbride, TM Hohl, PA Empey, and MN Wells. 2009. *River Protection Project System Plan*. ORP-11242, Rev. 4, U.S. Department of Energy, Office of River Protection, Richland, Washington.

Chu S. 2013. U.S. Department of Energy Nuclear Waste Fund Fee Adequacy Assessment Report, U.S. Department of Energy, Washington, D.C.

Cornell JA. 2002. *Experiments with Mixtures: Designs, Models, and the Analysis of Mixture Data*, 3rd Edition, John Wiley and Sons, New York, New York.

Crum JV, JD Vienna, DK Peeler, IA Reamer, and DJ Pittman. 2002. "The Effect of Glass Composition on Crystallinity and Durability for INEEL Run 78 Calcine Waste Simulant." *Environmental Issues and Waste Management Technologies in the Ceramic and Nuclear Industries VII*, 132:267−275, American Ceramic Society, Westerville, Ohio.

Crum JV, TB Edwards, RL Russell, PJ Workman, M Schweiger, RF Schumacher, DE Smith, DK Peeler, and JD Vienna. 2012. "DWPF Startup Frit Viscosity Measurement Round Robin Results." *J. Am. Ceram. Soc*. 95(7):2196-05.

Deng YN. 2014. *Dynamic (G2) Model Design Document*. 24590-WTP-MDD-PR-01-002, Rev. 13, River Protection Project, Waste Treatment Plant, Richland, Washington.

Dierks RD. 1980. *The Design and Performance of A 100-Kg/H, Direct Calcine-Fed Electric-Melter System for Nuclear-Waste Vitrification*. PNL-3387, Pacific Northwest Laboratory, Richland, Washington.

Draper, NR and H Smith. 1998. *Applied Regression Analysis*, Third Edition, John Wiley and Sons, New York, New York.

DOE. 1996. *Waste Acceptance Product Specifications for Vitrified High-Level Waste Forms (WAPS)*. DOE/EM-0093, U.S. Department of Energy, Office of Environmental Management, Washington, D.C.

DOE. 2000. *Design, Construction, and Commissioning of the Hanford Tank Waste Treatment and Immobilization Plant*. U.S. Department of Energy, Office of River Protection, Richland, Washington.

DOE. 2008. *Quality Assurance Requirements and Description*. DOE/RW-0333P, Rev. 21, U.S. Department of Energy, Office of Civilian Radioactive Waste Management, Washington, D.C.

DOE. 2011. *Quality Assurance*. DOE O 414.1D. U.S. Department of Energy, Washington, D.C.

DOE. 2013. *Nuclear Safety Management*. 10CFR830. U.S. Department of Energy, Washington, D.C.

DOE. 2014. *River Protection Project System Plan*. ORP-11242, Rev. 7, U.S. Department of Energy, Office of River Protection, Richland, Washington.

Efron B and R Tibshirani. 1994. *An Introduction to the Bootstrap*. Chapman and Hall/CRC Press, Boca Raton, Florida.

Feng XD, PR Hrma, JH Westsik, Jr., NR Brown, MJ Schweiger, H Li, JD Vienna, G Chen, GF Piepel, DE Smith, BP Mcgrail, SE Palmer, DS Kim, Y Peng, WK Hahn, AJ Bakel, WL Ebert, DK Peeler, and CY Chang. 1996. *Glass Optimization for Vitrification of Hanford Site Low-Level Tank Waste*. PNNL-10918, Pacific Northwest Laboratory, Richland, Washington.

Fox KM and TB Edwards. 2008. *Refinement of the Nepheline Discriminator: Results of a Phase II Study*. SRNS-STI-2008-00099, Savannah River National Laboratory, Aiken, South Carolina.

Fox KM and TB Edwards. 2009. *Experimental Results of the Nepheline Phase III Study*. SRNL-STI-2009-00608, Savannah River National Laboratory, Aiken, South Carolina.

Fox KM, DK Peeler, TB Edwards, DR Best, IA Reamer, RJ Workman, JC Marra, BJ Riley, JD Vienna, JV Crum, J Matyas, AB Edmondson, JB Lang, NM Ibarra, A Fluegel, A Aloy, AV Trofimenko, and R Soshnikov. 2008. *International Study of Aluminum Impacts on Crystallization in U.S. High Level Waste Glass*. SRNL-STI-2008-00057, Savannah River National Laboratory, Aiken, South Carolina.

Fox KM, JD Newell, TB Edwards, DR Best, IA Reamer, and RJ Workman. 2007. *Refinement of the Nepheline Discriminator: Results of a Phase I Study*. WSRC-STI-2007-00659, Westinghouse Savannah River Company, Aiken, South Carolina.

Fox KM, TB Edwards, DK Peeler, DR Best, IA Reamer, and RJ Workman. 2006. *Nepheline Formation Study for Sludge Batch 4 (SB4): Phase 3 Experimental Results*. WSRC-TR-2006-00093, Savannah River National Laboratory, Aiken, South Carolina.

Gan H, K Gilbo, AE Papathanassiu, WK Kot, and IL Pegg. 2015. *Calcium Phosphate Constraints in HLW Glasses: Phosphate Liquidus Model*. VSL-15R3420-1, Vitreous State Laboratory, Washington, D.C.

Gan H, X Lu, I Vidensky, C Paul, and IL Pegg. 2001. *Corrosion of K-3 Refractory and Metal Alloys in RPP-WTP HLW Glasses*. VSL-01R2550-1, Vitreous State Laboratory, Washington, D.C.

Gimpel RF. 2002. *WTP Calculation Sheet: Determining the LAW Glass Former Constituents and Amounts for G2 and Acm Models: 24590-LAW-M4C-LFP-00002, Rev. B,* ORP-56511, River Protection Project, Waste Treatment Plant, Richland, Washington.

Gimpel RF. 2009. Memo, "Incorporation of HLW Glass Shell V2.0 into the Flowsheets," to ED Lee, CCN: 184905, October 20, 2009, ORP-56505, River Protection Project, Waste Treatment Plant, Richland, Washington.

Gimpel RF. 2010. *Halide, Chromate, and Phosphate Impacts on LAW Glass for Dynamic Flowsheet: 24590-WTP-MCR-PET-09-0037, Rev. 1,* ORP-56504, River Protection Project, Waste Treatment Plant, Richland, Washington.

Hamel WF, LK Holton, and LE Demick. 2003. *An Assessment of the Factors Affecting the Ability to Increase the Na2O Loading in the Waste Treatment and Immobilization Plant (WTP) Low Activity Waste (LAW) Glass*. D-03-DESIGN-004, U.S. Department of Energy, Office of River Protection, Richland, Washington.

Hrma P and JD Vienna. 2003. "Relationship between Liquidus Temperature and Solubility." *Environmental Issues and Waste Management Technologies in the Ceramic and Nuclear Industries VIII* 143:159−167, American Ceramic Society, Westerville, Ohio.

Hrma P, BJ Riley, JV Crum, and J Matyas. 2014. "The Effect of High-Level Waste Glass Composition on Spinel Liquidus Temperature." *Journal of Non-Crystalline Solids*. 384:32-40. DOI 10.1016/j.jnonaysol.2013.02.014.

Hrma P, BM Arrigoni, and MJ Schweiger. 2009. "Viscosity of Many-Component Glasses." *Journal of Non-Crystalline Solids*, 355(14-15):891-902. DOI: 10.1016/j.jnoncrysol.2009.03.005.

Hrma P, GF Piepel, MJ Schweiger, DE Smith, DS Kim, PE Redgate, JD Vienna, CA Lopresti, DB Simpson, DK Peeler, and MH Langowski. 1994. *Property/Composition Relationships for Hanford High-Level Waste Glasses Melting at 1150°C*. PNL-10359, Pacific Northwest Laboratory, Richland, Washington.

Hrma P, J Matyas, and DS Kim. 2003. "Evaluation of Crystallinity Constraint for HLW Glass Processing." *Environmental Issues and Waste Management Technologies in the Ceramic and Nuclear Industries VIII* 143:133−140, American Ceramic Society, Westerville, Ohio.

Hrma P, JD Vienna, BK Wilson, TJ Plaisted, and SM Heald. 2006. "Chromium Phase Behavior in a Multi-Component Borosilicate Glass Melt." *Journal of Non-Crystalline Solids*, 352:2114-2122. DOI: 10.1016/j.jnoncrysol.2006.02.051.

Hrma P, MJ Schweiger, CJ Humrickhouse, JA Moody, RM Tate, TT Rainsdon, NE Tegrotenhuis, BM Arrigoni, J Marcial, CP Rodriguez, and BH Tincher. 2010. "Effect of Glass-Batch Makeup on the Melting Process." *Ceramics-Silikaty*, 54(3):193−211.

Hrma P. 2002. "Crystallization in High-Level Waste Glasses." *Environmental Issues and Waste Management Technologies in the Ceramic and Nuclear Industries VII* 132:243−256, American Ceramic Society, Westerville, Ohio.

Hrma P. 2010. "Crystallization During Processing of Nuclear Waste Glass." *Journal of Non-Crystalline Solids*, 356(52-54):3019-3025. DOI: 10.1016/j.jnoncryso1.2010.03.039.

Jain V and SM Barnes. 1991. "Effect of Glass Pour Cycle on the Crystallization Behavior in the Canistered Product at the West Valley Demonstration Project." *Nuclear Waste Management* IV 23.

Jain V, RA Palmer, and SM Barnes. 1992. "Glass Composition Development and Nuclear Waste Vitrification System Testing − the West Valley Experience." In *Physics of Non-Crystalline Solids*, edited by LD Pye and HJ Stevens, Taylor & Francis, New York.

Jantzen CM and D Lambert. 1999. *Inspection and Analysis of the Integrated DWPF Melter System (IDMS) after Seven Years of Continuous Operation*. WSRC-MS-99-00336, Westinghouse Savannah River Company, Aiken, South Carolina.

Jantzen CM and KG Brown. 2007a. "Predicting the Spinel-Nepheline Liquidus for Application to Nuclear Waste Glass Processing: Part I. Primary Phase Analysis, Liquidus Measurement, and Quasicrystalline Approach." *Journal of the American Ceramic Society* 90(6):1866-1879.

Jantzen CM and KG Brown. 2007b. "Predicting the Spinel-Nepheline Liquidus for Application to Nuclear Waste Glass Processing. Part II: Quasicrystalline Freezing Point Depression Model." *Journal of the American Ceramic Society*, 90(6):1880-1891.

Jantzen CM, AD Cozzi, and NE Bibler. 2004. "High Level Waste Processing Experience with Increased Waste Loadings." *Ceramic Transactions* 168:31−49, American Ceramic Society, Westerville, Ohio.

Jantzen CM, NE Bibler, DC Beam, CL Crawford, and MA Pickett. 1993. *Characterization of the Defense Waste Processing Facility (DWPF) Environmental Assessment (EA) Glass Standard Reference Material (U)*. WSRC-TR-92-346, Rev. 1, Westinghouse Savannah River Company, Aiken, South Carolina.

Jantzen CM. 1986. *Devitrification of Scale Melter Glass in Riser Heater*. DPST-86-461, Savannah River Laboratory, Aiken, South Carolina.

Jantzen CM. 1991a. "Relationship of Glass Composition to Glass Viscosity, Resistivity, Liquidus Temperature, and Durability: First-Principle Process Product Models for Vitrification of Nuclear Waste." *Ceramics Transactions,* 23:37−51, American Ceramic Society, Westerville, Ohio.

Jantzen CM. 1991b. *Characterization of Off-Gas System Pluggages, Significance for DWPF and Suggested Remediation*. WSRC-TR-90-205, Westinghouse Savannah River Company, Aiken, South Carolina.

Jenkins KD, RC Chen, R Gimpel, Y Deng, MR Gross, and C Peredo. 2013. *Flowsheets Bases, Assumptions, and Requirements (BARD)*. 24590-WTP-RPT-PT-02-005, Rev. 7, River Protection Project, Hanford Tank Waste Treatment and Immobilization Plant, Richland, Washington.

Jenkins, KD, R Gimpel, and YN Deng. 2013. *2013 Tank Utilization Assessment (TUA) Part 1: Potential Impact of Advanced Glass Models on the WTP*, 24590-WTP-RPT-PE-13-003, Rev. 0, River Protection Project, Hanford Tank Waste Treatment and Immobilization Plant, Richland, Washington.

John AS, H Gan, M Chaudhuri, WK Kot, and IL Pegg. 2004. "Spinel Crystallization in HLW Glass Melts: Cation Exchange Systematics and the Role of Rh_2O_3 in Spinel Formation." *Ceramic Transactions* 279−288, American Ceramic Society, Westerville, Ohio.

Kim D, JD Vienna, DK Peeler, KM Fox, A Aloy, AV Trofimenko, and KD Gerdes. 2008. "Improved Alumina Loading in High Level Waste Glasses." *Waste Management 2008,* p. 10382.

Kim D, JD Vienna, P Hrma, MJ Schweiger, J Matyas, JV Crum, DE Smith, WC Buchmiller, JS Tixier, Jr., JD Yeager, and KB Belew. 2003. *Development and Testing of ICV Glasses for Hanford LAW*. PNNL-14351, Pacific Northwest National Laboratory, Richland, Washington.

Kim DS and JD Vienna. 2012. *Preliminary ILAW Formulation Algorithm Description*: *24590-LAW-RPT-RT-04-0003, Rev. 1*. ORP-56321, River Protection Project, Hanford Tank Waste Treatment and Immobilization Plant, Richland, Washington.

Kim DS, DK Peeler, and P Hrma. 1995. "Effect of Crystallization on the Chemical Durability of Simulated Nuclear Waste Glasses." *Ceramic Transactions* 61:177−185, American Ceramic Society, Westerville, Ohio.

Kim DS, MJ Schweiger, CP Rodriguez, WC Lepry, JB Lang, JV Crum, JD Vienna, FC Johnson, JC Marra, and DK Peeler. 2011. *Formulation and Characterization of Waste Glasses with Varying Processing Temperature*. PNNL-20774, Pacific Northwest National Laboratory, Richland, Washington.

Kim DS. 2013. Letter, "Estimation of Low-Activity Waste Glass Mass." to AA Kruger, PNNL-SA-92798, January 8, 2013, Pacific Northwest National Laboratory, Richland, Washington.

Kim DS. 2013. Letter, "Estimation of Low-Activity Waste Glass Mass." to AA Kruger, PNNL-SA-92798, January 8, 2013, Pacific Northwest National Laboratory, Richland, Washington.

Kot WK, H Gan, and IL Pegg. 2005. *Preparation and Testing (T1% and PCT) of HLW Matrix Glasses to Support WTP Property-Composition Model Development*. VSL-05R5780-2, Vitreous State Laboratory, The Catholic University of America, Washington, D.C.

Kot WK, H Gan, and IL Pegg. 2006. *Preparation and Testing of Glasses to Support Development of WTP IHLW Formulation Algorithm*. VSL-06R1240-1, Rev. 0, Vitreous State Laboratory at The Catholic University of America, Washington, D.C.

Kot WK, K Gilbo, H Gan, I Joseph, and IL Pegg. 2015. *Enhanced HLW Glass Property-Composition Models – Phase 2*. VSL-15R3400-1, The Catholic University of America, Washington, D.C.

Kroll JO, JD Vienna, MJ Schweiger, GF Piepel, and SK Cooley. 2016. *Results from Phase 1, 2, and 3 Studies on Nepheline Formation in High-Level Waste Glasses Containing High Concentrations of Alumina*. DRAFT, Pacific Northwest National Laboratory, Richland, Washington.

Kruger AA, IL Pegg, A Feng, and WK Kot. 2013. *Sulfate Solubility in RPP-WTP HLW Glasses*. VSL-06R6780-1, ORP-56325, Vitreous State Laboratory, The Catholic University of America, Washington, D.C.

Li H, JD Vienna, P Hrma, DE Smith, and MJ Schweiger. 1996. "Nepheline Precipitation in High-Level Waste Glasses: Compositional Effects and Impact on the Waste Form Acceptability." *MRS Proceedings*, 465:261-268. Cambridge University Press, Cambridge, United Kingdom.

Li H, JD Vienna, P Hrma, DE Smith, and MJ Schweiger. 1997. "Nepheline Precipitation in High-Level Waste Glasses: Compositional Effects and Impact on the Waste Form Acceptability." *Scientific Basis for Nuclear Waste Management XX* 465:261−268, Materials Research Society, Pittsburgh, Pennsylvania.

Matlack KS, H Gan, M Chaudhuri, WK Kot, W Gong, T Bardakci, IL Pegg, and I Joseph. 2008. *Melt Rate Enhancement for High Aluminum HLW Glass Formulations: VSL-08R1360-1*. ORP-44236, Vitreous State Laboratory, The Catholic University of America, Washington, D.C.

Matlack KS, H Gan, M Chaudhuri, WK Kot, W Gong, T Bardakci, IL Pegg, and I Joseph. 2010a. *DM100 and DM1200 Melter Testing with High Waste Loading Glass Formulations for Hanford High-Aluminum HLW Streams: VSL-10R1690-1*. ORP-44198, Vitreous State Laboratory, The Catholic University of America, Washington, D.C.

Matlack KS, H Gan, W Gong, IL Pegg, CC Chapman, and I Joseph. 2007a. *High Level Waste Vitrification System Improvements: VSL-07R1010-1*. ORP-56297, Vitreous State Laboratory, The Catholic University of America, Washington, D.C.

Matlack KS, I Joseph, W Gong, IS Muller, and IL Pegg. 2007b. *Enhanced LAW Glass Formulation Testing: VSL-07R1130-1*. ORP-56293, Vitreous State Laboratory, The Catholic University of America, Washington, D.C.

Matlack KS, I Joseph, W Gong, IS Muller, and IL Pegg. 2009a. *Glass Formulation Development and DM10 Melter Testing with ORP LAW Glasses: VSL-09R1510-2*. ORP-56296, Vitreous State Laboratory, The Catholic University of America, Washington, D.C.

Matlack KS, IS Muller, I Joseph, and IL Pegg. 2014. *Melter Tests to Define LAW Halide, Chromium and Phosphate Concentrations*. VSL-14R3070-1, Vitreous State Laboratory at The Catholic University of America, Washington, D.C.

Matlack KS, IS Muller, W Gong, and IL Pegg. 2006c. *DuraMelter 100 Tests to Support LAW Glass Formulation Correlation Development: VSL-06R6480-1*. ORP-56324, Vitreous State Laboratory, The Catholic University of America, Washington, D.C.

Matlack KS, M Chaudhuri, H Gan, IS Muller, WK Kot, W Gong, and IL Pegg. 2005. *Glass Formulation Testing to Increase Sulfate Incorporation*: *VSL-04R4960-1*. ORP-51808, Vitreous State Laboratory, The Catholic University of America, Washington, D.C.

Matlack KS, W Gong, IS Muller, I Joseph, and IL Pegg. 2006a. *LAW Envelope A and B Glass Formulations Testing to Increase Waste Loading: VSL-06R6900-1,* ORP-56322, Vitreous State Laboratory, The Catholic University of America, Washington, D.C.

Matlack KS, W Gong, IS Muller, I Joseph, and IL Pegg. 2006b. *LAW Envelope C Glass Formulation Testing to Increase Waste Loading: VSL-05R5900-1*. ORP-56323, Vitreous State Laboratory, The Catholic University of America, Washington, D.C.

Matlack KS, WK Kot, and IL Pegg. 2015a. *Support for HLW Direct Feed - Phase 2*. VSL-15R3440-1, Vitreous State Laboratory, Washington, D.C.

Matlack KS, WK Kot, H Gan, and IL Pegg. 2010b. *Glass Formulation Development and Testing for DWPF High-Al_2O_3 HLW Sludges: VSL-10R1670-1*. ORP-56290, Vitreous State Laboratory, The Catholic University of America, Washington, D.C.

Matlack KS, WK Kot, W Gong, W Lutze, IL Pegg, and I Joseph. 2009b. *Effects of High Spinel and Chromium Oxide Crystal Contents on Simulated HLW Vitrification in DM100 Melter Tests: VSL-09R1520-1*. ORP-56327, Vitreous State Laboratory, The Catholic University of America, Washington, D.C.

Matlack, KS, WK Kot, IL Pegg, and I Joseph. 2015b. *High Waste Loading Glass Formulation Development for High-Zr HLW*. VSL-15R3250-1, Vitreous State Laboratory, Washington, D.C.

Matyas J, AR Huckleberry, CP Rodriguez, JB Lang, AT Owen, and AA Kruger. 2012. *HLW Glass Studies: Development of Crystal Tolerant HLW Glasses*. PNNL-21308, Pacific Northwest National Laboratory, Richland, Washington.

Matyas J, AR Huckleberry, CP Rodriguez, JB Lang, AT Owen, and AA Kruger. 2013. "Crystal-Tolerant Glass Approach for Mitigation of Crystal Accumulation in Continuous Melters Processing Radioactive Waste." *Journal of the American Ceramic Society* (Submitted).

Matyas J, JD Vienna, A Kimura, M Schaible, and RM Tate. 2010a. "Development of Crystal-Tolerant Waste Glasses." *Advances in Materials Science for Environmental and Nuclear Technology*, 222:41-50.

Matyas J, JD Vienna, M Schaible, C Rodriguez, JV Crum, A Kimura, and RM Tate. 2010b. *Development of Crystal-Tolerant High-Level Waste Glasses*. PNNL-20072, Pacific Northwest National Laboratory, Richland, Washington.

Matyas J, M Schaible, and JD Vienna. 2011. "Determination of Stokes Shape Factor for Single Particles and Agglomerates." *Advances in Materials Science for Environmental and Nuclear Technology II*, 227:195-202.

McCloy JS and JD Vienna. 2010. *Glass Composition Constraint Recommendations for Use in Life-Cycle Mission Modeling*. PNNL-19372, Pacific Northwest National Laboratory, Richland, Washington.

McCloy JS, C Rodriguez, C Windisch, C Leslie, MJ Schweiger, BJ Riley, and JD Vienna. 2010. "Alkali/Alkaline-Earth Content Effects of Properties of High-Alumina Nuclear Waste Glasses." *Ceramic Transactions* 222:63-76, American Ceramic Society, Westerville, Ohio.

McCloy JS, MJ Schweiger, CP Rodriguez, and JD Vienna. 2011. "Nepheline Crystallization in Nuclear Waste Glasses: Progress toward Acceptance of High-Alumina Formulations." *International Journal of Applied Glass Science* 2(3):201-214. DOI: 10.1111/j.2041-1294.2011.00055.x.

McElroy JL, JE Mendel, WF Bonner, and MH Henry. 1979a. *Quarterly Progress Report − Research and Development Activities − High-Level Waste Immobilization Program: January through March 1979*. PNL-3050-1, Pacific Northwest Laboratory, Richland, Washington.

McElroy JL, JE Mendel, WF Bonner, and MH Henry. 1979b. *Quarterly Progress Reports Research and Development Activities − High-Level Waste Immobilization Program: January through December 1978*. PNL-2999, Pacific Northwest Laboratory, Richland, Washington.

McElroy JL. 1976. *Quarterly Progress Report Research and Development Activities Waste Fixation Program, January through March 1976*. BNWL-2070, Pacific Northwest Laboratory, Richland, Washington.

Mendel JE, WA Ross, FP Roberts, YB Katayama, J Westsik, JH, RP Turcotte, JW Wald, and DJ Bradley. 1977. *Annual Report on the Characteristics of High-Level Waste Glasses*. BNWL-2252, Pacific Northwest Laboratory, Richland, Washington.

Mika M, MJ Schweiger, JD Vienna, and P Hrma. 1997. "Liquidus Temperature of Spinel Precipitating High-Level Waste Glasses." *Proc. Sci. Basis Nucl. Waste Manag.*, 465:71-78.

Montgomery DC, EA Peck, GV Vining. 2013. *Introduction to Linear Regression Analysis*, Fifth Edition. John Wiley and Sons, New York, New York.

Muller I, K Gilbo, I Joseph, and IL Pegg. 2013. *Enhanced LAW Glass Property-Composition Models – Phase 1*. *VSL-13R2940-1*, Vitreous State Laboratory, The Catholic University of America, Washington, D.C.

Muller I, K Gilbo, I Joseph, and IL Pegg. 2014. *Enhanced LAW Glass Property-Composition Models – Phase 2. VSL-14R3050-1*. Vitreous State Laboratory, The Catholic University of America, Washington, D.C.

Muller IS and IL Pegg. 2003a. *Baseline LAW Glass Formulation Testing: VSL-03R3460-1*. ORP-55237, Vitreous State Laboratory, The Catholic University of America, Washington, D.C.

Muller IS and IL Pegg. 2003b. *LAW Glass Formulation to Support AP-101 Actual Waste Testing Final Report: VSL-03R3470-2*. Vitreous State Laboratory, The Catholic University of America, Washington, D.C.

Muller IS and IL Pegg. 2003c. *LAW Glass Formulation to Support Melter Runs with Simulants: VSL-03R3460-2*. ORP-55237, Vitreous State Laboratory, The Catholic University of America, Washington, D.C.

Muller IS, AC Buechele, and IL Pegg. 2001. *Glass Formulation and Testing with RPP-WTP LAW Simulants: VSL-01R3560-2*. ORP-56327, Vitreous State Laboratory, The Catholic University of America, Washington, D.C.

Muller IS, G Diener, I Joseph, and IL Pegg. 2004. *Proposed Approach for Development of LAW Glass Formulation Correlation: VSL-04L4460-1, Rev. 2*. ORP-56326, Vitreous State Laboratory, The Catholic University of America, Washington, D.C.

Muller IS, H Gan, K Gilbo, IL Pegg, and I Joseph. 2015b. *LAW Glass Property-Composition Models for K-3 Refractory Corrosion and Sulfate Solubility, VSL-15R3270-1*. Vitreous State Laboratory, the Catholic University of America, Washington, D.C.

Muller IS, I Joseph, and IL Pegg. 2005. *Comparison of LAW Simulant, Actual Waste, and Melter Glasses: VSL-05R5460-1, Rev. 0*. Vitreous State Laboratory, The Catholic University of America, Washington, D.C.

Muller IS, I Joseph, and IL Pegg. 2006a. *Preparation and Testing of LAW High Phosphorus and High-Chromium Glasses: VSL-06R6480-2, Rev. 0*. Vitreous State Laboratory, The Catholic University of America, Washington, D.C.

Muller IS, I Joseph, and IL Pegg. 2006b. *Preparation and Testing of LAW High-Alkali Correlation and Augmentation Matrix Glasses Final Report: VSL-06R6480-3, Rev. 0*. Vitreous State Laboratory, The Catholic University of America, Washington, D.C.

Muller IS, I Joseph, F Perez- Cardenas, and IL Pegg. 2008. *LAW Glass Testing and VHT Model Assessment*, VSL-08R1410-1, Rev. 0, Vitreous State Laboratory, The Catholic University of America, Washington, D.C.

Muller IS, IL Pegg, AC Buechele, H Gan, C Kim, ST Lai, G Del Rosario, and Q Yan. 1998. *Glass Formulation and Testing with TWRS LAW Simulants*, ORP-56328, The Catholic University of America, Washington, D.C.

Muller IS, KS Matlack, H Gan, I Joseph, and IL Pegg. 2010. *Waste Loading Enhancements for Hanford LAW Glasses: VSL-10R1790-1*. ORP-48578, Vitreous State Laboratory, The Catholic University of America, Washington, D.C.

Muller IS, KS Matlack, IL Pegg, and I Joseph. 2015a. *Test Plan: Enhanced LAW Glass Correlation*. *VSL-15T3680-1*. Vitreous State Laboratory at The Catholic University of America, Washington, D.C.

Muller IS, WK Kot, HK Pasieka, K Gilbo, FC Perez-Cardenas, I Joseph, and IL Pegg. 2012. *Compilation and Management of ORP Glass Formulation Database: VSL-12R2470-1*, ORP-53934, Vitreous State Laboratory, The Catholic University of America, Washington, D.C.

Nocedal J and S Wright. 2006. *Numerical Optimization*. 2nd ed. Springer Science & Business Media, New York, New York.

OCRWM. 2008. *Civilian Radioactive Waste Management System Waste Acceptance System Requirements Document (WASRD)*. DOE/RW-0351, Rev. 5, ICN-01, U.S. Department of Energy, Office of Civilian Radioactive Waste Management, Washington, D.C.

Peeler DK, DS Kim, JD Vienna, MJ Schweiger, and GF Piepel. 2015. *Office of River Protection Advanced Low-Activity Waste Glass Research and Development Plan*. PNNL-24883, Pacific Northwest National Laboratory, Richland, Washington.

Peeler DK, JD Vienna, MJ Schweiger, and KM Fox. 2015. *Advanced High-Level Waste Glass Research and Development Plan*. PNNL-24450, Pacific Northwest National Laboratory, Richland, Washington.

Peeler DK, TB Edwards, DR Best, IA Reamer, and RJ Workman. 2006. *Nepheline Formation Study for Sludge Batch 4 (SB4): Phase 2 Experimental Results*. WSRC-TR-2006-00006, Savannah River National Laboratory, Aiken, South Carolina.

Peeler DK, TB Edwards, IA Reamer, and RJ Workman. 2005. *Nepheline Formation Study for Sludge Batch 4 (SB4): Phase 1 Experimental Results*. WSRC-TR-2005-00371, Savannah River National Laboratory, Aiken, South Carolina.

Perez J and IL Pegg. 2006. "High-Level Waste Glass Formulation Algorithm Verification Testing Guidance." CCN 127601, River Protection Project, Waste Treatment Plant, Richland, Washington.

Perez JM. 2006. *Practical and Historical Bases for a Glass Viscosity Range for Joule-Heater Ceramic Melter Operation*. Email to JD Vienna, Dtd, Dec. 22, 2006, CCN: 150054, River Protection Project, Hanford Tank Waste Treatment and Immobilization Plant, Richland, Washington.

Piepel GF, JM Szychowski, and JL Loeppky. 2002. "Augmenting Scheffé Linear Mixture Models with Squared and/or Crossproduct Terms." *Journal of Quality Technology* 34:297-314.

Piepel GF, SK Cooley, A Heredia-Langner, SM Landmesser, WK Kot, H Gan, and IL Pegg. 2008. *IHLW PCT, Spinel $T_{1\%}$, Electrical Conductivity, and Viscosity Model Development: VSL-07R1240-4, Rev. 0*. ORP-56320, Vitreous State Laboratory, The Catholic University of America, Washington, D.C.

Piepel GF, SK Cooley, IS Muller, H Gan, I Joseph, and IL Pegg. 2007. *ILAW PCT, VHT, Viscosity, and Electrical Conductivity Model Development: VSL-07R1240-4, Rev. 0*. ORP-56502, Vitreous State Laboratory, The Catholic University of America, Washington, D.C.

Piepel, GF and SK Cooley. 2009. "Automated Method for Reducing Scheffé Linear Mixture Experiment Models". *Quality Technology and Quantitative Management*, 6:255-270.

Rankin WN, PE O'rourke, PD Soper, MB Cosper, and BC Osgood. 1982. *Evaluation of Corrosion and Deposition in the 1941 Melter*. DPST-82-231, Savannah River Laboratory, Aiken, South Carolina.

Rielley E, Muller IS and IL Pegg. 2003. *Preparation and Testing of LAW Marix Glasses Final Report: VSL-04R4480-1*. Vitreous State Laboratory, The Catholic University of America, Washington, D.C.

Riley BJ, JA Rosaria, and P Hrma. 2001. *Impact of HLW Glass Crystallinity on PCT Response*. PNNL-13491, Pacific Northwest National Laboratory, Richland, Washington.

Rodriguez CP, J McCloy, MJ Schweiger, JV Crum, and A Winschell. 2011. *Optical Basicity and Nepheline Crystallization in High Alumina Glasses*. PNNL-20184, Pacific Northwest National Laboratory, Richland, Washington.

Ross WA and JE Mendel. 1979. *Annual Report on the Development and Characterization of Solidified Forms for High-Level Wastes: 1978*. PNL-3060, Pacific Northwest Laboratory, Richland, Washington.

Schweiger M, B Riley, J Crum, P Hrma, C Rodriguez, B Arrigoni, J Lang, D Kim, J Vienna, F Raszewski, D Peeler, T Edwards, D Best, I Reamer, W Riley, P Simmons, and R Workman. 2011. *Expanded High-Level Waste Glass Property Data Development: Phase I*. PNNL-17950, Pacific Northwest National Laboratory, Richland, Washington.

Stan Development Team. 2015. *Stan Modeling Language User's Guide and Reference Manual*. Version 2.10.0. http://mc-stan.org/.

Taylor AS, TB Edwards, JC George, TK Snyder, and DK Peeler. 2004. *The SRNL Glass Composition – Properties (Compro™) Database*. WSRC-RP-2004-00704, Savannah River National Laboratory, Aiken, South Carolina.

Vienna JD and DS Kim. 2007. *Halide, Chromate, and Phosphate Impacts on LAW Glass Salt Limits*. Memorandum to Larry Petkus, Dtd. October 2, 2007, CCN: 150795, River Protection Project, Hanford Tank Waste Treatment and Immobilization Plant, Richland, Washington.

Vienna JD and DS Kim. 2008. *Preliminary IHLW Formulation Algorithm Description*. 24590-HLW-RPT-RT-05-001, Rev. 0, River Protection Project, Hanford Tank Waste Treatment and Immobilization Plant, Richland, Washington.

Vienna JD, A Fluegel, DS Kim, and P Hrma. 2009. *Glass Property Data and Models for Estimating High-Level Waste Glass Volume*. PNNL-18501, Pacific Northwest National Laboratory, Richland, Washington.

Vienna JD, A Jiřička, PR Hrma, DE Smith, TH Lorier, RL Schulz, and IA Reamer. 2001b. *Hanford Immobilized LAW Product Acceptance Testing: Tanks Focus Area Results*. PNNL-13744, Pacific Northwest National Laboratory, Richland, Washington.

Vienna JD, DS Kim, DC Skorski, and J Matyas. 2013. *Glass Property Models and Constraints for Estimating the Glass to Be Produced at Hanford by Implementing Current Advanced Glass Formulation Efforts*. PNNL-22631, Rev. 1, ORP-58289, Pacific Northwest National Laboratory, Richland, Washington.

Vienna JD, DS Kim, IS Muller, GF Piepel, and AA Kruger. 2014. "Toward Understanding the Effect of Low-Activity Waste Glass Composition on Sulfur Solubility." *Journal of the American Ceramic Society*, 97(10):3135–3142. DOI: 10.1111/jace.13125.

Vienna JD, JO Kroll, P Hrma, JB Lang, and JV Crum. 2016. "Submixture Model to Predict Nepheline Precipitation in Waste Glasses." *International Journal of Applied Glass Science*, 2016:1-16. DOI: 10.1111/ijag.12207.

Vienna JD, P Hrma, A Jiricka, DE Smith, TH Lorier, IA Reamer, and RL Schulz. 2001a. *Hanford Immobilized LAW Product Acceptance Testing: Tanks Focus Area Results*. PNNL-13744, Pacific Northwest National Laboratory, Richland, Washington.

Vienna JD, P Hrma, MJ Schweiger, and MH Langowski. 1996a. "Compositional Dependence of Elemental Release from HLW Glasses by the Product Consistency Test: A One Component-at-a-Time Study." *Ceramic Transactions* 72:307−316, American Ceramic Society, Westerville, Ohio.

Vienna JD, P Hrma, MJ Schweiger, MH Langowski, PE Redgate, DS Kim, GF Peipel, DE Smith, CY Chang, DE Rinehart, SE Palmer, and H Li. 1996b. *Effect of Composition and Temperature on the Properties of High-Level Waste (HLW) Glass Melting above 1200°C*. PNNL-10987, Pacific Northwest National Laboratory, Richland, Washington.

Vienna JD, P Hrma, WC Buchmiller, and JS Ricklefs. 2004. *Preliminary Investigation of Sulfur Loading in Hanford LAW Glass*. PNNL-14649, Pacific Northwest National Laboratory, Richland, Washington.

Wilson BK, P Hrma, J Alton, J Plaisted, and JD Vienna. 2002. "The Effect of Composition on Spinel Equilibrium and Crystal Size in High-level Waste Glass." *Journal of Materials Science*, 37:5327-5331.

Appendix A

Statistical Methods for Evaluating and Validating Models Fit to Experimental Data

Appendix A

Statistical Methods for Evaluating and Validating Models Fit to Experimental Data

There are many statistical methods (both numerical and graphical) for assessing models. *Evaluation methods* assess a model with the data used to develop the model. Such data are referred to as *model development data*. The goals of model evaluation are to assess: (i) how well a model fits the data used to develop it, (ii) whether there are any outlying or influential data points that significantly affect the fitted model, and (iii) whether the assumption of ordinary least squares regression are satisfied. Problems detected by model evaluation such as violation of assumptions, detection of outlying data points, or detection of model inadequacy require implementing various remedies in the model development process until the problem(s) are corrected.

When the model being evaluated acceptably fits the data used to develop the model, *model validation* methods should be applied using data not used to develop the model. Such data are referred to as *model validation data*. If model validation data are not available, *cross-validation methods* can be applied using the model development data. Cross-validation methods leave out one or more data points at a time, so that some of the data are used for model development and some for model validation. Such methods are also referred to as data-splitting validation methods, where part of the data is used for model development and evaluation, while the other part is used for validation.

Section A.1 discusses statistical methods for evaluating models fit to experimental data. Section A.2 discusses statistical methods for validating models using experimental data not used to fit the model. Draper and Smith (1998) and Montgomery et al. (2013) are textbook references that discuss statistical methods for evaluating and validating models.

A.1 Statistical Methods for Model Evaluation

Model evaluation techniques used in this report include, Studentized residuals, three R^2 statistics, the root mean squared error (*RMSE*), and predicted versus measured (PvM) plots with X% prediction intervals. Each of these is explained briefly below. The following notation is used in the subsequent descriptions and definitions:

n = number of data points used to fit a model

p = number of parameters (coefficients) in a model estimated by fitting the model to data

y_i = measured property value (mathematically transformed, if appropriate for the model used) for the i^{th} data point

$\hat{y}_i$ = predicted property value (mathematically transformed, if appropriate for the model used) for the i^{th} data point made using the model fitted to all n data points

$\hat{y}_{(i)}$ = predicted property value (mathematically transformed, if appropriate for the model used) for the i^{th} data point made using a model fitted to all n data points except the i^{th}

$\bar{y}$ = average (mean) of the n measured property values (mathematically transformed, if appropriate for the model form used).

The model evaluation methods are now briefly described for situations where ordinary least squares regression is appropriate for fitting a model to data. The descriptions and formulas of the various model evaluation quantities are different if weighted least squares regression, generalized least squares regression, or nonlinear least squares regression are appropriate. Because none of these latter methods were used in this report, the model evaluation methods and formulas are not discussed only for ordinary least squares regression.

RMSE

The RMSE is calculated by the formula

$$RMSE = \sqrt{\frac{\sum_{i=1}^{n} (\hat{y}_i - y_i)^2}{n - p}} \tag{A.1}$$

If the fitted model is adequate and does not have a statistically significant lack-of-fit (LOF), this statistic provides an estimate of the experimental and measurement uncertainty standard deviation associated with melting glasses and measuring the associated property. The statistic *RMSE* is included as standard output in most regression software, and has units the same as the property values y_i (including any mathematical transformation of the property in the model).

Studentized Residual

A Studentized residual (s_i) for a given data point is the difference in measured and predicted property values (i.e., a residual $r_i = y_i - \hat{y}_i$) divided by its standard deviation. The formula for a Studentized residual is given by

$$s_i = \frac{r_i}{RMSE\left[1 - \mathbf{a}_i^T \left(\mathbf{A}^T \mathbf{A}\right)^{-1} \mathbf{a}_i\right]^{0.5}}, \tag{A.2}$$

where r_i and *RMSE* are as previously defined, $\boldsymbol{a}_i$ is the composition (column) vector for the i^{th} modeling data point expanded in the form of the model, $\boldsymbol{A}$ is an $n \times p$ matrix of the compositions (and temperatures in the case of viscosity or electrical conductivity) in the modeling dataset expanded in the form of the model, the superscript T denotes the transpose of a vector or matrix, and the superscript "-1" indicates a matrix inverse.

Patterns in plots of the s_i versus $\hat{y}_i$ may indicate (i) a violation of the ordinary least squares regression assumptions and suggest a property transformation to remedy the situation, or (ii) indicate model inadequacy. Studentized residuals are typically viewed in plots on the y-axis with various quantities on the x-axis. The majority of the Studentized residuals should fall within the range of ± 2.0 and almost all should fall within ± 3.0. Comparing Studentized residuals to such a range provides an easy criterion for judging whether a data point is outlying. Points with very large (in absolute value) Studentized residuals

should not automatically be eliminated from the modeling data set. Rather, a subject matter expert should assess whether the property value may be wrong, or whether the composition has an extreme value of one or more components that make it very influential. These are appropriate reasons for removing one or more outlying data points from a modeling dataset.

R^2 Statistics

Three R^2 statistics are discussed, which all generally quantify the proportion of variation in the property values y_i accounted for by the fitted model. Three different R^2 statistics are useful in evaluating models fitted to glass property-composition data. These are denoted as R^2, R^2_{Adj}, and R^2_{Pred}, which are discussed subsequently. In general, all three quantify the proportion of variation in the property values y_i accounted for by the fitted model, with some differences in the specifics.

The (ordinary) R^2 statistic is given by

$$R^2 = 1 - \frac{\sum_{i=1}^{n} (\hat{y}_i - y_i)^2}{\sum_{i=1}^{n} (y_i - \bar{y})^2}, \tag{A.3}$$

where the notation was defined previously. R^2 is interpreted as the fraction of variability in the property data (transformed if appropriate) accounted for by the fitted model.

The adjusted R^2 statistic is given by

$$R^2_{Adj} = 1 - \frac{\sum_{i=1}^{n} (\hat{y}_i - y_i)^2 \Big/ (n-p)}{\sum_{i=1}^{n} (y_i - \bar{y})^2 \Big/ (n-1)}, \tag{A.4}$$

where the notation was defined previously. R^2_{Adj} is interpreted as the adjusted fraction of variability in the property data (transformed if appropriate) accounted for by the fitted model. The adjustment is for the number of parameters (p) and number of data points (n) used in fitting the model. Increasing the number of parameters (coefficients) in a model will always increase R^2, but R^2_{Adj} may decrease if the addition model terms and coefficients do not significantly improve the fit.

The predicted R^2 statistic is given by

$$R^2_{Pred} = 1 - \frac{\sum_{i=1}^{n} (\hat{y}_{(i)} - y_i)^2}{\sum_{i=1}^{n} (y_i - \bar{y}_w)^2}, \tag{A.5}$$

where the notation was defined previously. R^2_{Pred} is interpreted as the leave-one-out cross-validation fraction of variability in the property data (transformed if appropriate) accounted for by the fitted model.

This statistic is calculated by a method equivalent to leaving each data point out of the model fit, and then evaluating how well the model predicts the property for that data point. R^2_{Pred} estimates the fraction of variability that would be explained in predicting new observations drawn from the same composition space. However, computational simplifications (using a vector-matrix formula) do not require refitting a model with each data point removed.

Generally, the three R^2 statistics take values between 0 and 1. However, R^2_{Adj} and R^2_{Pred} can take negative values for a poor fitting model, a model that contains many more terms than needed to fit the data, or a model fitted to data with one or more very influential data points. Among the three R^2 statistics, typically $R^2_{Pred} \leq R^2_{Adj} \leq R^2 \leq 1$. More than a small difference between R^2 and R^2_{Adj} indicates that the model may contain more terms than needed to achieve essentially the same goodness of fit. A substantial difference between R^2 and R^2_{Pred} is indicative of one or more data points being very influential in determining the fit of the model. Some reduction from R^2 to R^2_{Pred} is expected because R^2 corresponds to using all data to fit the model, whereas R^2_{Pred} corresponds to leaving each data point out of the fit when evaluating the performance of the model for that point. In general, a model will tend to predict better for data used to fit it than for data not used to fit it.

Predicted versus Measured Plot and Prediction Intervals

A predicted versus measured plot shows how well model-predicted values $\hat{y}_i$ compare to the measured values y_i for the glasses in the model-development dataset. Predicted property values $\hat{y}_i$ are plotted on the *y*-axis and measured property values y_i are plotted on the *x*-axis. A 45º line (i.e., with slope one) is included in the plot for reference purposes, and represents the ideal of predicted values equaling measured values. Plotted points falling above this line correspond to glasses for which the model overpredicts the property, while plotted points falling below this line represent glasses for which the model underpredicts the property. A preponderance of plotted points in a portion of the plot on the x-axis (measured values) falling above or below the line indicates that the model tends to yield biased predictions for that range of measured property values. Plotted points far from the line are outlying or potentially influential data points.

In this report, either 90% or 95% prediction intervals (PI) have been added to many of the predicted vs. measured plots. The use of 90% or 95% depends on whether the property is for process control (90%) or product acceptability (95%). The formula for a *X*% two-sided PI for an individual response value for a given composition $\boldsymbol{x}$ is given by

$$\hat{y}(\mathbf{x}) \mp t_{1-\alpha/2}(n-p)RMSE\sqrt{1+\mathbf{a}^T(\mathbf{A}^T\mathbf{A})^{-1}\mathbf{a}}\,, \qquad \text{(A.6)}$$

where all notation has been defined previously. An X% prediction interval (X% PI) provides X% confidence that the interval includes a future single observation of the property (or its transformation) for a glass of the specific composition. When an X% PI overlaps the 45º line in the plot, it indicates that the predicted property value is not statistically different than the measured value with X% confidence.

The model evaluation techniques discussed above are included in the output of many software packages that use ordinary least squares regression to fit models to data. In some cases, different notation and terminology may be used, but the concepts and formulas are the same (with the exception that there are variations of Studentized residuals). See Draper and Smith (1998) or Montgomery et al. (2001) for further discussion of the concepts.

A.2 Statistical Methods for Model Validation

Model validation methods assess how well a fitted model predicts property values for glasses not used in fitting the model. The glasses used for validation ideally should be in the same composition region as the data used to fit the property-composition models, because (in general) fitted empirical and semi-empirical models should not be used to extrapolate much beyond the region covered by the modeling data. Also, ideally the validation data should be evenly distributed over the model composition region of model validity to properly assess predictive ability over the region. However, this is difficult to achieve in practice because validation data are typically not designed, but often consists of whatever extra data are available.

Validation generally consists of using a fitted model to predict property values for a set of validation data, and then comparing the predicted property values to the measured values from the validation dataset. Several methods for comparing predicted and measured values of properties are described following.

Validation R^2

Statistical summary comparisons of predicted and measured property values are useful to see if differences are larger than their expected uncertainties. One such comparison is the *validation* R^2 statistic, which is given by

$$R^2_{Val} = 1 - \frac{\sum_{i=1}^{n} (\hat{y}_i - y_i)^2}{\sum_{i=1}^{n} (y_i - \bar{y})^2}, \qquad \text{(A.7)}$$

where the notation was defined previously. R^2_{Val} is interpreted as the fraction of variability in the property values (transformed if appropriate) in the validation dataset accounted for by the fitted model. Note that R^2_{Val} is defined in Equation (A.7) exactly the same as the ordinary R^2 defined in Equation (A.3), except that model validation data are used to assess model predictive performance instead of the model development data. Hence, the y_i, $\hat{y}_i$, and $\bar{y}$ values in Equation (A.7) correspond to the model validation data.

Generally $R^2_{Val} \le R^2_{Pred} \le R^2_{Adj} \le R^2 \le 1$ for model validation. However, R^2_{Val} can take negative values (when a model predicts a validation dataset very poorly) and can take values larger than R^2_{Pred}, R^2_{Adj}, or R^2 (when a model predicts a particular validation dataset better than it predicts the model development dataset).

When there is no appropriate separate validation dataset, the modeling dataset may be split into modeling and validation subsets. In this report, the data are split into five subsets, each containing roughly 20% of the modeling dataset. Then, each such subset was used as the validation dataset, and the remaining four subsets were combined and used as the modeling subset. See Section 1.4 for the specifics.

Validation RMSE

Another useful summary statistic for model validation is *validation RMSE* ($RMSE_{Val}$). This statistic is calculated the same as given in Equation (A.1), except using the model validation dataset instead of the model development dataset. The statistic may also be calculated for a validation subset when the modeling dataset is split into subsets, as described previously.

Predicted Versus Measured Plots and Prediction Intervals

Predicted and measured values for a model validation dataset can be compared by plotting the predicted versus the measured property values for each data point. Such plots are the same as described in Section A.1, except model validation data are used instead of model development data. Also, X% PIs may be added to such plots, as described in Section A.1. One would expect that at least X% of the validation data points would have X% PIs that overlap the 45º line in the predicted vs. measured plot if the model predicts as well for the validation dataset as it did the model development dataset. If the percentage of X% PIs overlapping the 45º line is substantially less than X%, it may be an indication that (i) the model overfits the model development dataset, or (ii) the model validation dataset may focus more on subregions of the composition region where the model does not predict as well.

Pacific Northwest
NATIONAL LABORATORY

Proudly Operated by **Battelle** *Since 1965*

U.S. DEPARTMENT OF
ENERGY

902 Battelle Boulevard
P.O. Box 999
Richland, WA 99352
1-888-375-PNNL (7665)

www.pnnl.gov